

الجمهورية الجزائرية الديمقراطية الشعبية
République Algérienne Démocratique et Populaire
وزارة التعليم العالي و البحث العلمي
Ministère de l'enseignement supérieur et de la recherche scientifique

Université Mohamed Khider - Biskra
Faculté des Sciences et de la Technologie
Département de Génie Civil et Hydraulique
Référence :.....



جامعة محمد خيضر - بسكرة
كلية العلوم و التكنولوجيا
قسم الهندسة المدنية و الري
المرجع :

Thèse présentée en vue de l'obtention du diplôme de

Doctorat en Génie Civil

Spécialité : Modélisation et Analyse des Structures

Nonlinear Behaviour Analysis of Composite Thin Beams and Plates

**Analyse du Comportement Non-linéaire des Poutres Minces
et des plaques en Matériaux Composites**

Présentée par

Souhia Bouadjadja

Soutenue publiquement le: 07 Décembre 2020

Devant le jury composé de :

Mr. Rachid Chebili	Professeur	Président	Université de Biskra
Mr. Abdelouahab Tati	Professeur	Rapporteur	Université de Biskra
Mr. Djamel Hamadi	Professeur	Examineur	Université de Biskra
Mr. Khelifa Guerraiche	Maitre de Conférence 'A'	Examineur	Université de Batna2

Acknowledgements

Faith, confidence, belief in God wisdom is the secret that keeps me powerful, patient, an optimist at each difficult moment during my life trip. So, thank you so much, God, for anything, everything, I love you.

First of all, I am deeply grateful to my parents for their care, support, assistance, love and advice and their belief in me, who made me the person that I am today. I would like to thank my brother, sisters for their encouragement and help.

Writing a thesis is not an easy task and it never contains only the work of a single person. I am deeply thankful to my academic tutor, my supervisor Professor Abdelouahab Tati, who gave substance to my work. Professor Tati encouraged me along my whole path and was always instrumental in the development of my research and my thinking by his judicious advice and his always positive attitude. Next, I would like to thank all the professors and staff of the University of Biskra, who helped me to progress in my work. Also, I am thankful to Dr. Belhi Guerira and all the engineers in the Mechanical laboratory for their useful discussions and help during my experimental work.

I am very grateful to Professor E.Carrera who accepted my request to work under Dr. A. Pagani in the MUL2 group of research, Department of Mechanical Engineering and Aerospace, Politecnico di Torino, Italy. Dr. A. Pagani was always professional, helpful, kind and he always accepted my questions and help me to learn and understand more in my domain of research. Also, MUL2 team who always manage everything in good ways.

Finely, I would like to thank a friend, person, student who helped me or gave me advice or encouraged me during my path in this work.

Souhia Bouadjadja

“Imagination is more important than knowledge”
“It will never be enough. . . science”

Abstract

In engineering applications, it is well known that the minimum weight criteria with high performance is essential in the design of certain structures like aircraft components, aerospace vehicles and civil structures.. etc. This task could be a challenge especially when the design of wing structures such as aircraft wings, rotor blades, robotic arms is the subject. The behavior of such structures is highly nonlinear due to the deformation of their geometry. The solution of such problems becomes very complex, especially with the use of composite materials. The effects of large displacements may play a primary role in the correct prediction of the behavior of these structural members, which continue to be modeled as a flexible beams. In this way, another difficult task can be imposed here when some structural elements like plates and shells which can undergo inplane thermo-mechanical stresses that affect their dynamic and static behaviors. This problem has stimulated several researchers to work on the subject to provide accurate predictions of free vibration of laminated plates, subjected to inplane thermal or mechanical stresses. The main aim of the present work is the contribution in the analytical, experimental and numerical analysis of nonlinear behavior of some structural elements. The nonlinearities considered in this thesis are geometric nonlinearities arising from the large displacements and nonlinearities arising when a part of structure as plates, may lose their stiffness under inplane thermal or mechanical loading effect. An analytical model has been developed for beams large deflection analysis followed by an experimental program for the same purpose. Furthermore, a beam finite element based on Euler-Bernoulli beam theory, taking in consideration composite material has been formulated for nonlinear bending analysis. A four noded finite element based on first order shear deformation theory has been used to study the effect of thermal and mechanical inplane loading on dynamic behavior of laminated plates. The obtained results have been verified and validated with the available results in the literature.

Keywords: Nonlinear analysis, Composite material, Analytical, Experimental, beams, Laminated plates, Finite element.

ملخص

من المعروف في التطبيقات الهندسية، أن معيار الحد الأدنى للوزن مع الأداء العالي، يعد ضرورة في تصميم بعض الهياكل مثل مكونات الطائرات، المركبات الفضائية والهياكل المدنية. هذه المهمة ستكون تحدياً خصوصاً عند تصميم هياكل الأجنحة مثل أجنحة الطائرات، شفرات الدوار، الأذرع الآلية. يكون سلوك مثل هذه الهياكل غير خطي بدرجة كبيرة بسبب تشوه شكلها الهندسي فيصبح حل هذه المشكلات معقداً للغاية، لا سيما مع استخدام المواد المركبة. قد تلعب تأثيرات الإزاحات الكبرى دوراً رئيسياً في التنبؤ الصحيح لسلوك هؤلاء الأعضاء الهيكلية، والتي لا تزال تعتبر كروافد مرنة. ويزداد الأمر صعوبة عندما تتعرض بعض هذه العناصر الهيكلية مثل الألواح والهياكل القشرية إلى الاجهادات الحرارية أو الميكانيكية الداخلية التي تؤثر على سلوكها الديناميكي و الاستاتيكي. وقد حفزت هذه المشكلة العديد من الباحثين للعمل على الاهتزاز الحر للألواح المصفحة المعرضة للاجهادات الحرارية و الميكانيكية. الهدف الرئيسي من العمل هو المساهمة في دراسة السلوك غير الخطي لبعض العناصر الهيكلية، تحليلياً و تجريبياً ورقمياً. اللاخطية التي تم اعتبارها في هذه الأطروحة هي اللاخطية الهندسية الناشئة عن عمليات الإزاحات الكبرى و اللاخطية الهندسية التي تنشأ عندما يتعرض جزء من الهيكل كالصفائح، لفقدان صلابته تحت تأثير التحميل الحراري أو الميكانيكي. تم تطوير نموذج تحليلي من أجل دراسة الإزاحات الكبرى للروافد متبوع برنامج تجريبي من أجل نفس الهدف. بالإضافة الى، تم صياغة عنصر محدود استناداً على نظريته برنولي للروافد من أجل دراسة الانحناء الاخطي للروافد. و قد تم دراسة تأثير التحميل الحراري و الميكانيكي على السلوك الديناميكي للألواح المصفحة باستعمال طريقة العناصر المحدودة استناداً لنظرية تشوه القص من الدرجة الأولى. تم التحقق من النتائج التي تم الحصول عليها و التحقق من صحتها مع النتائج المتاحة

الكلمات المفتاحية : التحليل اللاخطي، المواد المركبة، التحليلي، تجريبي، الروافد، اللوحات المصفحة، العناصر المحدودة.

List of Publications and Communications

International Publications

- A. Tati, **S. Bouadjadja**, Y. Bada. Free Vibration of Thermally Stressed Angle-Ply Laminated Composite Using First-Order Shear Deformation Theory Model with Assumed Natural Shear Strain. *Journal of The Institution of Engineers (India): Series C*, 937:947-100,2018.
- **S. Bouadjadja**, A. Tati, B. Guerira. Analytical and Experimental Investigation on Large Deflection Analysis of Composite Cantilever Beams. *Journal of Mechanics of Advanced Materials and Structures*,1:9, 2020.
- **S. Bouadjadja**, A. Tati, A. Sadgui. Nonlinear Bending Analysis of Composite Cantilever Beams. *Australian Journal of Basic and Applied Sciences*, 28:34-13, 2019.

International Communications

- **S. Bouadjadja**, A. Tati. Nonlinear Bending Analysis of a Cantilever Beams. Arab Conference on Mechanical Engineering (ARCME'17),10-11 December 2017, Biskra- Algeria.
- **S. Bouadjadja**, A. Tati, A. Sadgui. Nonlinear Bending Analysis of Composite Cantilever Beams.The Third International Conference on Advances in Mechanical, Industrial and Mechatronics Engineering (ICAMIME 2019),19-20 April 2019,Tunis-Tunisia.
- A. Sadgui, A. Tati, **S. Bouadjadja**. First-order Shear Deformation Theory Model for the Bending Analysis of Functionally Graded Isotropic and Sandwich Plates. The First International Conference on Materials, Environment, Mechanical and Industrial Systems (ICMEMIS'19), 29-30 June 2019, Djalfa-Algeria.

- A. Sadgui, A. Tati, **S. Bouadjadja**. Bending and Free Vibration Analysis of Functionally Graded Sandwich Plates. Congrès Algérien de Mécanique (CAM), 23-26 February 2020, Ghardaia-Algeria.

Contents

Acknowledgements	i
Abstract	iii
List of Publications and Communications	v
List of Figures	xv
List of Tables	xvii
List of Symbols and Abbreviations	xviii
General Introduction	1
I Literature Review	7
1 Basic Concepts of Nonlinear Phenomena	8
1.1 Introduction	8
1.2 Sources of Nonlinearity	12
1.2.1 Geometric nonlinearities	13
1.2.2 Material nonlinearities	14
1.2.3 Kinematic nonlinearity	15
1.2.4 Force nonlinearity	15
1.3 Importance of Nonlinear Analysis	16
1.4 Solution of Nonlinear Systems	17

1.4.1	Direct iteration method	19
1.4.2	Newton-Raphson method	21
1.4.3	Riks method	23
1.5	Conclusion	27
2	Previous Works on Nonlinear Analysis of Composite Beams and Plates	28
2.1	Introduction	28
2.2	Composite Beams Analysis	30
2.2.1	Analytical analysis: brief historical review	30
2.2.2	Nonlinear finite element beams analysis	34
2.2.3	Nonlinear dynamics of beams	42
2.3	Composite Plates Analysis	45
2.4	Conclusion	48
II	Nonlinear Beams Analysis	49
3	Experimental Study	50
3.1	Introduction	50
3.2	Material Manufacture and Specimen Preparation	51
3.2.1	Material characterization	53
3.3	Experimental Set-Up	60
3.4	Experiments Results	63
3.5	Conclusion	67
4	Analytical Model for Composite Beams	68
4.1	Introduction	68
4.2	Theoretical Approach	69
4.2.1	Constitutive equations	71
4.2.2	Resultant efforts	74
4.2.3	Neutral axis position change	75
4.2.4	Cantilever beam with tip concentrated load	76

4.3	Simpson's Rule	79
4.4	Validation of the Analytical Formulation	81
4.4.1	Isotropic cantilever beam subjected to tip concentrated load	81
4.4.2	Composite cantilever beams subjected to tip concentrated load	83
4.4.3	Comparison with the current experimental large displacements of (PG) and (RSF) beams.	86
4.5	Factors affecting large displacements variation	88
4.5.1	Effect of fiber orientation	88
4.5.2	Effect of degree of anisotropic	90
4.5.3	Effect of slenderness ratio	92
4.6	Conclusion	93
5	Numerical Analysis of Nonlinear Bending of Beams	95
5.1	Introduction	95
5.2	Strain Tensor (Measures of Deformations)	96
5.3	Finite Element Formulation	100
5.3.1	Displacement field	100
5.3.2	Strain-displacement relationships	101
5.3.3	Stress-strain relationships	101
5.3.4	Displacement interpolation and shape functions	107
5.3.5	Evaluation of stiffness matrix	109
5.4	Resolution Method	111
5.4.1	Load increments	112
5.5	Validation of The Present Finite Element	112
5.5.1	Isotropic cantilever beam subjected to tip concentrated load	112
5.5.2	Composite cantilever beams subjected to tip concentrated load	114
5.6	Parametric Study	116
5.6.1	Effect of fiber orientation angle	116
5.6.2	Effect of slenderness ratio	118
5.7	Conclusion	120

6 Numerical Analysis of Thermo-mechanical Loading Effect on Free Vibration of Laminated Composite Plates **122**

6.1 Introduction 122

6.2 Mathematical Formulation 123

 6.2.1 Displacement field and kinematics 123

 6.2.2 Constitutive equations 125

 6.2.3 Stress resultants 127

6.3 Finite Element Formulation 128

 6.3.1 Displacement interpolation and shape functions 129

 6.3.2 Strain-displacement relationship matrices 130

 6.3.3 Derivation of the elementary matrices 131

 6.3.4 Assumed natural shear strain method 134

 6.3.5 Natural vibration of pre-stressed plates 135

6.4 Effect of Thermal Loading on Free Vibration of Angle-Ply Laminated Composite Plates 137

 6.4.1 Convergence of the first natural frequency 139

 6.4.2 Convergence of the critical temperature 140

 6.4.3 Free vibration of angle-ply laminated composite plates, under thermal loading 140

 6.4.4 Effect of the side-to-thickness ratio on fundamental natural frequency . 144

 6.4.5 Effect of side-to-thickness ratio on the critical temperature 144

6.5 Effect of Mechanical Loading on Free Vibration of Angle-Ply Laminated Composite Plates 145

 6.5.1 Convergence of the first natural frequency 146

 6.5.2 Convergence of buckling critical Load 148

 6.5.3 Free vibration of angle-ply laminated composite plates, under mechanical loading 149

6.6 Conclusion 151

General Conclusion	152
Suggestions for Future Works	156
Bibliography	156

List of Figures

1.1	Linearity in structural systems..	10
1.2	Nonlinearities in solid mechanics..	13
1.3	Typical force displacement curve..	19
1.4	Direct iteration scheme..	20
1.5	The Newton-Raphson scheme..	22
1.6	The Modified Newton-Raphson scheme..	23
1.7	The Riks method, normal plane scheme..	24
1.8	The Riks method, circular arc scheme..	25
2.1	Deflection curves;(a)Bernoulli’s description ,(b)Euler’s investigation..	31
2.2	(a) Continuous and (b) stepwise graded structures.	39
3.1	The initial materials, E-glass fiber, polyester resin.	51
3.2	Laminated plate [0/90/90/0].	52
3.3	Dedicated cutting machine.	52
3.4	Static tensile tests of (PG) and (RSF) specimens.	53
3.5	The final fracture of some specimens.	55
3.6	Tensile stress-strain tests for (PG) specimens.	55
3.7	Tensile stress-strain tests for (RSF) specimens.	56
3.8	Tensile stress-strain tests for [0] specimens.	56
3.9	Tensile stress-strain tests for [90] specimens.	57
3.10	Calcination steps.	58
3.11	Bending experiments for (PG) beams.	61

3.12	Bending experiments for (RSF) beams.	61
3.13	Bending experiments for (GFP) laminated beams.	63
3.14	Experimental tip displacements for (PG) specimens.	64
3.15	Experimental tip displacements for (RSF) specimens.	65
3.16	Experimental tip displacements for (GFP) specimens.	66
4.1	Deformed geometry of a cantilever beam.	70
4.2	A lamina with reference axes (X,Y,Z) and fiber axes (1,2,3).	72
4.3	Neutral axis positions.	75
4.4	Schematic view of a cantilever.	77
4.5	Simpson's 1/3 rule.. . . .	79
4.6	Composite Simpson's 1/3 rule.. . . .	80
4.7	Cantilever beam subjected to tip load.	81
4.8	Non-dimensional deflections as a function of load parameter for isotropic cantilever beam subjected to tip load.	82
4.9	Laminated cantilever beam subjected to tip load.	83
4.10	Load-displacement curves for a $[0/90]_{3s}$ cantilever beam.	84
4.11	Load-displacement curves for a $[20/-70_2/20]_{2a}$ cantilever beam.	85
4.12	Deflection shape of a $[0/90]_{3s}$ cantilever beam for various loads.	85
4.13	Load-displacements curves for a (PG) cantilever beam.	87
4.14	Load-displacements curves for a (RSF) cantilever beam.	88
4.15	Effect of fiber orientation angle on non-dimensional deflections for a symmetric angle-ply (GFP) beam under tip load.	89
4.16	Effect of fiber orientation angle on non-dimensional deflections for antisymmetric angle-ply (GFP) beam under tip load.	89
4.17	Effect of modulus ratio on non-dimensional deflections for a symmetric angle-ply beam with various fiber orientation angles under tip load.	91
4.18	Effect of modulus ratio on non-dimensional deflections for antisymmetric angle-ply beam with various fiber orientation angles under tip load.	91

4.19	Effect of slenderness ratio on non-dimensional deflections for a symmetric angle-ply (GFP) beam under tip load with various orthotropy ratio values.	92
4.20	Effect of slenderness ratio on non-dimensional deflections for antisymmetric angle-ply (GFP) beam under tip load with various orthotropy ratio values.	93
5.1	Transformation of a point and a vector.	96
5.2	Transformation of a vector.	98
5.3	Transformation of a vectors.	98
5.4	A lamina with reference axes (x,y,z) and fiber axes (1,2,3).	103
5.5	Neutral axis position.	106
5.6	Cantilever beam under tip load.	113
5.7	Load-deflections curves for cantilever beam with tip load.	114
5.8	Laminated cantilever beam under tip load.	114
5.9	Load-deflections curves for $[0/90]_{3s}$ cantilever beam.	115
5.10	Simply supported laminated beam under concentrated load.	116
5.11	Cantilever laminated beam under tip load.	117
5.12	Effect of fiber orientation angle on non-dimensional deflections for a symmetric angle-ply (GFP) simply supported beam under concentrated load.	117
5.13	Effect of fiber orientation angle on non-dimensional deflections for anitsymmetric angle-ply (GFP) beam under tip load.	118
5.14	Effect of slenderness ratio on non-dimensional deflections for a symmetric angle-ply (GFP) beam under tip load with various anisotropy ratio values.	119
5.15	Effect of slenderness ratio on non-dimensional deflections for antisymmetric angle-ply (GFP) simply supported beam under concentrated load with various anisotropy ratio values.	119
6.1	Geometry and nodal variables of the element.	129
6.2	Sampling point $\bar{\gamma}_{xz}^A$ and $\bar{\gamma}_{yz}^A$	136
6.3	Geometry and boundary conditions.	139

6.4	Natural frequency ϖ^2 vs temperature $\bar{\lambda}$ of 10-layer angle-ply square laminated composite plates ($L/h = 5$)	142
6.5	Natural frequency ϖ^2 vs temperature $\bar{\lambda}$ of 10-layer angle-ply square laminated composite plates ($L/h = 10$)	143
6.6	Natural frequency ϖ^2 vs temperature $\bar{\lambda}$ of 10-layer angle-ply square laminated composite plates ($L/h = 100$)	143
6.7	Geometry and boundary conditions.	146
6.8	Natural frequency ϖ^2 vs in plane compression load N/N_{cr} of anti-symmetric 2 layers square laminated plate ($L/h = 10$).	149
6.9	Natural frequency ϖ^2 vs in plane compression load N/N_{cr} of anti-symmetric 4 layers square laminated plate ($L/h = 10$).	150
6.10	Natural frequency ϖ^2 vs in plane compression load N/N_{cr} of anti-symmetric 2 layers square laminated plate ($L/h = 100$).	150
6.11	Natural frequency ϖ^2 vs in plane compression load N/N_{cr} of anti-symmetric 4 layers square laminated plate ($L/h = 100$).	151

List of Tables

3.1	Mechanical properties of materials.	54
3.2	Mechanical properties of (GFP) laminate.	59
4.1	Non-dimensional deflections as a function of load parameter for isotropic cantilever beam subjected to tip load.	82
4.2	Analytical horizontal and vertical displacements of symmetric laminated $[0/90]_{3s}$ cantilever beam end.	84
4.3	Comparison Analytical horizontal and vertical displacements of antisymmetric laminated $[20/-70_2/20]_{2a}$ cantilever beam end.	84
4.4	Horizontal and vertical displacements of (PG) cantilever beam end.	86
4.5	Horizontal and vertical displacements of (RSF) cantilever beam end.	87
5.1	Non-dimensional deflections as a function of load parameter for isotropic cantilever beam subjected to tip load.	113
5.2	Horizontal and vertical displacements of symmetric laminated $[0/90]_{3s}$ cantilever beam	115
6.1	Convergence of non-dimensional natural frequency $\varpi \times 10$ for $\bar{\lambda}$ of 10-layer cross-ply $[0/90/\dots]_{10}$ square laminated composite plate with $(L/h = 5)$	139
6.2	Convergence of non-dimensional critical temperatures $\bar{\lambda}_{cr}$ of 3-layer cross-ply $[0/90/0]$ square laminated composite plates for different L/h ratios	140
6.3	Effect of the non-dimensional temperature $\bar{\lambda}$ on non-dimensional natural frequency $(\varpi^2)L/h = 100$	141

6.4	Effect of the non-dimensional temperature $\bar{\lambda}$ on non-dimensional natural frequency $(\varpi^2)L/h = 10$	141
6.5	Effect of the non-dimensional temperature $\bar{\lambda}$ on non-dimensional natural frequency $(\varpi^2)L/h = 5$	141
6.6	Non-dimensional frequency $\bar{\omega}$ for ($\bar{\lambda} = 0$) of 10-layer angle-ply square laminated composite plates.	144
6.7	Non-dimensional critical temperatures $\bar{\lambda}_{cr}$ of 10-layer angle-ply $[\theta/ - \theta/\dots]_{10}$ square laminated composite plates ($\theta = 0^\circ, 15^\circ$).	144
6.8	Non-dimensional critical temperatures $\bar{\lambda}_{cr}$ of 10-layer angle-ply $[\theta/ - \theta/\dots]_{10}$ square laminated composite plates ($\theta = 30^\circ, 45^\circ$).	145
6.9	Convergence of non-dimensional natural frequency of 4-layered angle-ply square laminated composite plate with different (L/h) values.	147
6.10	Convergence of non-dimensional natural frequency of 2-layered angle-ply square laminated composite plate with different (L/h) values.	147
6.11	Convergence of non-dimensional buckling critical load of 2-layered angle-ply square laminated composite plate with different fiber orientation angle and different (L/h) ratios.	148
6.12	Convergence of non-dimensional buckling critical load of 4-layered angle-ply square laminated composite plate with different fiber orientation angle and different (L/h) ratios.	148

List of Symbols and Abbreviations

Symbols

A_{ij}, B_{ij}, D_{ij} and H_{ij}	Elasticity matrices of the laminate
A, B, D	Elasticity scalars of the laminate
E_1^k, E_2^k	Young modulus of the material in the 1 and 2 directions of the kth layer
G_{12}^k, G_{23}^k and G_{13}^k	Shear modulus in the 1–2, 2–3 and 1–3 planes of the kth layer
$\{K\}$	Curvature vector
K_s	Beam Curvature
$[K_e]$	The elementary stiffness matrix
$[K_g^e]$	The elementary geometrical matrix
$[m]$	The inertia matrix
$[M]$	The mass matrix
M_x, M_y and M_{xy}	Moment resultants
N_x, N_y and N_{xy}	Normal stress resultants
$N_\alpha(x, y)$	The bilinear Lagrange shape functions associated with node α
$P_i(y)$ and $Q_i(x)$	Interpolation functions
$\{\delta\}$	Elementary displacement vector

Q_{ij}^{k0}	The reduced stiffness components in local coordinates system of the kth layer
Q_{xz}, Q_{yz}	Transverse shear stress resultants
\bar{Q}_{11}^k	The reduced stiffness components in laminate coordinates system of the kth layer
\bar{Q}_{eq}^k	The equivalent stiffness coefficient
$[T]$	Transformation matrix
T	The kinetic energy
u, v	In-plane displacement vector components
u_0, v_0	In-plane displacement vector components at the mid-plane of the laminate ($z = 0$)
U	The strain potential energy
w	Out-of-plane displacement vector component
W	The external forces work
x, y and z	Coordinates of point within the plate or the beam
α_1^k, α_2^k	Coefficients of thermal expansion of the kth layer in local coordinates system
α_x^k, α_y^k and α_{xy}^k	Coefficients of thermal expansion of the kth layer in laminate coordinates system
γ_{12}^k	In-plane shear strain of the kth layer in local coordinates system
$\gamma_{13}^k, \gamma_{23}^k$	Transverse shear strain of the kth layer in local coordinates system
$\{\gamma_s\}$	Transverse shear strain vector
$\bar{\gamma}_{xz}^A, \bar{\gamma}_{yz}^A$	The sampling points
δ^α	Displacement vector component associated with node α

$\delta(x, y)$	The displacement vector component of a given point $M(x, y)$ within an element
ΔT	The temperature rise
ΔT_{cr}	Critical temperature rise
$\{E\}$	Strain vector
$\{\varepsilon^0\}$	Membrane strain vector
E_{11}^k, E_{22}^k	Membrane strain of the kth layer in local coordinates system
E_{xx}^k, E_{yy}^k	Membrane strain of the kth layer in laminate coordinates system
θ	Fibers orientation angle with respect to laminate coordinates system
λ	Loading factor
λ_{cr}	Critical loading factor
ν_{12}^k, ν_{21}^k	Poisson's ratios
Π	The total potential energy
$\sigma_{11}^k, \sigma_{22}^k$	Normal stresses of the kth layer in local coordinates system
$\sigma_{xx}^k, \sigma_{yy}^k$	Normal stresses of the kth layer in laminate coordinates system
τ_{13}^k, τ_{23}^k	Transverse shear stresses of the kth layer in local coordinates system
τ_{xy}^k	In-plane shear stress of the kth layer in local coordinates system
τ_{xz}^k, τ_{yz}^k	Transverse shear stresses of the kth layer in laminate coordinates system

φ_x	Rotation angle of the plate with respect to the y-axis
φ_y	Rotation angle of the plate with respect to the x-axis
Ψ	Rotation angle of the beam
Ψ^m	Rotation angle of the free end of the beam
ω	The natural frequency

Abbreviations

(PG)	PlexiGlass
(RSF)	Composite of Random Short Fiber with unsaturated polyester resin
(GFP)	Laminate of E-Glass Fiber with Polyester resin
MPI	Maghred Pipe Industries
GEBT	Geometrically Exact Beam Theory
FSDT	First order Shear Deformation Theory
HSAPT	High order Sandwich Panel Theory
CUF	Carrera Unified Formulation
FGM	Functionally Graded Materials
FEM	Finite Element Method
DQM	Differential Quadrature Method

General Introduction

Material is the basic element of all natural and man-made structures. Figuratively speaking it materializes the structural conception. Technological progress is associated with continuous improvement of existing material properties as well as with expansion of structural material classes and types. Usually, new materials emerge due to necessity to improve the structure efficiency and performance, but as a rule, new materials themselves in turn provide new opportunities to develop updated structures and technology, while the latter presents material science with new problems and tasks. One of the best manifestations of this interrelated process in development of materials, structures, and technology is associated with composite materials.

Because of their high strength-to-weight ratio, long fatigue life, resistance to corrosion, high damping, structural simplicity, and possible use for aeroelastic tailoring, advanced laminated structures made of fiber-reinforced composite materials, such as boron-epoxy, graphite-epoxy, and boron-aluminum, etc. . . , have emerged as primary materials for advanced aerospace vehicle structures, automotive parts, civil engineering. They show great promise for improved performance. Moreover, the inherent anisotropy is an important property of composite materials and one of the basic reasons for their success.

Engineers and scientists from applied sciences are involved in one or more of the following activities:

- Studying engineering systems or their components.
- Developing mathematical models of physical systems.
- Carry out numerical simulations of the mathematical models.

- Conduct experiments to determine and understand characteristics of the system.
- Design the components of a system.
- Manufacture the components and integrate them to build a system.

Manufacturing a system or its components can take place only after the components are designed to meet the functionality and other requirements. On the other hand, design is an iterative process of selecting materials and configurations to meet the design requirements and cost-effectiveness. During each stage of the design, analysis is carried out for the selected configuration (i.e. geometry, materials and loads). Analysis is deterministic and involves analytically determining the response of the system or its components with the help of a mathematical model and a numerical method. A mathematical model of a system or its components is a collection of relationships - algebraic, differential, and/or integral - among the quantities that describe the response.

The minimum weight criteria with high performance is essential in the design of aircraft, aerospace vehicles and civil structures until today. This task will be a challenge, especially when the design of wing structures such as aircraft wings, rotor blades, robotic arms or some kind of bridges, is the subject. The behavior of such structures is highly nonlinear due to the deformation of their geometry and the solution of such problems becomes very complex, especially with the use of composite materials. The effects of large displacements may play a primary role in the correct prediction of the behavior of these members, which continue to be modeled as flexible beams. In this way, another difficult task can be imposed here when some structural elements as plates and shells can undergo inplane thermo-mechanical stresses that affect their stiffness (eg: high speed aircrafts, rockets and launch vehicles, trainees) and consequently, their dynamic and static behavior. This problem has stimulated the researchers to provide an accurate prediction of free vibration of laminated plates, subjected to inplane thermal or mechanical stresses.

The search for ways to represent the true nonlinearity of structures goes back to Renaissance times, and presents theories of nonlinear elastic and inelastic behavior are the result of approximately more than two hundred years of steady development. But recently the computer has made it possible to put much of this knowledge in use in the design . In recent years, nonlinear mechanics has gained an important position in our modern technology, and its need and importance to our future technology is growing at a much faster rate. In order to understand material and structural behavior and determine the nonlinear response and of structures, we must develop new methodologies and mathematical modeling that adequately represent such types of problems [1, 2, 3, 4]. The nonlinearities considered in this thesis are geometric nonlinearities arising from the large displacements and moderate rotations considering small strain case of composite beams. In addition, geometric nonlinearities arising when a part of structure as plates, may lose their stiffness under inplane thermal or mechanical loading, which affect their dynamic and static behavior.

Thesis objectives

The main objective of the present work is to contribute in nonlinear behavior analysis of beams and plates. This investigation will be carried out analytically, experimentally and numerically. This work is divided in two parts. The first part is destined for beams analysis, which an analytical model is firstly developed to analyze the large deflection of laminated cantilever beams. Secondly, an experimental program is prepared in order to carried out several bending experiments on isotropic and composite cantilever beams. In addition, a finite element beam based on the Euler-Bernoulli beam theory, will be formulated for beams large deflection analysis. In the second part, the effect of thermo-mechanical loading on free vibration of laminated composite plates is investigated.

The general lay-out of the thesis is as follows:

- **Chapter 1** presents basic concepts of nonlinear phenomena. Different types of nonlinearities in solid mechanics are introduced, including geometric, material, kinematic, and force nonlinearities. The importance of nonlinear analysis in structural mechanics is also addressed. In addition, general solving procedures of nonlinear equations system have been presented.
- In **Chapter 2**, brief historical review on analytical analysis of large deflection isotropic beams is given. A few available papers on analytical analysis of large deflection composite beams are also presented. Previous works on geometrically nonlinear analysis of isotropic, anisotropic, sandwich and functionally graded beams using finite element method have been reviewed. In addition, the nonlinear dynamic response analysis of isotropic and composite beams are presented. Free vibration analysis of composite plates under inplane thermo-mechanical loading have been finelly reviewed.
- In **Chapter 3**, several bending experiments are carried out on isotropic and composite cantilever beams to verify the analytical as well as the finite element formulations in chapters 4 and 5, respectively. Three different types of materials are considered for these experiments, where the manufacturing of materials and the preparation of specimens are firstly addressed. The characterization of used materials is also presented and described by the measurement of their properties through a series of static tensile tests. Furthermore, a calcination has been carried out to define more properties that could not be measured by tensile tests. The experiments setup are described in detail and their results are presented and commented.

- An analytical formulation has been carried out in **Chapter 4**, to analyze the large deflection of composite beams. The proposed formulation is based on the elastica beam model, according to the classical Euler-Bernoulli beam theory. The present formulation is prepared to be able to deal with symmetric and non-symmetric laminated beams. Simpson method has been used to solve the nonlinear equations. Subsequently, for the purpose of validation, the obtained results have been compared with both analytical models and experimental studies existing in the literature. Furthermore, for the sake of comparison, the obtained results of the present formulation have been also compared with those obtained from the performed experiments in chapter 3. In addition, the varying parameters, such as fiber orientation angle, anisotropic ratio E_1/E_2 and slenderness ratio are examined in order to discover and understand their effect on the deflections variation of laminated beams.
- In **Chapter 5**, one-dimensional finite element formulation, based on the Euler-Bernoulli beam theory has been developed for the nonlinear bending analysis of symmetric and non-symmetric laminated beams. The present element has been defined by two nodes and three degree of freedom per node. The principle of total potential energy has been used for the derivation of stiffness and geometrical matrices. The direct iterative method has been used to solve the nonlinear equations. Subsequently, for the purpose of validation the present element has been compared with the available analytical models, experimental studies from the literature as well as the present analytical model presented in chapter 4. In addition, a parametric study is presented in order to examine the effect of some parameters such as fiber orientation angle and slenderness ratio on the deflection variation of laminated beams with different boundary conditions.
- Free vibration of laminated composite plates under thermal and mechanical loading effect have been analyzed in **Chapter 6**, using a four-nodded rectangular finite element based on first order shear deformation theory with assumed natural shear strain. Total potential energy and Hamilton' principles have been used to derivate stiffness, geometric

and mass matrices. The convergence of the natural frequency for unloaded plates case and the critical temperature as well as the buckling critical load has been checked. The effects of thickness to side ratio, anisotropy degree of single layer and fibers orientation angle, on free vibration and critical temperature and critical buckling load have been also analyzed.

- Finally, the **General Conclusion** contains summary and conclusions of the present research. It also presents contributions and suggestions for the future work.

Part I

Literature Review

Chapter1

Basic Concepts of Nonlinear Phenomena

1.1 Introduction

"No problem in nonlinear engineering is simple no matter how small or how unimportant it may appear to be. Its the nonlinear behavior is the one that makes this problem complex and you need to have a complete understanding of this nonlinear behavior in order to provide a reasonable solution."

Modern technological advances challenge engineers to carry out increasingly complex and costly projects, which are subject to severe reliability and safety constraints. These projects cover domains such as space travel, aeronautics and high constructions, where reliability and safety are of crucial importance. One of the main responsibilities in such domains is the design of structural components task. The practicing design engineer, who deals with the design of structural components in general, is often confronted with a challenging problems that could appear with the introduction of any new technology, especially the design of lighter components with high performance because it is important to say that one of the main interests in the design phase of these projects is the minimum weight criteria.

In this light, for a proper understanding, analysts need mathematical models that allow them to simulate the behavior of complex physical systems. These models are then used during the design phase of the projects. Nonlinear analysis is a broad, interdisciplinary field characterized by a mixture of analysis, topology, and applications. Its concepts and techniques provide the tools for developing more realistic and accurate models for a variety of phenomena encountered in fields ranging from engineering [4].

The future of engineering is becoming increasingly nonlinear, and both the engineering student and the practicing engineer should be prepared for it. The material (informations) included in this chapter is carefully selected in order to provide a good start in understanding and comprehending important aspects of nonlinear analysis, so that the engineering student can start preparing himself for the very challenging nonlinear problems of the present and the future.

In order to understand nonlinearity in solid mechanics, it is important to define and understand linearity first. A linear system is defined such that the relationship between input and output is linear. Specifically, in structural mechanics, the relationship between applied loads (input) and displacements (output) is linear. When an applied load is doubled, the displacement will also be doubled. So, response is directly proportional to load. Mathematically, linearity can be explained using a linear operator [5]. Linearity may be a good representation of the reality or may only be the inevitable result of assumptions made for analysis purposes. In the following, the fundamental assumptions of linear analysis of structures.

- The structures are composed of linearly elastic material; that is, the stress-strain relationship for the structural material follows Hooke's law, which stress is directly proportional to strain.
- The deformations of the structures are so small that the squares and higher powers of member slopes, rotations, and axial strains are negligible in comparison with unity, and the equations of equilibrium can be based on the undeformed geometry of the structure.

The reason for making these assumptions is to obtain linear relationships between applied loads and the resulting structural deformations. An important advantage of linear force-deformation relations is that the principle of superposition can be used in the analysis. This principle states essentially that the combined effect of several loads acting simultaneously on a structure equals the algebraic sum of the effects of each load acting individually on the structure.

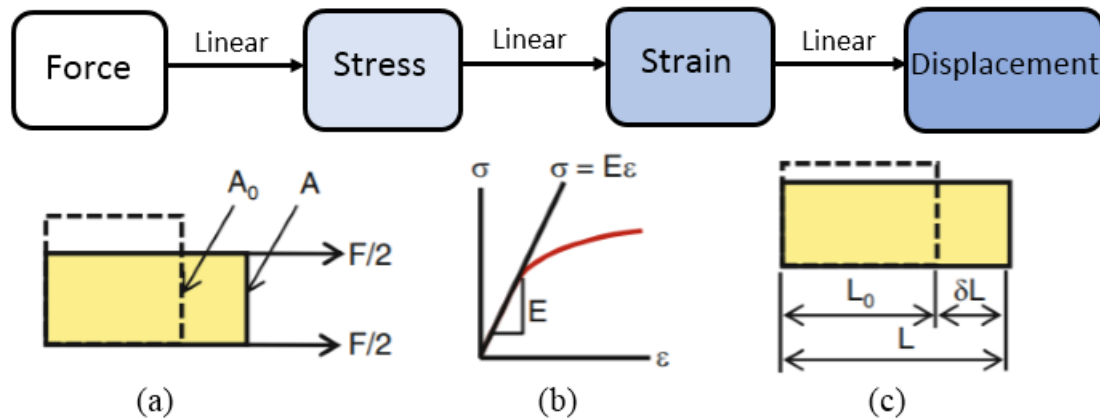


Figure 1.1: Linearity in structural systems [5].

We are fortunate that so many practical problems can be solved by so simple an approximation. However, any of the convenient assumptions that lead to a linear analysis may be at odds with reality and many physical situations present nonlinearities too large to be ignored, such as:

- Adjacent parts may make or break contact.
- A contact area may changes as load changes.
- Elastic material may become plastic, or the material may not have a linear stress-strain relations at any stress level.
- *Part of the structure may lose stiffness because of the buckling or the failure of the material.*
- *Displacement and rotations may become large enough that equilibrium equations must be written for the deformed configuration rather than the original configuration.*

- Large rotations cause pressure loads to change in direction, and also to change in magnitude if there is the change in a area to which they are applied [6].

We do not have to abandon the treatment of many physical problems from the linear point of view. It certainly depends upon the problem and to what extent the results are going to be used. If one is looking for accurate results or some phenomena that will be missed by the linear analysis, then a nonlinear analysis is required.

Linearized formulations are insufficient to explain many phenomena, for example, the minimum weight criteria in the design of aircraft, aerospace vehicles, coupled with the evergrowing use of light polymeric materials that can undergo large displacement without exceeding their specific elastic limits, prompted a renewed interest in the nonlinear analysis of structures subjected to various static and dynamic loading conditions. Due to the geometry of deformation, the behavior of such structures is highly nonlinear and the solution of such problems must be obtained using the nonlinear theories. It must be noted, however, that nonlinear analysis procedures are more complex and therefore more computing time consuming. Significant advances have been made in the last decade or so, thanks to the availability of high speed computers, in developing various analytic and numerical techniques to solve different type of nonlinear problems in structural mechanics [7].

In nonlinear analysis the aim is to trace the history of all material points in structure as it undergoes progressive loading. We have argued that, generally, the only practical way to do this is by a series of linear analyses [8]. Nonlinearity makes a problem more complicated because equations that describe the solution must incorporate conditions not fully known until the solution is known, the actual configuration, loading conditions, state of stress, and support conditions. The solution cannot be obtained in a single step of analysis. We must take several steps, update the tentative solution after each step, and repeat until a convergence test is satisfied. The usual linear analysis is only the first step in this sequence. Nonlinear analysis can treat a great variety of problems. But in a sense it is more restrictive than linear analysis because the principle of superposition does not apply, we cannot scale results in proportion to load or combine results from different load cases as in linear analysis. Accordingly, each different

load case requires a separate analysis. Also, if a loading consists of component loads that are sequentially applied, results may not be independent of the order in which loads are applied [6].

In nonlinear analysis an attempt is made to improve the analytical simulation of the behavior of the structures in some respect. The fundamental aim to improve the quality of design by providing the engineer with a more reliable prediction of the performance of the system that is under design or investigation. In making this closer link between structural analysis and actual behavior, the traditional distinction between the terms "analysis" the determination of forces and displacements under given loads and "design" the proportioning of members and connections to resist the determined effects-becomes blurred [8].

In using nonlinear analysis the uncertainty regarding actual behavior may be reduced. In the process, However, the element of art in modeling the structure and in handling the equations of analysis is increased. In modeling the analyst must decide what source of nonlinearity are apt to be significant and how to represent them. In dealing with the resulting nonlinear equations, decisions must be made regarding how to reduce them to a system suitable for practical computation and, then, the method for solving the reduced system [8]. Thus we see that nonlinear effects may vary in type and may be mild or severe. An analyst must understand the physical problem and must be acquainted with various solution strategies. A single strategy will not always work well, and may not work at all for some problems. Several attempts may be needed in order to obtain a satisfactory results [9].

1.2 Sources of Nonlinearity

In general, there are many different ways of categorizing different nonlinearities. However, it is generally accepted that four different sources of nonlinearity can exist in solid mechanics. The occurrence of these nonlinearities in their relation among applied loads, stresses, strains, displacements, and boundary conditions Figure 1.2, [5].

In linear elastic analysis the material is assumed to be unyielding and its properties invariable, and the equations of equilibrium are formulated on the geometry of undeformed structure or, in the case of self-strained structures, on an initial reference configuration. Subsequent deformations are assumed to be so small as to be insignificant in their effect on the equilibrium and the mode of system response.

Nonlinear analysis offers several options for addressing problems resulting from the above assumptions. We may consider only the geometric nonlinearity. That is, we may continue to treat the structural material as elastic but include the effects of deformations and finite displacements in formulating the equations of equilibrium. It is also possible to consider only the material nonlinearity, that is, the effect of changes member material properties under load. And, as third general option, we may include effects of both geometric and material nonlinearity in the analysis. In each case, the possibility of coupling of internal actions must be considered, it may be a dominant feature of the analysis [8].

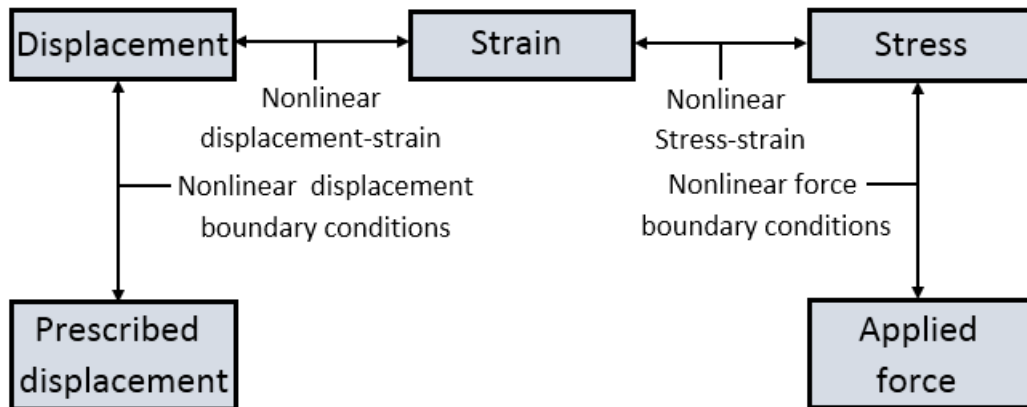


Figure 1.2: Nonlinearities in solid mechanics [5].

1.2.1 Geometric nonlinearities

In dealing with the nonlinear behavior of deformable bodies, such as beams, plates, shells, the relationship between strains and displacements is nonlinear. This type of nonlinearity is the most commonly treated in literature. As a direct consequence of the nonlinear strain-displacement relations, the governing differential equations will turn out to be nonlinear.

This is true in spite of the fact that the relationship between curvatures and displacement components are assumed to be linear. Another way of looking in this, consider the total strain energy of the deformable elastic body, which is in the form of the extensional and the bending energy. The extensional strain energy involves higher order nonlinear terms than quadratic in the normal displacement component, whereas the bending strain energy remains quadratic in the displacement components [7].

By other words, When the deformation of a solid reaches a state for which the undeformed and deformed shapes are substantially different a state of finite deformation occurs. In this case it is no longer possible to write linear strain–displacement or equilibrium equations on the undeformed geometry [10]. Thus, *geometric nonlinearities* are associated with the effect of a change in geometry due to load application on the overall structural response. In general, *geometric nonlinearities* represent the cases when the relations among kinematics quantities (displacements-strains) are nonlinear, which Such nonlinearities occur when displacements are large.

1.2.2 Material nonlinearities

The introduction of new materials and their application at severe thermal and mechanical environments to highly deformable structural elements have generated an interest in nonlinear analysis techniques. These techniques together with the availability of high-speed computers have made the solutions of materially nonlinear problems a reality [7]. Material or physical nonlinearity represents the case when the relation between stress and strain is not linear. The simplest form of non-linear material behaviour is that of elasticity for which the stress is not linearly proportional to the strain. More general situations are those in which the loading and unloading response of the material is different. Typical here is the case of classical elastic–plastic behaviour [10]. Thus, the generalized Hooke’s law is not valid any more in treatment of the nonlinear stress-strain behavior of the material of the deformable body. The effect of material nonlinearity on the behavior of structures components is an important consideration in the analysis of structural systems.

1.2.3 Kinematic nonlinearity

Kinematic nonlinearity is also called boundary nonlinearity, as the displacement boundary conditions depend on the deformations of the structure. In general, structural equations solve for unknown displacements in the domain with given applied loads and prescribed displacement boundary conditions. When the boundary conditions change as a function of displacements, both the displacements and boundary conditions are unknown. In such a case, it is difficult to solve the structural equations as both sides have unknown terms. In general, there are two possible cases for kinematic nonlinearity. The first one is when the location on the boundary where boundary conditions are applied is known, but the values are unknown. The second case is that both the location on the boundary where boundary conditions are applied and the values on the boundary conditions are unknown. The most common example is the contact constraint between two bodies. As two bodies are in contact, the displacements on the contact boundary are limited such that they cannot penetrate each other. At the same time, it is usually unknown which part of the boundary will be in contact. This kind of problem is more difficult than the first one [5].

1.2.4 Force nonlinearity

Similar to kinematic nonlinearity, force nonlinearity occurs when the applied force depend on deformation. Since force is a vector, its magnitude and/or direction can change according to the deformation of the structure. Force nonlinearity is often accompanied by geometric nonlinearity. The most common example in solid mechanics is pressure loads of fluids. In the deployment of an airbag, for example, the direction and magnitude of pressure loads vary according to the deployment shape of the airbag. Although the contact condition is considered as boundary nonlinearity, the contact force can also be considered as force nonlinearity. As contact boundary varies, the contact force on boundary also varies. Thus, in the contact problem, both the contact boundary and contact forces are unknown [5].

1.3 Importance of Nonlinear Analysis

The advent of powerful computers in recent years has paved the way for the development and implementation of several nonlinear analysis methods, which vary in terms of applicability, efficiency, and accuracy. The main motivation behind such developments has been the urgent need for such tools in the field of structural design as well as in experimental and theoretical research.

The use of nonlinear analysis in the design of structures has not so far been utilized to its full potential. Despite its considerable demand on computing resources, accurate nonlinear analysis allows a better assessment of structural safety and reliability than can be achieved by other simplified methods. This realization represents a major drive behind the efforts to improve the efficiency of nonlinear analysis methods, and will combine with the rapid advancements in the field of computing to lead to the inevitable inclusion of nonlinear analysis as part of the design process.

A more immediate application of nonlinear analysis is in experimental and theoretical research work, where the main concern is to establish accurate rather than efficient solutions. On the experimental side, nonlinear analysis can be employed in the design of test setups, as well as in the choice of test specimens and loading configurations. On the theoretical side, nonlinear analysis can be instrumental in achieving better understanding of complex structural behaviour, and provides an abundance of information for parametric studies on realistic engineering problems.

Another factor that calls for the necessity of nonlinear analysis can be attributed to the development of high-strength materials in areas such as aerospace engineering, mechanical engineering, and high-rise building construction, where the weight of the structure design is of major concern. Application of such materials in these areas, though enabling structural engineers to achieve a lighter design, will normally introduce certain degrees of nonlinearity in the structural response. It is the responsibility of structural engineers to ensure that all the operational functions of the design structure are not impaired by such nonlinear effects under the

working or extreme loading conditions. Obviously, the role of nonlinear analysis has become much more important than ever due to the increasing use of light, high-strength materials in industry. It should be noted that, in addition to the stringent design requirements, the advancement in solution methods, the expansion in computer memory, and, most directly, the drastic decline in computing costs are other factors that make room for nonlinear analysis.

1.4 Solution of Nonlinear Systems

Many phenomena in physics shows nonlinear behaviors, and linear systems are approximation of nonlinear systems under limited conditions. For example, the relation between the deflection of a beam and applied load at its tip is linear when the deflection is small. This includes small strain, small displacement, and small rotation in solid mechanics. However, as the deflection becomes large, the relation becomes nonlinear. In this sense, a linear system is an approximation of a nonlinear one [5].

In addition, solving linear system has several advantages compared to solving nonlinear ones. First, linear systems are easier to solve. All the linear systems can be solved using the system of linear equations. On the other hand, nonlinear systems, cannot be solved in such simple form. In fact, nonlinear systems are often solved using a sequence of linear equations. Thus, the computational cost of a linear analysis usually much less than that nonlinear analysis. Second, once the problem is well posed, the solution of linear system always exists and it is unique. However, there is no guarantee that nonlinear system has a unique solution [5].

Nonlinearities appear in the formulation of physical problems for two reasons :

- The physical parameters that are supposedly independent of displacements in linear model, such as Young's modulus, The coefficients of conductivity, etc, may become functions of displacements.
- Terms that are nonlinear in relation to the unknowns of the problem appear in the partial differential equation, even when the physical properties are independent of displacements.

There are many numerical procedures used to solve nonlinear problems, which are iterative in nature. Here three iterative procedures are presented in the following.

If we suppose that we wish to solve the nonlinear matrix equation

$$\left[A\left(\left\{U\right\}\right)\right] \left\{U\right\} = \left\{F\right\} \quad (1.1)$$

Assuming that the solution $\left\{U\right\}^{(r-1)}$ at the $(r-1)$ st iteration is known, and we researching the solution $\left\{U\right\}^{(r)}$ at the r th iteration. So $\left\{U\right\}^{(r)}$ is the solution to be determined. At the beginning of the iteration, that is, when $r=1$, the solution $\left\{U\right\}^{(0)}$ is guessed consistent with the problem data. Using the solution from the $(r-1)$ st, we compute the coefficient matrix $\left[A\left(\left\{U\right\}^{(r-1)}\right)\right]$. Since $\left[A\right]$ is evaluated using estimated vector $\left\{U\right\}$, in general

$$\left[A\left(\left\{U\right\}^{(r-1)}\right)\right] \left\{U\right\}^{(r)} \neq \left\{F\right\} \quad (1.2)$$

Hence, we are left with a residual

$$\left\{R\right\} \equiv \left[A\left(\left\{U\right\}^{(r-1)}\right)\right] \left\{U\right\}^{(r)} - \left\{F\right\} \quad (1.3)$$

A plot of the equilibrium path, $\left\{R\right\} = 0$, is shown in Figure 1.3 . For any value $\left\{U\right\}^{(r)}$, $\left[A\left(\left\{U\right\}^{(r)}\right)\right]$ denotes the secant of the curve at $\left\{U\right\}^{(r-1)} = \left\{U\right\}^{(r)}$, and $\left(\frac{\partial R}{\partial U^{r-1}}\right)\Big|_{U^r}$ denotes the tangent of the curve at $\left\{U\right\}^{(r-1)} = \left\{U\right\}^{(r)}$. F is the known force.

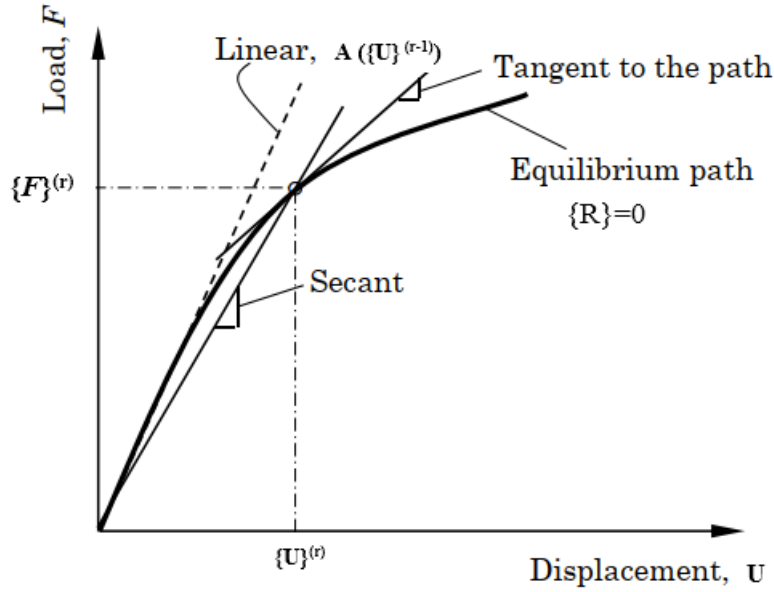


Figure 1.3: Typical force displacement curve [3].

The objective of the iteration process is to reduce this residual to a very small negligible value, ε :

$$\sqrt{\sum_{I=1}^N R_I^2} \leq \varepsilon \quad (1.4)$$

Alternatively, the iteration may proceed until the difference between the solutions from two consecutive iterations, is less than the tolerance ε

$$\sqrt{\frac{\sum_{I=1}^N (U_I^{(r)} - U_I^{(r-1)})^2}{\sum_{I=1}^N (U_I^{(r)})^2}} \leq \varepsilon \quad (1.5)$$

1.4.1 Direct iteration method

The direct iteration technique, also known as the Picard iteration method of successive substitution, is the simplest iterative procedure here. We begin with an initial guess for u , say $u^{(0)}, u^{(0)}=0$ and determine the first approximation of u by solving the equation

$$u^{(1)} = (K(u^{(0)}))^{-1} F \quad (1.6)$$

$u^{(1)} \neq u$, and a second approximation for u is sought by using the last approximation to evaluate K

$$u^{(2)} = (K(u^{(1)}))^{-1} F \quad (1.7)$$

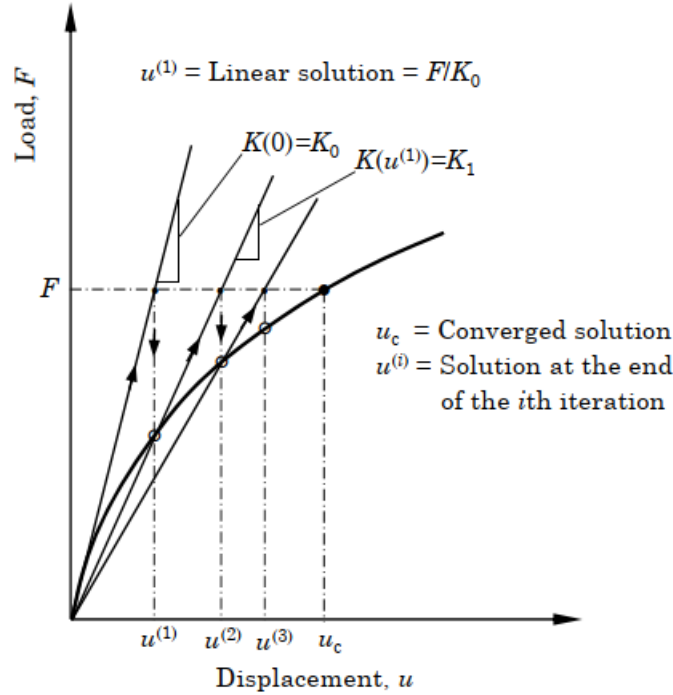


Figure 1.4: Direct iteration scheme [3].

This procedure is continued until the difference between two consecutive approximations of u differ by a preselected value. Thus, the algorithm and criterion for convergence can be written as

Algorithm

$$u^{(r)} = (K(u^{(r-1)}))^{-1} F \quad (1.8)$$

Convergence Criterion

$$\sqrt{\frac{(u^{(r)} - u^{(r-1)})^2}{(u^{(r)})^2}} \leq \varepsilon \quad (1.9)$$

1.4.2 Newton-Raphson method

The most popular technique for solving nonlinear algebraic equations that results from discretization of a structure is the Newton-Raphson method. This iterative technique uses the tangent stiffness at a point on the equilibrium curve to approximate a point further along the curve at particular load or displacement. The unknown load or displacement at this intermediate is back out of the equilibrium equation, a new tangent stiffness is computed, and iteration continues until the load or displacement value is achieved within a specified tolerance. An interesting historical development of the Newton-Raphson method and its origins is given in [11].

Suppose that the solution $u^{(r-1)}$ is known at $(r - 1)$ st iteration and the residual $\{R\}$ is expanded about the known solution $u^{(r-1)}$ in Taylor's series,

$$\{R\} = R(u^{(r-1)}) + \left(\frac{\partial R}{\partial u}\right)\Big|_{u^{(r-1)}} \delta u + \frac{1}{2} \left(\frac{\partial^2 R}{\partial u^2}\right)\Big|_{u^{(r-1)}} (\delta u)^2 + \dots = 0 \quad (1.10)$$

Where δu is the increment,

$$\delta u^{(r)} = u^{(r)} - u^{(r-1)} \quad (1.11)$$

Omitting the terms of order 2 and higher

$$\left(\frac{\partial R}{\partial u}\right)\Big|_{u^{(r-1)}} \delta u = -R(u^{(r-1)}) \quad (1.12)$$

$$\left(K_T(u)^{(r-1)}\right)\Big|_{u^{(r-1)}} \delta u = -R(u^{(r-1)}) \quad (1.13)$$

Where K_T is the slope (tangent) of the curve $\{R\}$ at $u^{(r-1)}$

$$K_T(u)^{(r-1)} = \frac{\partial R}{\partial u}\Big|_{u^{(r-1)}} \quad (1.14)$$

The residual or imbalanced force, $R(u^{r-1})$ is gradually reduced to zero if the procedure converges. The solution at r th iteration is given by

$$u^{(r)} = u^{(r-1)} + \delta u^{(r)} \quad (1.15)$$

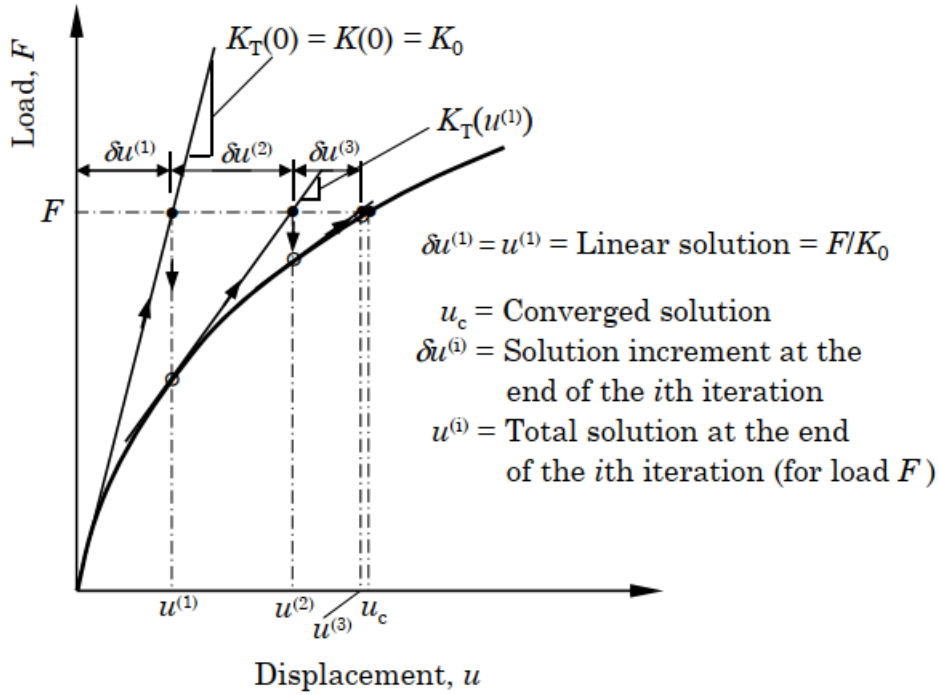


Figure 1.5: The Newton-Raphson scheme [3].

A variation is the modified Newton-Raphson technique in which the tangent stiffness matrix is kept constant and not updated for iterations within an increment. The approach often takes more iterations to obtain convergence.

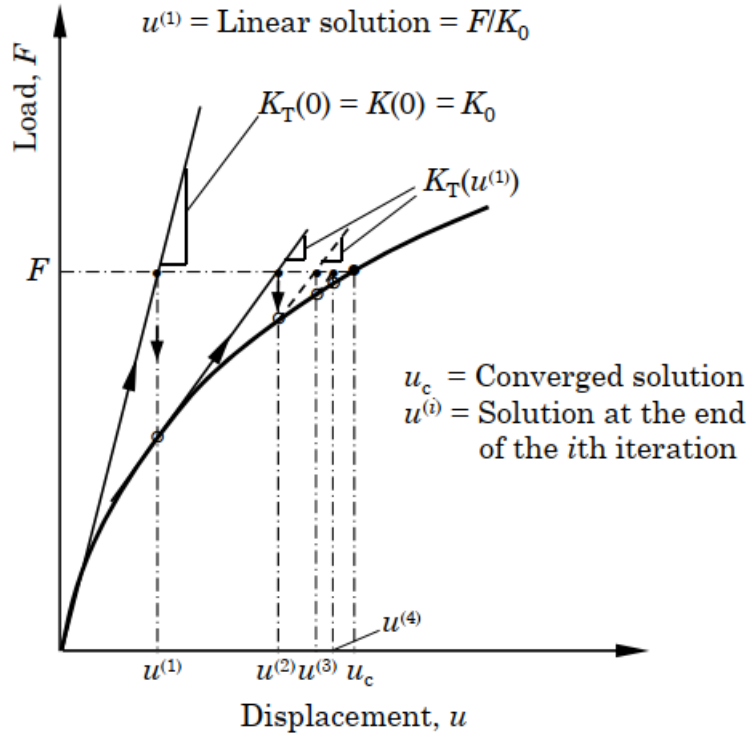


Figure 1.6: The Modified Newton-Raphson scheme [3].

1.4.3 Riks method

Difficulties arise because Newton-Raphson method fails to trace the nonlinear equilibrium path at limit points where the tangent stiffness matrix becomes singular and the iteration procedure diverges. Near horizontal limit points, displacement control traverses the singularities since a unique load exists for each displacement. Likewise, near vertical limit points load control passes limit points because unique displacement for each load. Riks [12] and Wempner [13] suggested a procedure to predict the nonlinear equilibrium path through limit points. The method, known as the *Riks-Wempner method* provides the Newton-Raphson method and its modifications with a technique to control progress along the equilibrium path. Also, Sabir and Lock [14] have devised a code capable to switching between load and displacement control to traverse any limit point.

A more elegant, but more complex, technique has been formulated by Riks [15]. Riks adds a constraint equation to the system equations which prescribes a fixed distance from the starting point about which the solution is sought.

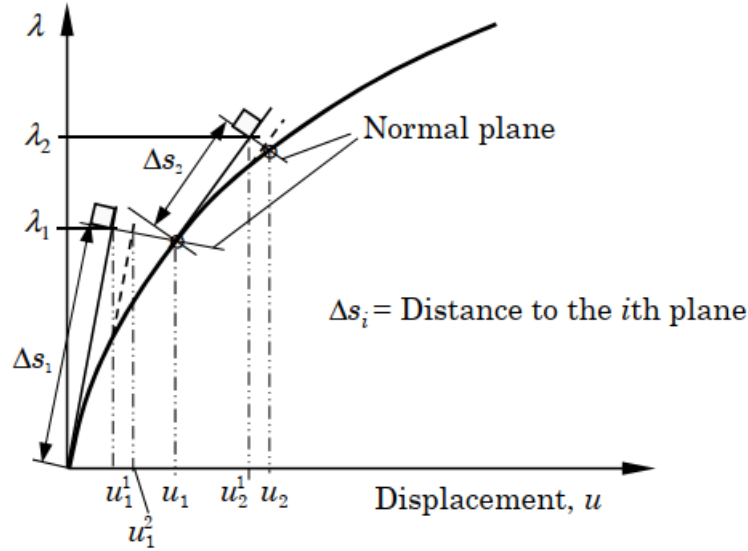


Figure 1.7: The Riks method, normal plane scheme [3].

Riks' method has been reformulated for finite elements by Crisfield [16] and Ramm [17]. Crisfield [16] suggested using a circular arc in place of the normal.

We wish to solve Eq (1.1) for u as a function of the sources term F . If F is independent of the geometry, we can write it as

$$F = \lambda \bar{F} \quad (1.16)$$

Where λ is a scalar, called load parameter, which is considered as an unknown parameter. Eq (1.3) becomes

$$\left\{ R \right\} = K(u)u - \lambda \bar{F} \quad (1.17)$$

Now suppose that the solution $(u_n^{(r-1)}, \lambda_n^{(r-1)})$ at $(r - 1)$ st iteration of the n th load step is known and we wish to determine the solution $(u_n^{(r)}, \lambda_n^{(r)})$ at the r th iteration. Expanding R which is now a function of λ and u , in Taylor's series about the known solution, we have

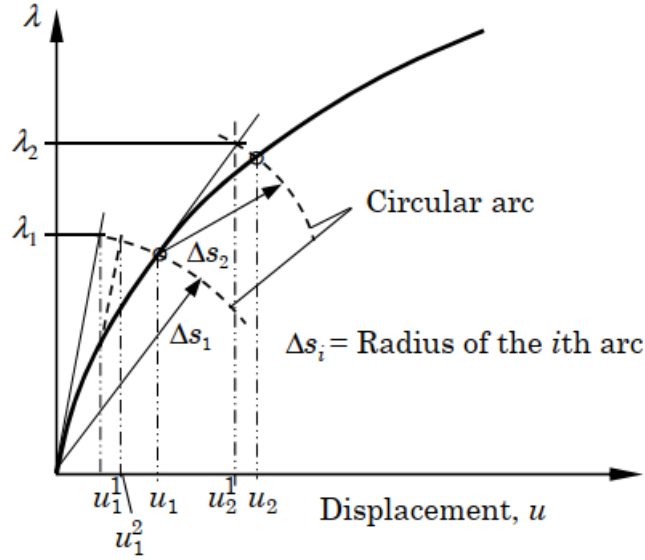


Figure 1.8: The Riks method, circular arc scheme [3].

$$R(u_n^{(r)}, \lambda_n^{(r)}) = R(u_n^{(r-1)}, \lambda_n^{(r-1)}) + \left(\frac{\partial R}{\partial \lambda} \right)^{(r-1)} \delta \lambda_n^{(r)} + \left(\frac{\partial R}{\partial u} \right)^{(r-1)} \delta u_n^{(r)} + \dots = 0 \quad (1.18)$$

Omitting the higher-order terms involving the increments $\delta \lambda_n^{(r)}$ and $\delta u_n^{(r)}$, we obtain

$$0 = R_n^{(r-1)} - \bar{F} \delta \lambda_n^{(r)} + (K_T)^{(r-1)} \delta u_n^{(r)} \quad (1.19)$$

The incremental solution at the current iteration of the n th load step is given by

$$\begin{aligned} \delta u_n^{(r)} &= -K_T^{-1} (R_n^{(r-1)} - \bar{F} \delta \lambda_n^{(r)}) \\ &\equiv \delta \bar{u}_n^{(r)} + \delta \lambda_n^{(r)} \delta \hat{u}_n \end{aligned} \quad (1.20)$$

Where $\delta u_n^{(r)}$ is the usual increment in displacement due to known out-of-balance force vector $R_n^{(r-1)}$ with known $\lambda_n^{(r-1)}$ and K_T is the tangent at the beginning of the current load increment

$$\delta \bar{u}_n^{(r)} = -K_T^{-1} R_n^{(r-1)} \quad (1.21)$$

$\delta \hat{u}_n$ is the tangential solution

$$\delta \hat{u}_n = K_T^{-1} \bar{F} \quad (1.22)$$

Note that K_T is evaluated using the converged solution u_{n-1} of the last load step

$$K_T = \left(\frac{\partial R}{\partial u} \right) \Big|_{u=u_{n-1}} = K(u_{n-1}) + \left(\frac{\partial k}{\partial u} \right) \Big|_{u=u_{n-1}} u_{(n-1)} \quad (1.23)$$

and $\delta \hat{u}_n$ is computed at the beginning of each load step.

The solution at the r th iteration of the current load step is given by

$$u_n = u_{n-1} + \Delta u_n^{(r)} \quad (1.24)$$

$$\Delta u_n^{(r)} = \Delta u_n^{(r-1)} + \delta u_n^{(r)}, \lambda_n^{(r)} = \lambda_n^{(r-1)} + \delta \lambda_n^{(r)} \quad (1.25)$$

1.5 Conclusion

Basic concepts of nonlinear phenomena are given in this introductory chapter. Different types of nonlinearities in solid mechanics are introduced, including geometric, material, kinematic, and force nonlinearities. The importance of nonlinear analysis in structural mechanics is also addressed. General solving procedures of nonlinear equations system have been presented. It has been concluded that the role of nonlinear analysis has become much more important than ever due to the increasing use of light, high-strength materials in industry. Thus, the geometric nonlinearity is the most important nonlinearity that could appear in the design of some structural elements also the most commonly treated in literature.

Chapter2

Previous Works on Nonlinear Analysis of Composite Beams and Plates

2.1 Introduction

One of the most important thing engineers and scientists do is to model natural phenomena. They develop conceptual and mathematical models to simulate physical events, whether they are aerospace, biological, chemical, geological, or mechanical. The mathematical models are developed using laws of physics and they are often described in terms of algebraic, differential, and/or integral equations relating various quantities of interest. A mathematical model can be broadly defined as a set of relationships between variables that express the essential features of a physical system or process in analytical terms. The relationships that govern the system take the form of algebraic, differential and integral equations. Mathematical models of physical phenomena are often based on fundamental scientific laws of physics such as the principle of conservation of mass, the principle of conservation of energy. Note that the engineering systems are governed by laws of continuum mechanics. Mathematical models of engineering systems are often characterized by a very complex equations that posed on geometrically regions. Consequently, many of the mathematical models, until the advent of electronic computation, were drastically simplified in the interest of analytically solving them. Over the last three decades, the computer has made it possible, with the help of mathematical models and

numerical methods, to solve many practical problems of science and engineering. A new and growing body of knowledge connected with the use of numerical methods and computers exists to analyze mathematical models of physical systems, and this body is known as computational mechanics [3].

The minimum weight criteria with high performance has been essential in the design of aircraft, aerospace vehicles and civil structures until today. This task will be a challenge especially when the design of wing structures such as aircraft wings, rotor blades, robotic arms or bridges is the subject. The behavior of such structures is highly nonlinear due to the deformation of their geometry and the solution of such problems becomes very complex, especially with the use of composite materials. The effects of large displacements may play a primary role in the correct prediction of the behavior of these members, which continue to be modeling as a flexible beams.

In this way, another difficult task can be imposed here when some structural elements as plates and shells can undergo inplane thermo-mechanical stresses that affect their stiffness, (eg: high speed aircrafts, rockets and launch vehicles, trains) and consequently, their dynamic and static behavior. This problem has stimulated the researchers to provide an accurate prediction of free vibration of laminated plates, subjected to inplane thermal or mechanical stresses [18, 19].

In this light, much of work has been done in order to better understanding as well as improve the description of such complex behaviors, where some of chosen papers from the literature available are presented in this chapter as a review includes:

- Analytical beams analysis: brief historical review.
- Nonlinear finite element beam analysis.
- Nonlinear dynamics of beams.
- Free vibration of composite laminated plates under thermo-mechanical loading.

2.2 Composite Beams Analysis

2.2.1 Analytical analysis: brief historical review

The geometrical nonlinear analysis of elastic structures has been among fundamental topics in structural mechanics and continue to be an important axis of research attract an immense number of researchers especially when the large displacements of beams is the subject. It has been observed by looking into past development on the subject that an excellent analytical model was presented for geometrically nonlinear analysis by the so-called elastica. The elastica addresses flexural beams problems which the analysis was basically concentrated on the determination of the exact shape of deflection curve. This task has been performed using different types of analytical techniques, such as elliptic integrals as well as various kinds of numerical methods of analysis. Numerical procedures were also extensively used to solve the complicated differential equations when analytical methods were used.

The history of beams theory dates from 16th century. The differential equation of the deflection was first derived by the brothers, Jacob and Johann Bernoulli, of the well-known Bernoulli family of mathematicians. However, because the constant of proportionality was not correctly evaluated, it was rederived later by the suggestion of Daniel Bernoulli, L. Euler (1707–1783) and proceeded to solve the various problems of the elastica. Interested readers can find more details about the history of theory of structures in [20]. After the works of Bernoulli on the deflection curve, large deflection of elastic beams has been the focus of many researchers, since 1940's.

In 1945, The large deflection problem of elastic cantilever beam under tip concentrated vertical load at the free end was studied classically for the first time by Bisshopp and Drucker [21]. Lau [22] also investigated the flexible uniform cantilever beam loaded with the combined loading, consisting of a uniformly distributed load along its span and a concentrated load at its free end, by using the power series method. He proved that superposition does not apply to large

et al. [31], Tari [32], Batista [33]). When a simply-supported beam is subjected to moment at ends, large deflections have been calculated by Chucheesakul et al. [34, 35].

Because of the difficulties involved in solving the nonlinear differential equations, elliptic integral solutions have imposed challenges in the solution evaluations and as well as implementations which have led the researchers in employing, or in some cases devising alternative approaches such as numerical integration methods.

Moreover, a simple numerical method was proposed by wang [36, 37] to solved nonlinear bending of cantilever and simply supported beams under tip concentrated and uniformly distributed loads. Schile and Sierakowski [38] studied large deflection of simply supported beams in four-point bending. Ohtsuki [39] also studied the same problem numerically using the Runge–Kutta method in combination with elliptic integrals to analyze a thin elastic simply supported beam under a symmetrical three-point bending. Shooting optimization technique was utilized by Wang and Kitipornchai [40] to determine large deflections of beam under both concentrated forces and uniformly distributed loading. Numerical methods are developed by Lee and Oh [41] for solving the elastica and buckling load of simply supported tapered beam subjected to compressive end load. Lee [42] used a numerical integration procedure to analyze Post-buckling of uniform column under a combined load consisting of a uniformly distributed axial load and concentrated load at the free end. Lee [43] investigated numerically the large deflection of cantilever beams made of a Ludwick type material subjected to combined concentrated vertical tip point and uniformly distributed forces. The same problem was recently studied by Solano-canillo [44] with a bending moment formulation. Beléndez et al [45,46] also studied large deflection of beams, both theoretically and experimentally. The genetic algorithm was suggested by Kumar et al. [47] and numerically explored in the context of large deflection analysis of elastic beams. A new technique was developed by Dado and Al-sadder [48] to analyze large deflection of non-prismatic beam when the angle of rotation was represented by polynomial function on the variable position along the deflected beam axis. Shvartsman [49] solved numerically large deflection problem of non-uniform cantilever beam under tip concentrated follower load. Wang et al. [50] applied the homotopy analysis method (HAM) to investigate the large deflection of a cantilever beam under a vertical tip point load. Banerjee

et al. [51] employed non-linear shooting and Adomian's decomposition methods to approximate large deflection solution a cantilever beam under arbitrary loading. Mutyalarao et al [52] used numerical integration to solve large deflection of uniform beam under tip concentrated follower load, which the effect of inclination of load in relation with the angle of rotation was studied. Nallathambi et al. [53] studied large deflection of curved cantilever beam by fourth order Runge-Kutta method, whereas Shvartsman [54] studied the same problem by direct numerical method. A new perturbation method was proposed by He et al. [55] to solve nonlinear large deflection problem of initially curved beams under two different boundary conditions.

A detailed look at the works mentioned above reveals that most of the publication based on the Euler-Bernoulli beam theory which assume that shear rigidity sufficiently large during the process of bending deformation. In other words, the effect of shear deformations of the cross-section of a beam is neglected. For this phenomena Timoshenko beam theory taken into account the effect of shear deformations.

Large deflection problems of shear deformable cantilever beams were studied by Sinclair [56] using the Timoshenko theory. Goto et al. [57] published a closed form solutions for elastic beam with axial and shear deformations, using elliptic integrals. However, the authors were adopted the Timoshenko beam theory of finite displacements with finite strains and that with small strains. Atanackovic and Spasic [58] proposed a new shear model for plane elastica. For large deflection analysis based on the Timoshenko beam theory, Li and Song [59] solved large thermal deflections of Timoshenko beams under transverse non-uniform temperature rise. Molyeddin and Fereidoon [60] formulated a method for calculating large deflections of a beam under three-point bending. Li and Lee [61] analyzed the effect of the horizontal reaction force at the support position on the large deflection of short simply-supported Timoshenko beams subjected to general transverse loading. Large deflection and rotation of simply supported beam based on Timoshenko beam theory have been studied by Li and Li [61].

It has been shown in the literature that when the large deflection of composite beams studied analytically the work is rare. Thus, a few available papers are presented in the following. Minguet and Dugundji [62] have developed a theory to predict large deflections of laminated beams. Also some experiments using flat composite cantilevered beams have been performed. Minguet and Dugundji employed an updated Lagrangian elemental coordinate system which represents rigid body motion of the element exactly via Euler angles. The midplane is allowed to stretch but higher-order terms are not included. A unified methodology based on geometrically nonlinear and three-dimensional elasticity, for nonhomogeneous, anisotropic beams analysis was presented by Atilgan and Hodges [63]. An exact solution for the bending of thin and thick cross-ply laminated beams was investigated by Khdeif and Reddy [64].

2.2.2 Nonlinear finite element beams analysis

On the other hand, numerical methods are extremely powerful tools for engineering analysis. With the advent of computers, there has been a tremendous explosion in the development and use of numerical methods. Of these, the nonlinear finite element analysis has received much attention by many researchers due to new industrial needs especially in the mechanical and aerospace fields.

2.2.2.1 Isotropic beams analysis

The first application of finite element method in nonlinear analysis of structures was proposed in 1960 by Turner et al. [65]. Authors have originally presented an incremental approach to analyze the structures geometrically nonlinear using finite element method. In the following, several excellent books for interesting readers. These books either fully devoted to nonlinear finite elements or partially containing significant sections on the subject. Books dealing only with nonlinear finite element analysis include Oden, 1972 [66], Crisfield, 1991 [67], Kleiber, 1989 [68], and Zhong, 1993 [69]. In addition, some of books which partially devoted the subject are Bathe, 1982 [70], Belytschko and Hughes, 1983 [71] and Cook, Plesha and Malkus, 1989 [9], Zienkiewicz and Taylor, 2000 [10].

Moreover, Tada and Lee [72] adopted nodal coordinates and direction cosines of a tangent vector regarding the deformed configuration of elastic flexible beams. The stiffness matrices were obtained by using the equations of equilibrium and Galerkin's method. Their method was applied to a flexible cantilever beam loaded at the free end. Yang [73] proposed a matrix displacement formulation for the analysis of elastica problems related to beams and frames. Wood and Zienkiewicz [74] used a continuum mechanics approach with a Lagrangian coordinate system and isoparametric element for beams, frames, arches, and axisymmetric shells. The Newton–Raphson method was used to solve the nonlinear equilibrium equations. Large displacement with small strain analysis of structures with rotational degrees of freedom was investigated by Argyris et al [75]. Argyris and Symeonidis [76] presented a nonlinear finite element analysis of elastic structures subject to nonconservative forces. An updated Lagrangian and a total Lagrangian formulation of a three-dimensional beam element for large displacement and large rotation analysis are presented by Bathe and Bolourchi [70]. Crisfield [16, 77] proposed a new Incremental/iterative solution procedures for non-linear structural analysis. A new arc-length method including line searches and accelerations is presented by Crisfield [78], which it is applied to the geometrically nonlinear analysis of beams. A consistent co-rotational formulation is presented by Crisfield [79] for non-linear three-dimensional beams analysis. Ramm and Osterrieder [17] carried out the geometric and material nonlinear analysis of open-sectioned and thin-walled rectilinear beams using an updated Lagrangian formulation. Batoz and Jameux [80, 81] obtained an exact displacement field for 2D beam and arch structures, and four different strain expressions with the Total Lagrangian Description are used to show the importance of displacement and strain expressions. Ramm and Osterrieder [17] carried out the geometric and material nonlinear analysis of open-section and thin-walled rectilinear beams using an updated Lagrangian formulation. Hsiao and Hou [82] used the small deflection beam theory, by including the axial force, to solve the large rotation of frame problems by assuming that the strains are small. The total stiffness matrix was formulated by superimposing the bending, geometric, and linear beam stiffness matrices. An incremental iterative method based on the Newton–Raphson method, combined with a constant arc length control method, was used

for the solution of the nonlinear equilibrium equations. Chajes [83] applied the linear and nonlinear incremental methods, as well as the direct method, to investigate the geometrically nonlinear behavior of elastic structures. The governing equations were derived for each method, and a procedure outline was provided regarding the plotting of the load–deflection curves. An incremental Total Lagrangian Formulation for curved beam elements that includes the effect of large rotation increments is developed by Dvorkin et al. [84]. The geometrically nonlinear formulation of three-dimensional curved beam elements with large rotations has been investigated by Lo [85]. Three-dimensional curved beam elements were presented by Ibrahimbegovic [86] for geometrically nonlinear analysis. Also, a finite element formulation for three-dimensional beams undergoing large displacement and large rotations but small strains was proposed by Mikdad and Ibrahimbegovic [87]. A three-dimensional elastoplastic beam element being capable of incorporating large displacement and large rotation is developed and examined by Park and Lee [19]. A geometrical nonlinear analysis eccentric 3D-beam cross-sections element with arbitrary cross-section has been investigated by Gruttmann et al. [88]. Co-rotational and Lagrangian formulations have been addressed by Teh and Clarke [89] for elastic three-dimensional beam finite elements. Large displacements tests and total-Lagrangian finite element analyses of flexible beams have been studied by Pai et al. [90]. A new finite element formulation for geometrically nonlinear three-dimensional beam theories based on interpolation of strain measures has been developed by Zupan and Saje [91]. A new 2D Euler–Bernoulli beam element for large displacement analysis using the total Lagrangian formulation has been proposed by Nanakorn and Vu [92]. Magisano et al. [93] investigated the geometrically nonlinear analysis of beams and shells using solid finite elements and highlighted the advantages of mixed stress/displacement formulations when applied to the path-following analysis and Koiter asymptotic method. By using the Carrera Unified Formulation (CUF) and a total Lagrangian approach, the unified theory of beams including geometrical nonlinearities has been introduced by Pagani and Carrera [94].

2.2.2.2 Anisotropic beams analysis

All works mentioned in the previous section have been basically focused on addressing the geometrically nonlinear finite element isotropic beams analysis, However, there are another problems have been emerging when composite materials are used. Thus, many efforts have been made in order to solve the large deflection problem of composite laminated beams, where are presented by the available papers in this section.

A more complete review on nonlinear laminated composites beams available has been given by Hodges [95]. A large displacement formulation for anisotropic beam analysis was presented by Borri and Merlini [96]. Singh et al. [97] considered the same theory using Von-Karman strain and one-dimensional finite element having twelve degrees of freedom per node to study the nonlinear bending of thin and thick unsymmetrically laminated beams. In contrast, the flexural linear and nonlinear analysis of composite beams under transverse loading based on higher order shear deformation theory is studied by Chandrashekhra and Bengera [98], wherein geometric nonlinearity is incorporated in the formulation by considering Von-Karman strain. A Nonlinear formulation and a finite-differences based numerical solution for a generic orthotropic beams of solid cross-sections was presented by Rand [99]. Furthermore, Creaghan and Palazotto [100] considered a finite element potential energy approach for large displacements and moderate rotations of composite beam structures, which it has been extended by Miller and Palazotto [101] using a large rotation theory. Also, the bending of thin and thick cross-ply laminated beams has been presented by Khdeif and Reddy [64]. An experimental and theoretical model on Aeroelastic Response of High-Aspect-Ratio Wings has been developed by Tang and Dowell [102]. A weighted residual formulation of equilibrium equations for nonlinear laminated beams analysis has been presented by Zielinski and Frey [103]. Also, the existing statically beam finite element based on FSDT was recently used to study the geometric nonlinear effects on static and dynamic responses in isotropic, composite and functionally graded material beams by Agarwal et al. [104]. Large deflection of multilayered Timoshenko beams using Von-Karman strain–displacement relations has been carried out by Di Sciuva and Icardi [105]. A geometric nonlinear model for composite beams with partial interaction has

been developed by Ranzi et al. [106] Yu and Blair [107] developed Geometrically Exact Beam Theory (GEBT) to give a general-purpose tool for nonlinear analysis of composite slender structures. Sofi et al. [108] presented a beam model based on Von Kármán's nonlinear theory and the classical lamination theory for the geometrically nonlinear analysis of laminated composite frame Structures. Nonlinear aeroelastic behaviors of curved laminated composite panels are investigated by An et al. [109]. An efficient nonlinear finite element model based on higher-order beam theory for two layered composite beams was developed by Alhaz Uddin et al. [110]. On the other hand, Pagani and Carrera [94] employed the Carrera Unified Formulation (CUF) to deal with the geometric nonlinear analysis of solid cross-section and thin-walled metallic beams. The promising results provided enough confidence for using the capabilities of that methodology to deal with the large displacements and post-buckling response of composite laminated beam [111].

2.2.2.3 Sandwich beams analysis

In 1992 Frostig et al. [112] presented a new theory based on variational principle for sandwich panels with flexible core, named high order sandwich panel theory (HSAPT). Geometrical nonlinearities were also considered in many papers to increase the accuracy of HSAPT. The large number of literatures that emphasis on nonlinear HSAPT are based on kinematic relations that assume large displacements with moderate rotations for face sheets and small deformations for core. For example in [113, 114, 115]. The nonlinear behavior of a composite sandwich beam in three-point bending was investigated by Gdoutos et al. [116]. Experimental and analytical study of geometrically nonlinear bending response of sandwich beams is presented by Sokolinsky et al. [117]. In the work of phan et al. [118], the face sheets undergo large displacements with moderate rotations, whereas the core strains assume to be linear and nonlinear von-Karman strain in two cases. The first and linear one was a case that loads just apply on face sheets and the second and nonlinear one was a case that a uniform compressive strain through the thickness is applied to sandwich beam. A new geometrically nonlinear high order theory for orthotropic sandwich beams is presented by Dariushi and Sadighi [119].

2.2.2.4 Functionally graded beams analysis

Although the laminated composite materials may offer various different solutions and provide the design flexibility to achieve desirable stiffness and strength, they have some disadvantages such as the geometric discontinuities that can lead to damage in the form of delamination, matrix cracking, and adhesive bond separation. These problems arise due to the discontinuity of the material properties within the structure. As a solution, materials that consist of two phases with continuous transition, so-called Functionally Graded Materials (FGM).

Functionally graded materials (FGMs) are inhomogeneous composites that have smooth and continuous variation of material properties in space. In most of the existing and potential future applications and in the simplest form, FGMs is mainly considered as a mixture of two different material ingredients change gradually from one to other as illustrated in Figure 2.2(a). The material ingredients can also change in a discontinuous way such as the stepwise gradation illustrated in Figure 2.2(b). This type of structure can also be considered an FGM. The most familiar FGM is compositionally graded from a refractory ceramic to a metal. it can incorporate incompatible functions such as the heat, wear, oxidation resistance of ceramics with the high toughness, high strength, machinability, and bonding capability of metals without severe internal thermal stress [120].

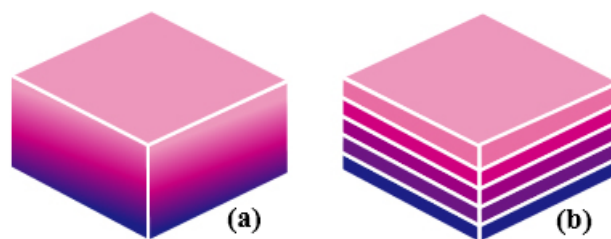


Figure 2.2: (a) Continuous and (b) stepwise graded structures.

Historically, the general idea of structural gradients first was advanced for composites and polymeric materials in 1972 [121, 122]. Various models were suggested for gradients for composition, in filament concentration, and in polymerization along with possible applications for the resulting graded structures. However, there was no actual investigation about how to de-

sign, fabricate, and evaluate graded structures until the 1980s. In 1985, Niino et al. [123] have proposed the use of continuous texture control in order to increase the adhesion strength and minimize the thermal stress in the ceramic coatings and joints being developed for the reusable rocket engine. In 1986, these types of materials were termed *functionally gradient materials*, Which soon became abbreviated to the now familiar,FGM. In 1995, as a consequence of a discussion at the Third International Symposium on FGMs held in Lausanne in 1994, it was decided to change the full name to *functionally graded materials* because it is more accurate both descriptively and grammatically [120].

Bringing it all together, it is fair to say that geometric nonlinear and large deflection analysis of FGM structures is an important subject in modern structural engineering, especially, FGM beams play an important role not only in classical structural applications, but we can find many applications in thermal, electric-thermal or electric-thermal–structural systems. In literature, a huge amount of papers can be found which deal with modeling and simulation of nonlinear static and dynamic problems of FGM beams. For example,an elasticity problem of functionally graded beam subjected to transverse loads has been solved by Sankar [124]. Agarwal at al. [125] studied the geometrically non-linear static and dynamic responses of functionally graded beams based on the total Lagrangian finite element formulation with the von Kármán’s geometric non-linearity. Kang and Li [126] examined the large deflection of a straight cantilever beam subjected to an end force. Material of the beam is assumed to be functionally graded, and nonlinear effects of material variation was investigated. Birman and Byrd [127] presented a review of the main developments in FGMs with an emphasis on the recent work published since 2000. Large deflections analysis of a FGM cantilever beam subjected to an end moment was investigated by Kang and Li [128]. Rahimi and Davoodinik [129] discussed the large deflection of a functionally graded cantilever beam under inclined end loading by fully accounting for geometric nonlinearities using analytical and Adomian decomposition methods, then Davoodinik and Rahimi [130] extended their works to the semi-analytical analysis of the flexible tapered functionally graded cantilever beam. Nonlinear static analyses of a cantilever Timoshenko beam composed of FGM under non-follower transversal uniformly distributed loads with large displacements and rotations has been studied by Kocatürk et al. [131]. Govern-

ing equations for Euler–Bernoulli and Timoshenko beams have been developed by Reddy [132] using von Kármán nonlinear strains for functionally graded beams. Almeida et al. [133] presented a finite element formulation based on the Total Lagrangian approach to analyze large deflections of straight FGM beams. Soleimani and Saadatfar [134] studied numerically the large deflection of FGM beams subjected to arbitrary loading conditions. Ma and Lee [135] gave exact solutions for nonlinear static responses of a shear deformable FGM beam under an in-plane thermal loading. Zamanzadeh et al. [136] studied a stability of FGM micro-beams subjected to non-linear electrostatic pressure and thermal changes. Based on a physical neutral surface and high order shear deformation theory nonlinear bending analysis of FGM beams has been investigated by Zhang [137]. Large deflections of slender nonlinearly elastic functionally graded composite beams subjected to a combined loading have been presented by Sitar et al [138]. Kien and Gan [139] used the first order shear deformation assumption to study the large deflection of tapered cantilever beams made of FGM, and subjected to an end force. Authors [140] presented in the same year a finite element procedure for the large deflection analysis of functionally graded beams resting on a two-parameter elastic foundation. Kien [141] studied the large displacement behaviour of tapered Euler-Bernoulli cantilever beams made of FGM and subjected to end forces. Under the effect of both thermal, and mechanical loads nonlinear bending analysis of tapered FGM beams have been studied by Nikham et al. [142]. Yoon et al. [143] presented a geometrically nonlinear finite element formulation for analysis of 3D FGM beams. A novel beam model has been derived by Li et al. [59] to investigate the nonlinearized bending behaviors of a two-dimensionally functionally graded (FG) beam based on the Euler–Bernoulli beam kinematic theory. An analytical investigation on the thermally induced non-linear response of slightly curved beams made of functionally graded materials has been presented by Dehrouyeh-Semnani [144].

2.2.3 Nonlinear dynamics of beams

If modern nonlinear dynamics has a father, it is Henri Poincare (1854-1912). Dynamic studies, prior to his studies in the 1880s, concentrated on obtaining analytic solutions of dynamic equations, as characterized by many astronomical investigations of planetary motions and by Lord Rayleigh's ubiquitous studies of nearly every moving mechanical system [145]. Since Poincare a huge number of investigators focused their efforts to perform on nonlinear dynamics analysis, especially, the nonlinear vibration of beams, where some of research work is discussed and presented in this section.

2.2.3.1 Isotropic beams vibration

Fertis [4, 146] and Fertis and Afonta [147, 148] applied the method of the equivalent systems to determine the free vibration of variable stiffness flexible members. Fertis [4, 146], and Fertis and Lee [149, 150] developed a method to be used for the nonlinear vibration and instabilities of elastically supported beams with axial restraints. They have also provided solutions for the inelastic response of variable stiffness members subjected to cyclic loadings. Wionowsky-Krieger [151] was the first one to analyze the nonlinear free vibration of hinged beams with an axial force. Prathap [152] worked on the nonlinear vibration of beams with variable axial restraints. Also, Prathap and Varadan [153] worked on the large amplitude vibration of tapered clamped beams. They used the actual nonlinear equilibrium equations and the exact nonlinear expression for the curvature. Mei and Decha-Umphai [154] developed a finite element approach in order to evaluate the geometric nonlinearities of large amplitude free- and forced-beam vibrations. Mei [155] Evensen [156], and other researchers also worked on nonlinear vibrations of beams.

Furthermore, a Galerkin finite element method has been presented for studying nonlinear vibrations of beams describable in terms of moderately large bending theory by Bhashyam and Prathap [157]. An analytical method for determining the vibration modes of geometrically nonlinear beams under various edge conditions has been presented by Qaisi [158]. Nayfeh and Nayfeh [159] have obtained the nonlinear modes and natural frequencies of a simply sup-

ported Euler–Bernoulli beam resting on an elastic foundation with distributed quadratic and cubic nonlinearities using the method of multiple scales and the invariant manifold approach. Also, the nonlinear vibrations of an Euler–Bernoulli beam with a concentrated mass attached to it are investigated by Karlik et al [160]. Azrar et al. [161] have developed a semi-analytical approach to the nonlinear dynamic response problem of beams based on Lagrange’s principle and the harmonic balance method. Authors [162] extended thier works, which semi-analytical approach to the non-linear dynamic response of beams based on multimode analysis has been presented. Nonlinear modal analysis approach based on invariant manifold method to obtain the nonlinear normal modes of a clamped-clamped beam for large amplitude displacements has been presented by Xie et al. [163]. Zhong and Guo [69] investigated the large-amplitude free vibration of simply supported Timoshenko beams with immovable ends. Pirbodaghi et al. [164] have used the first-order approximation of the homotopy analysis method to investigate the nonlinear free vibration analysis of Euler–Bernoulli beam.

2.2.3.2 Anisotropic beams vibration

On the other hand, the nonlinear vibration and dynamic response analysis of composite beams have been studied extensively over the years. For example, Singh and Rao [165], Kapania and Racitij [166] presented nonlinear vibration analysis of unsymmetrically laminated beams by using FEM based on refined classical lamination theory, first order shear deformation theory and higher order shear deformation theory, respectively. Ganapathi et al. [167] studied nonlinear free flexural vibration of cross-ply laminated beams using a cubic B-spline shear flexible straight/curved element. Patel et al. [168] studied nonlinear free flexural vibration and post-buckling of cross-ply laminated beams on a two parameter elastic foundation by using a three-noded shear flexible beam element. Malekzadeh and Vosoughi [169] studied a large amplitude vibration of symmetric laminated beams on nonlinear elastic foundations by using differential quadrature method (DQM) based on the classical lamination theory. Gunda et al. [170] studied a large amplitude vibration of cross-ply laminated composite beams with axially immovable ends with symmetric and asymmetric layup orientations by using the Ritz and finite element

methods based on the classical lamination theory. Also, large amplitude free vibration and postbuckling of cross-ply laminated beams on a nonlinear elastic foundation by using variational iteration method based on the classical lamination theory have been studied by Baghani et al. [171]. Slimani et al. [172] studied nonlinear vibration of cross-ply laminated beams by using polynomial finite element method with shape functions based on Legendre polynomials or sinusoidal functions. Li and Qiao [59] studied a large amplitude vibration of anisotropic laminated beams resting on a two-parameter elastic foundation by using a perturbation technique based on a refined higher order shear deformation theory. The nonlinear dynamic response of symmetric laminated composite beams subjected to combined in-plane and uniform lateral loadings have been investigated by Latifi et al. [173].

2.2.3.3 Functionally graded beams vibration

Moreover, in the following some of considerable research work was performed on nonlinear vibration of functionally graded beams. Kitipornchai et al. [174] studied the non-linear free vibration of functionally graded Timoshenko beams containing an open edge crack based on von Kármán geometric non-linearity. Ke et al. [175] studied the nonlinear vibration of functionally graded beams based on the Euler–Bernoulli beam theory and considering the von Kármán geometric nonlinearity. Based on the Euler–Bernoulli beam theory, authors [176] studied the nonlinear vibration of FGM beams with either exponential function or power law distribution of the material properties through the thickness direction, and presented that the vibration behavior of the FGM beams was different from the homogenous beams due to the stretching-bending coupling effect. Simsek [177] studied the non-linear transient analysis of a functionally graded (FG) beams with pinned–pinned supports due to a moving harmonic loading. Shooshtari and Rafiee [178] gave the nonlinear forced vibration of the FGM beams by using multiple time scales. Fallah and Aghdam [179, 180] presented large amplitude free vibration analysis of FGM Euler–Bernoulli beams resting on nonlinear elastic foundation subjected to both mechanical and thermal loadings. In addition, Fu et al. [181] carried out nonlinear free vibration analysis of piezoelectric FGM beams under thermal environment employing Euler–Bernoulli

beam theory. Lai et al. [182] obtained the accurate analytical solutions for large amplitude vibration of thin FGM beams using Euler–Bernoulli beam theory. Also, based on the same theory, Yaghoobi and Torabi [183] studied the nonlinear vibration behavior of FGM beams resting on nonlinear elastic foundation subjected to axial force. A theoretical study on free vibration behavior of pre-stressed FGM Timoshenko beam under large transverse deflection by a variational method has been investigated by Paul and Das [184].

2.3 Composite Plates Analysis

Stiff, strong and lightweight composite materials are being widely used in many structural members, such as multilayered composite beams, plates and shells. Since their first applications, composite laminated plates have been more and more employed in aeronautic, space and automotive industry. More in detail, layered composite plates are widely applied in external surface of aircrafts, ships, trains and other vehicles. This use can impose problems when these structural elements can undergo inplane thermo-mechanical stresses that affect their stiffness, and consequently ,their dynamic and static behavior. This problem has stimulated the researchers to provide an accurate prediction of free vibration of laminated plates, subjected to thermal or mechanical stresses [18, 19, 185].

Numerous works have been presented for isothermal stress free vibration, using analytic and finite elements methods. Srinivas et al. [186] presented a three-dimensional elasticity solution for the analysis of simply supported homogeneous and laminated rectangular plates. In 1973, Srinivas [187] presented a refined analysis of composite laminates for static and dynamic analyses of composite laminates. Noor [188] used a three-dimensional elasticity solution to investigate the free vibrations of multilayered composite plates. Reddy and Kuppusamy [189] presented a study related to the free vibration of laminated anisotropic plates. Di Sciuva [190] used a new displacement model for the analysis of bending, buckling and vibration of simply supported thick multilayered plates. Nayak et al. [191] used Reddy’s high-order theory for the analysis of dynamic behavior of composite sandwich plates. Zhen et al. [192] used a precise high-order theory finite element model to investigate the free vibration of laminates composite

and sandwich plates. Kant and Swaminathan [193] presented an analytical solution based on higher-order refined theory, for the free vibration of composite laminated and sandwich plates. Thermal buckling behavior has been of a great interest for various researchers in the past and in the present. Among the first studies that dealt with investigating thermal buckling of plates is that carried out by Gossard et al. [194]. Rayleigh–Ritz method has been used to calculate the critical buckling temperature of simply supported isotropic rectangular plates. Noor and Burton [195] used analytic three-dimensional elasticity solutions to tackle the thermal buckling problem of antisymmetric multilayered anisotropic plates analysis. Whitney and Ashton [196] used energy formulation for thermal buckling of simply supported symmetric, angle-ply layered composite plates. Zhen and Wanji [197] presented a study on buckling response of angle-ply laminated composite and sandwich plates using the global local higher-order theory with combination of geometric stiffness matrix. In 2013, Singh et al. [198] studied the buckling of laminated composite plates, subjected to mechanical and thermal loading, using meshless collocations. And recently, in 2017, Cetkovic [199] presented a study on thermal buckling of laminated composite plates, hinging on Reddy’s layerwise theory and its new version.

However, works carried out for thermally stressed laminated plates, free vibration, are rather less numerous in comparison with those devoted to thermal buckling and isothermal free vibration. Among the earlier works carried out on the vibration of laminated plates, subjected to thermal stresses is that presented by Lurie [200] on the lateral vibration as related to structural stability. Noor and Burton [201] used three-dimensional solutions to investigate the free vibrations and buckling of multilayered angle-ply anti-symmetric composite plates subjected to thermal stresses. They have presented numerical results displaying the effects of variations in both material characteristics and fiber orientation of different layers, in addition to the effects of initial thermal deformations on the vibration and buckling responses of the plates. Zhou et al. [202] observed the vibration of the thermally buckled composite plate, taking into account the initial deflection. They used a triangle-shaped finite element founded on the classical plate theory. Lee and Lee [203] studied the vibration of the thermally post-buckled composite plate by means of the theory of the first-order shear deformation plate (FSDT). Park et al. [19]

used the nonlinear finite element based on the FSDT to investigate the vibration of thermally post-buckled composite plates embedded with shape memory alloy fibers. Matsunaga presented [204] a first study on the vibration and stability of cross-ply laminated composite plates using a global higher-order plate theory, followed in 2001 [205] by a study on the vibration and stability of angle-ply laminated composite plates subjected to in-plane stresses. In 2005, [206] the author presented a two-dimensional global higher-order deformation theory used in the free vibration and stability problems of angle-ply laminated composite and sandwich plates subjected to thermal loading.

Recently, Khanna and Kaur [207] presented a study looking into the outcome of thermal gradient on vibration of nonuniform visco-elastic rectangular plates. Thus, to examine the effect of bilinear temperature on vibration of rectangular plate that is non-homogenous visco-elastic and of a nonuniform thickness, the authors used a theoretical model. They applied Rayleigh–Ritz technique to compute the deflection conforming to the first two modes of vibration, for different plate’s parameters, namely taper constant, aspect ratio, non-homogeneity constants and thermal gradient.

The first attention to the plates in pre-loaded configuration was given by Hermann and Armenakas [208, 209]. In their works, the authors identified a relationship between the equations of motion of a plate under initial stress and the general three-dimensional description obtained by considering the displacement field and a variational principle for elastic bodies. Buckling and lateral vibration of rectangular plates subjected to inplane loads have been investigated by Bassily and Dickinso [210], using Ritz method. Brunelle and Robertson [211] have investigated the the vibrational behavior of a thick, simply supported rectangular plate subjected to initial stress. Gianetti et al. [212] studied the transverse vibrations of rectangular plates with elastically restrained edges, subjected to inplane shear forces. Based on Higher-Order Deformation Theory, Doong and Chen [213, 214] investigated the vibration and the stability of an initially stressed laminated plate. The same problem has been studied by Dawe and Craig [215] for symmetrically laminated plates. In addition, The characteristics of fundamental modes of free vibration of initially stressed composite laminated plates have been presented

by Dhanaraj and Palaninathan [216]. Free vibration of isotropic and orthotropic square plates with square cutouts subjected to inplane forces have been analyzed by Lee and Lim [217]. Also, Natural frequencies, modal displacements and stresses of cross-ply laminated composite plates subjected to initial in-plane stresses have been analyzed by Matsunaga [218]. Chen and Fung [219] studied the non-linear vibration of initially stressed hybrid composite plates. The effects of inplane loading on vibration of composite plates have been studied by Carrera et al. [185].

2.4 Conclusion

Brief historical review on analytical analysis of large deflection isotropic beams is firstly given in this chapter. Some of the available papers on analytical analysis of large deflection of composite beams are also presented. Previous works on geometrically nonlinear analysis of isotropic, anisotropic, sandwich and functionally graded beams using finite element method have been reviewed. In addition, from the literature the nonlinear dynamic response analysis of isotropic and composite beams are presented. Free vibration analysis of composite plates under inplane thermo-mechanical loading have been finelly mentioned. It has been observed that the large deflection beam anlysis problem is rarely studied in the literature, especially when the composite materials are used.

Part II

Nonlinear Beams Analysis

Chapter3

Experimental Study

3.1 Introduction

In this work, several bending experiments were carried out on isotropic and composite cantilever beams to verify the analytical as well as the finite element formulations, which are presented in chapters 4 and 5 subsequently. Three different types of materials were considered for these experiments, where the manufacturing of materials and the preparation of specimens are firstly addressed in the current chapter. The characterization of used materials is also presented and described by the measurement of their properties through a series of static tensile tests. Furthermore, a calcination has been carried out to define more properties that could not be measured by tensile tests. In addition, the experiments setup are described in detail and their results are presented and commented.

3.2 Material Manufacture and Specimen Preparation

Three different types of materials were considered in this work. An isotropic Plexiglass (**PG**), a composite of random short fiber with unsaturated polyester resin (**RSF**). Also, laminated specimens of four layers with different fiber orientation angles(**GFP**) were fabricated by contact molding method. The initial materials, E-glass fiber with a density of $2.6g/m^3$ and polyester resin with a density of $1.2g/cm^3$, used in the manufacturing of the (**GFP**) specimens, were purchased from MPI (Maghreb Pipe Industries, Algeria). Figure 3.1, presents the initial used materials and E-glass fiber preparation steps.

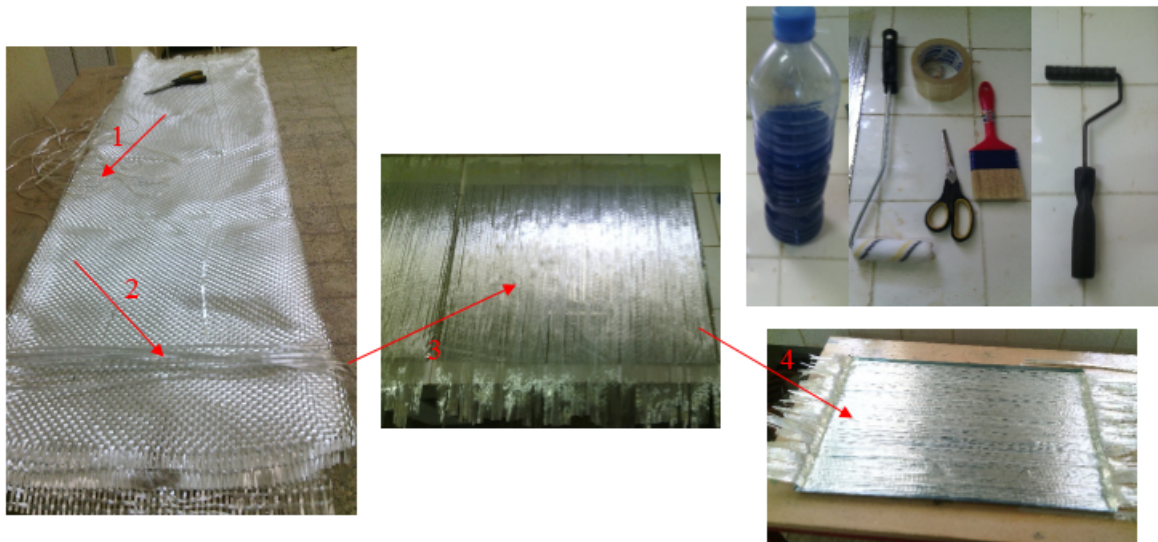


Figure 3.1: The initial materials, E-glass fiber, polyester resin.

Rectangular metallic mold with a length of $600mm$ and a width of $400mm$ is used for molding. Mold release agent is first applied to the mold for getting a high-quality surfaces and facilitate the release of the laminate from the mold. A long unidirectional glass fiber are prepared for two different angles orientation, $[0^\circ]$ fiber orientation for the first and the last layers then $[90^\circ]$ for the second and the third layers. When the agent has cured sufficiently, the fiber is manually placed on the mold. In the next step, the resin is applied by brushing. A metallic roller is used to consolidate the laminate and removing the entrapped air. The three layers remaining are added by the same way above the first one to build a symmetric laminate $[0/90/90/0]$. The

laminate was preserved at room temperature for a week to dry up. The thickness of individual ply is 0.5mm see Figure 3.2.



Figure 3.2: Laminated plate $[0/90/90/0]$.

The completed laminated plate was carefully released from the mold and it has been checked to ensure good quality without defects and then cut into specimens in a different fiber orientation angles, using a dedicated cutting machine Figure 3.3.



Figure 3.3: Dedicated cutting machine.

3.2.1 Material characterization

A series of static tensile tests were performed, using a universal testing machine (**INSTRON-5969**) in order to measure the mechanical properties of used materials. First, three specimens were prepared for each of the (**PG**) and (**RSF**) of size $(100 \times 10 \times 2mm^3)$. The (**GFP**) laminate, plate of a single layer with unidirectional glass fiber was fabricated by the same way in order to measure the mechanical properties, such as laminate Young's modulus E_1, E_2 , Poisson ratio ν_{12} . Also, six identical specimens of size $(100 \times 12 \times 2mm^3)$ were prepared for static tensile testing in the longitudinal $[0^\circ]$ and transverse $[90^\circ]$ unidirectional fiber orientation. The tests were conducted on specimens in the longitudinal way. The ends of the specimens were carefully mounted in the wedge grips of the machine to make sure that the specimen is aligned and centered. The specimens were loaded in tension to failure and during the loading, the whole test process was carefully recorded by the force/displacement as well as the strain/stress curves. Also, failure tensile stress, strain and specimens failure load were obtained. Figure 3.4, shows the tensile tests of both (**PG**) and (**RSF**) specimens.

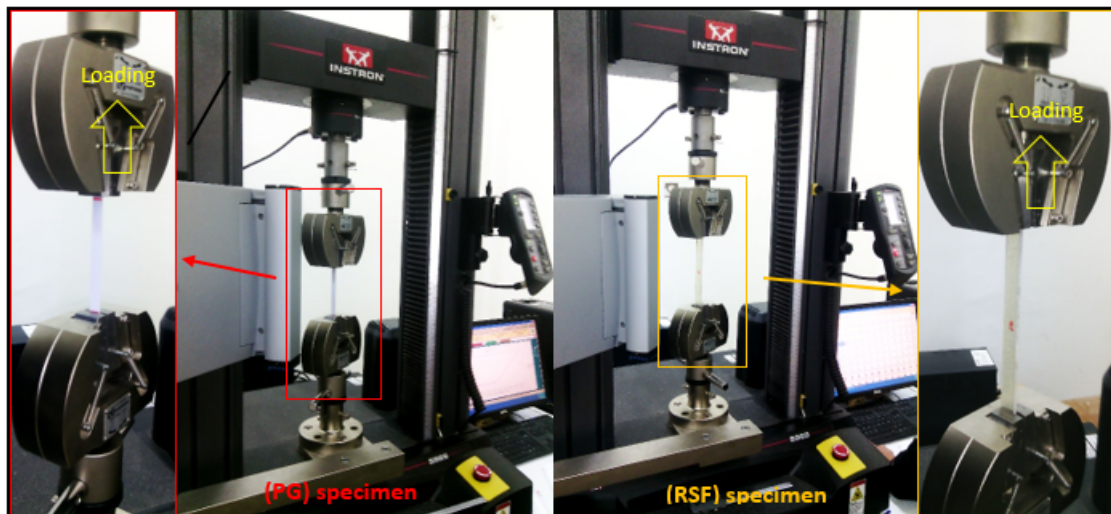


Figure 3.4: Static tensile tests of (**PG**) and (**RSF**) specimens.

Tensile modulus of elasticity, failure stress and strain of each specimen of used materials were determined. The obtained results of each material under consideration are averaged to eliminate the error and summarized in Table 3.1.

Table 3.1: Mechanical properties of materials.

property	(PG)	(RSF)	(GFP)	
			0°	90°
Failure tensile stress (MPa)	34.193	59.747	92.462	1.077
Failure tensile strain (mm/mm)	0.0195	0.0144	0.0228	0.0126
Specimen failure load (N)	1105.116	2537.905	1823.117	28.943
Modulus of elasticity (MPa)	2336.921	5711.623	5382.956- E_1	1914.862- E_2

Figure 3.6 to Figure 3.9 , show tensile stress-strain curves for three (PG) and (RSF) specimens as well as six specimens for (GFP) laminate used for material characterization.

Tests observations

- It can be seen from the stress/strain curves that the specimens of each material under consideration have identical behavior and the curves were practically superposed in the elastic region.
- In this study the used materials behave in two distinct phases, the first is the initial elastic region where the behavior is linear. This linear elastic phase is characterized by the elastic modulus. At the end of the elastic region the curves shows an elbow especially for composite material. Following this part, with increase of tensile stress the strain increase up to the brutal failure.
- The failure positions of the most specimens were near the center. Some specimens were clearly failed in the end of the grips. Then for (GFP) specimens, the damage mechanism was following the fibers direction. The following figures presents the final fracture of some specimens.

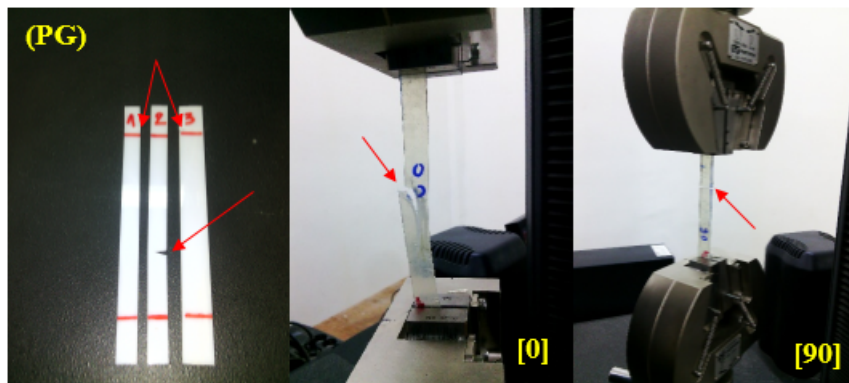


Figure 3.5: The final fracture of some specimens.

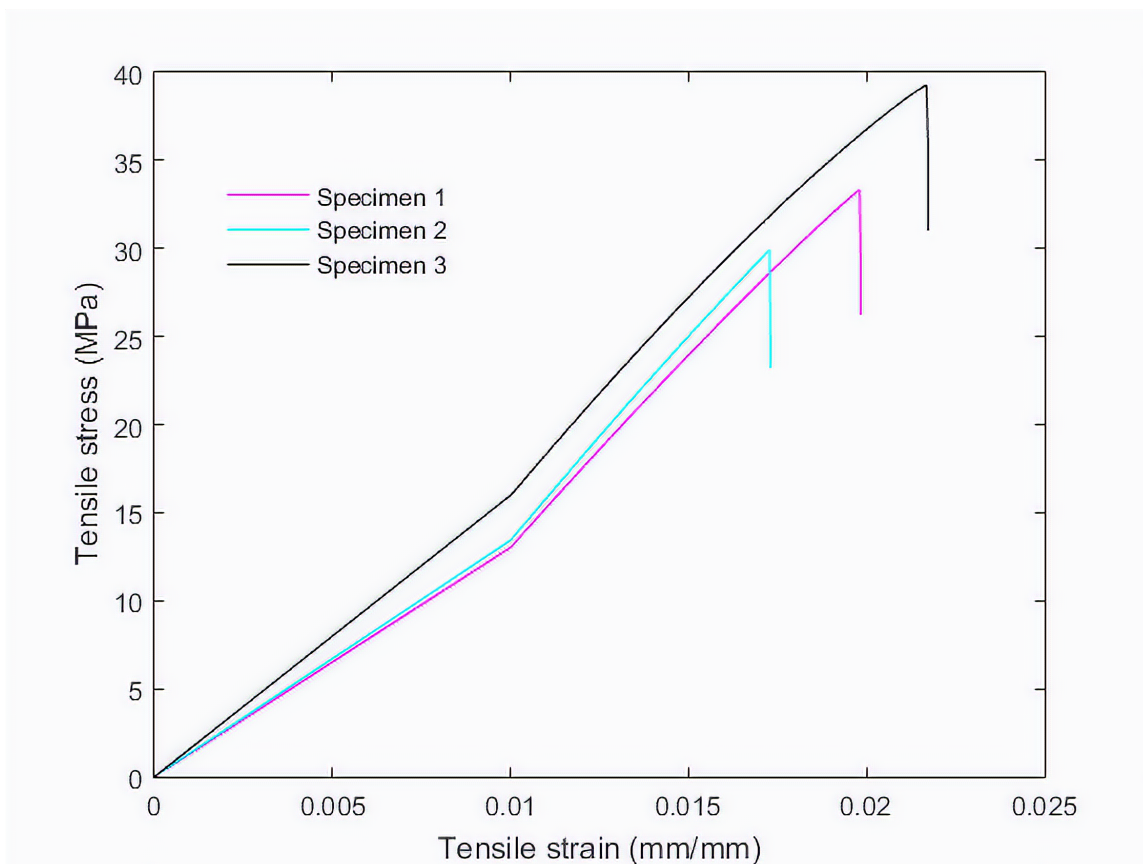


Figure 3.6: Tensile stress-strain tests for (PG) specimens.

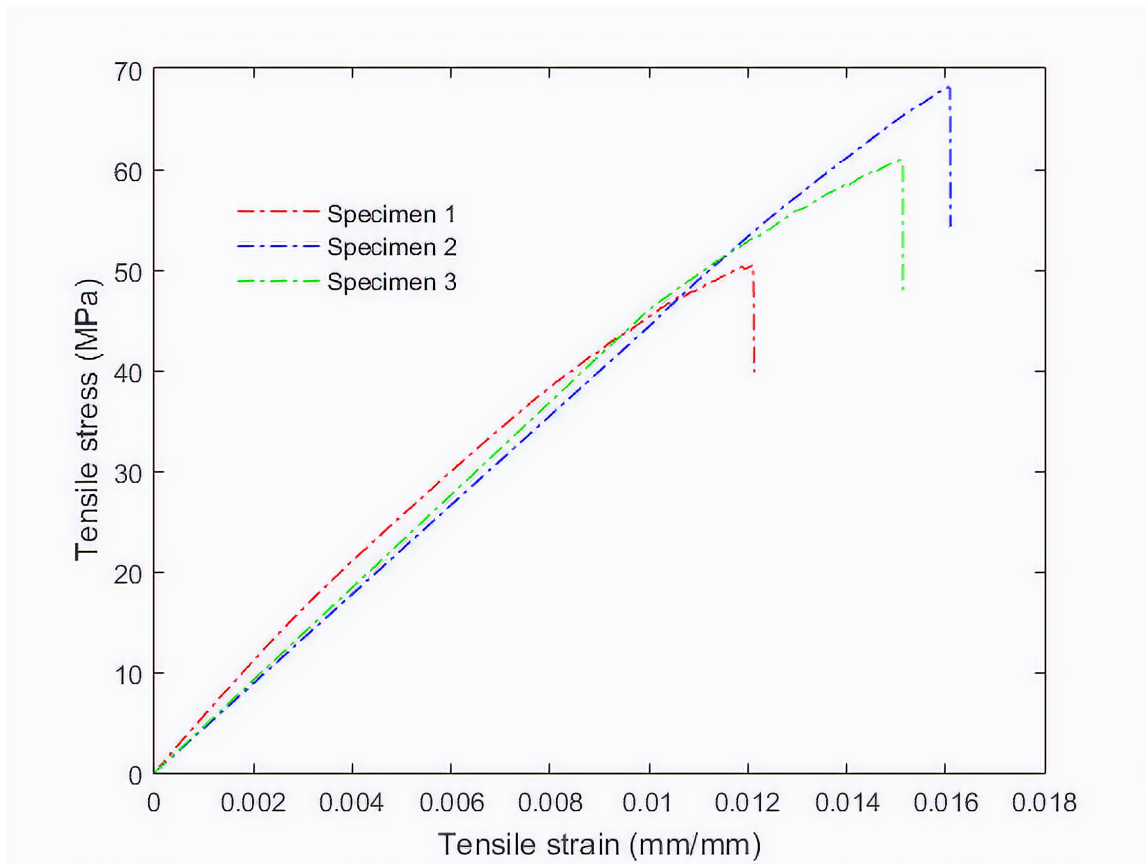


Figure 3.7: Tensile stress-strain tests for **(RSF)** specimens.

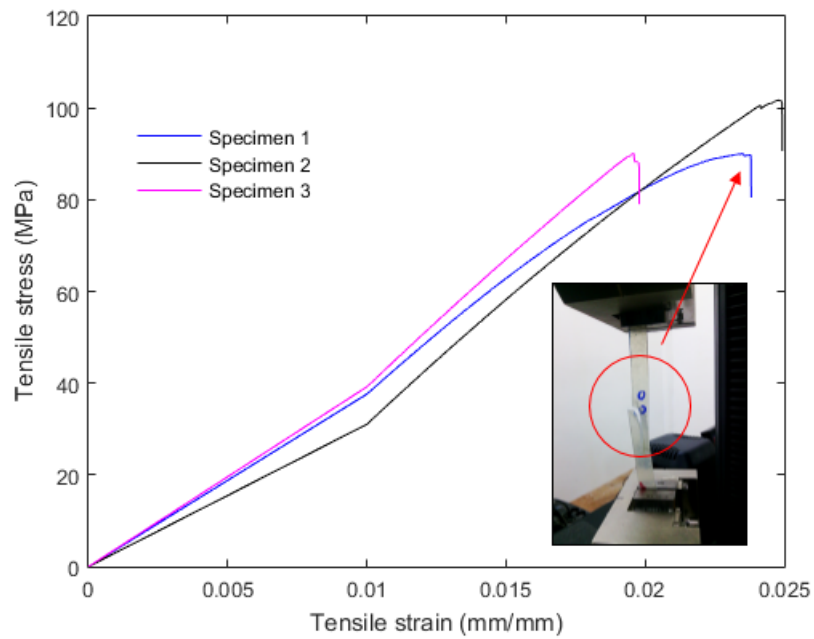


Figure 3.8: Tensile stress-strain tests for $[0]$ specimens.

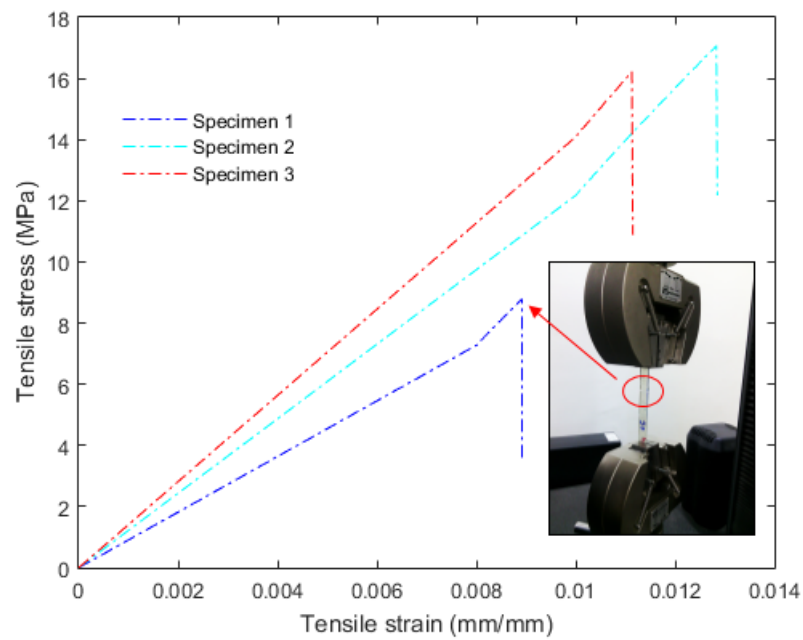


Figure 3.9: Tensile stress-strain tests for $[90]$ specimens.

Furthermore, calcination has also been carried out in order to measure the (GPF) laminate's properties. From location on the single layer of unidirectional glass fiber that was fabricated early, a square specimen of size $(50 \times 50 \times 1.5 \text{ mm}^3)$ was cut to be representative of material. It was cut using dedicated cutting machine. Also, a melting pot is used for heat treatment of prepared specimen. The first step was to weight the used specimen as well as a melting pot and both specimen with melting pot using a balance with (0.001 g) of precision. The obtained weights are (110.714 g) for melting pot and (4.430 g) for specimen then (115.143 g) for both of them. Then, the prepared specimen was put in a melting pot and baked in the temperature of $750 \text{ }^\circ\text{C}$ for approximately 2 hours. The next step was after the heat treatment of specimen, which we remarked that the polyester resin burnt and evaporated. However, The glass fibers remained the same in the melting pot. Then, the weight of the fibers was determined (0.822 g) . The mentioned steps above are summarized and presented in the following Figure 3.10.

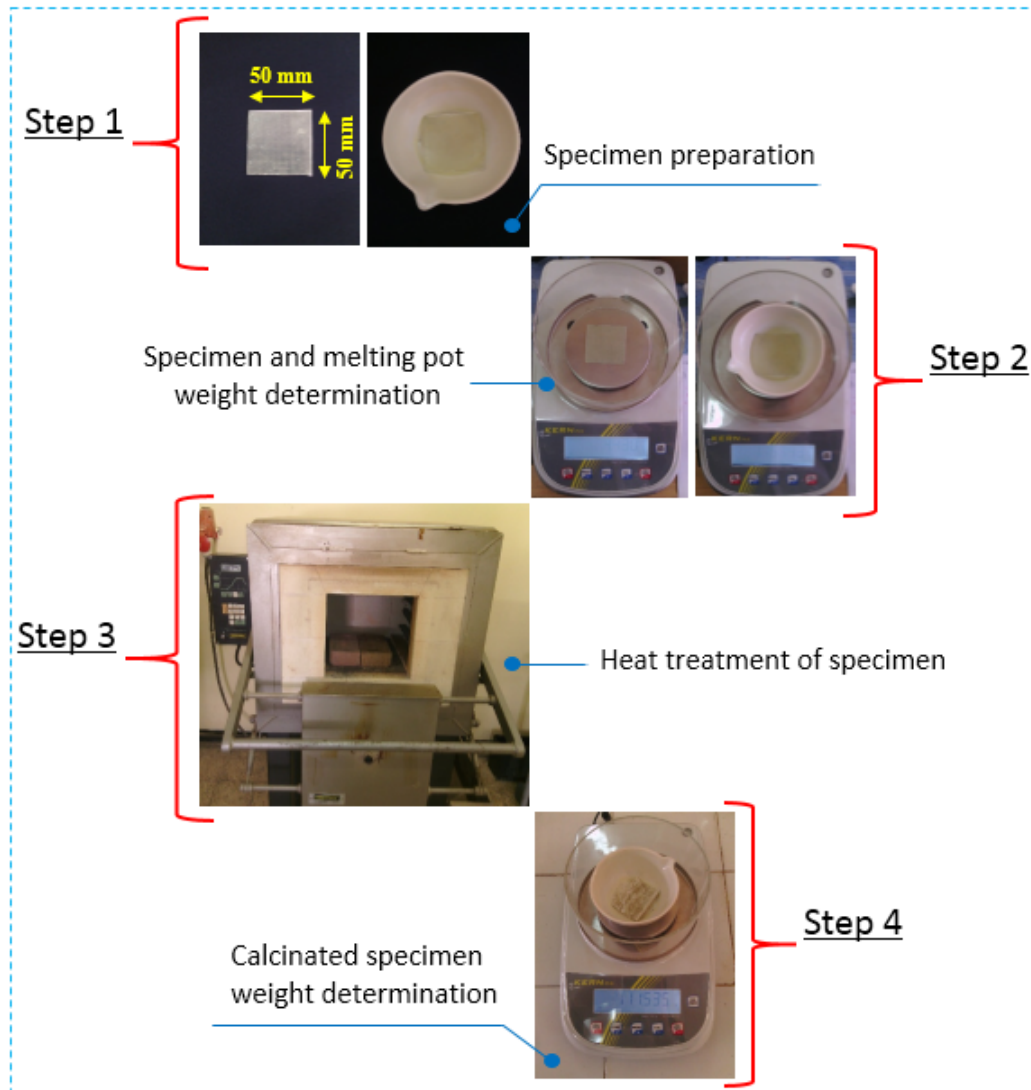


Figure 3.10: Calcination steps.

The Young's modulus and Poisson's ratio of glass fiber/polyester specimen can be expressed in term of the modulus, Poisson's ratios and volume fractions of the constituents and are calculated using the following mixing lows

$$E_1 = E_f V_f + E_m V_m \quad (3.1)$$

$$E_2 = \frac{E_f E_m}{V_m E_f + V_f E_m} \quad (3.2)$$

$$\nu_{12} = \nu_m V_m + \nu_f V_f \quad (3.3)$$

$$G_{12} = \frac{G_m G_f}{V_m G_f + V_f G_m} \quad (3.4)$$

Where

E_f = modulus of the fiber; E_m = modulus of the matrix

V_f = fiber volume fraction; V_m = matrix volume fraction

ν_f = Poisson's ratio of the fiber; ν_m = Poisson's ratio of the matrix

In this study, the calcination of a specimen under consideration aimed to measure the weight of glass fiber as well as polyester matrix in order to calculate the mechanical properties of (GFP) laminate. The obtained results are summarized in Table 3.2.

Table 3.2: Mechanical properties of (GFP) laminate.

Material	$E_1(MPa)$	$E_2(MPa)$	$G_{12}(MPa)$	ν_{12}
(GFP) laminate	9754	4797.87	1680.55	0.353

3.3 Experimental Set-Up

In this work, several bending experiments were performed on several cantelivered beams. For these experiments different beams size were cut and prepared of the used materials. The first group of beams consisted four (**PG**) specimens with a length of $L = 500mm$, a width of $W = 20mm$, a thickness of $t = 2mm$. In the second group of beams, twelve (**RSF**) specimens with a length of $L = 250mm$, a width of $W = 15mm$, a thickness of $t = 3mm$ were prepared. The third group was for (**GFP**) laminates, which several specimens with different fiber orientation angles $[0/90/90/0]$, $[90/0/0/90]$, $[45/ - 45/ - 45/45]$, $[-45/45/45/ - 45]$ were cut with a length of $L = 240mm$, a width of $W = 20mm$, a thickness of $t = 2mm$. . All specimens are numbered to be differentiated from each other.

A vertical metallic stand was used, in order to conduct the bending experiments on (**PG**) as well as (**RSF**) specimens. A serie of different metallic masses whith a metallic axis are used for loading. A graph paper sheet was placed on a vertical metallic stand, then a pencil was fixed on the tip of the beams. The pencil is used in order to drawing the deflection curve on the graph paper during the experiments. First, the beams were accuratly fixed from one end in the stand using a metallic bolt and loaded from the free end. The horizontality of beams was checked before loading, then an horizontal line was drawn on the graph paper with the undeformed beam's level in order to make a reference with for deflection curve. The beams were loaded by hand carefully then after each load a point was marked on the graph paper with the level of the tip of deflected beams in order to record the corresponding displacements of each load. Then, the horizontal and the vertical displacements of each point were measured from the deflection curve drawn on the graph. The following figures show the bending experiments for (**PG**) as well as for (**RSF**) beams.

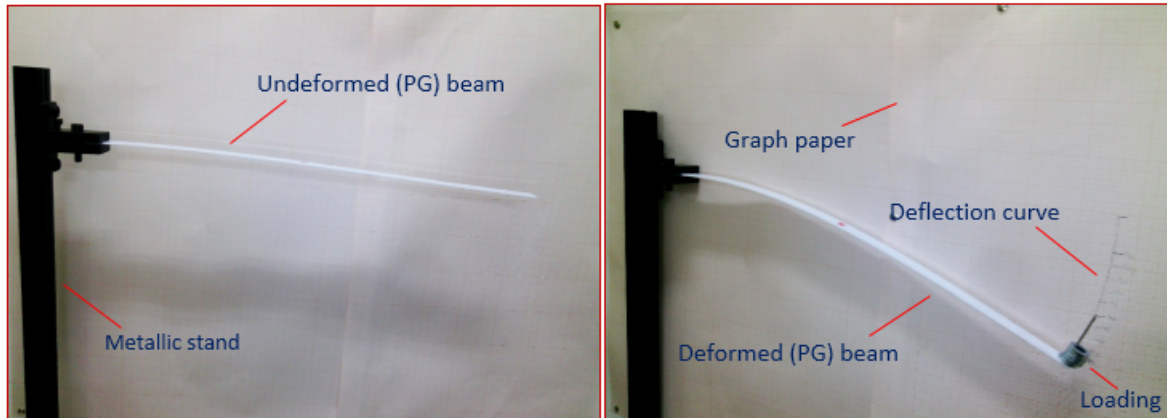


Figure 3.11: Bending experiments for **(PG)** beams.

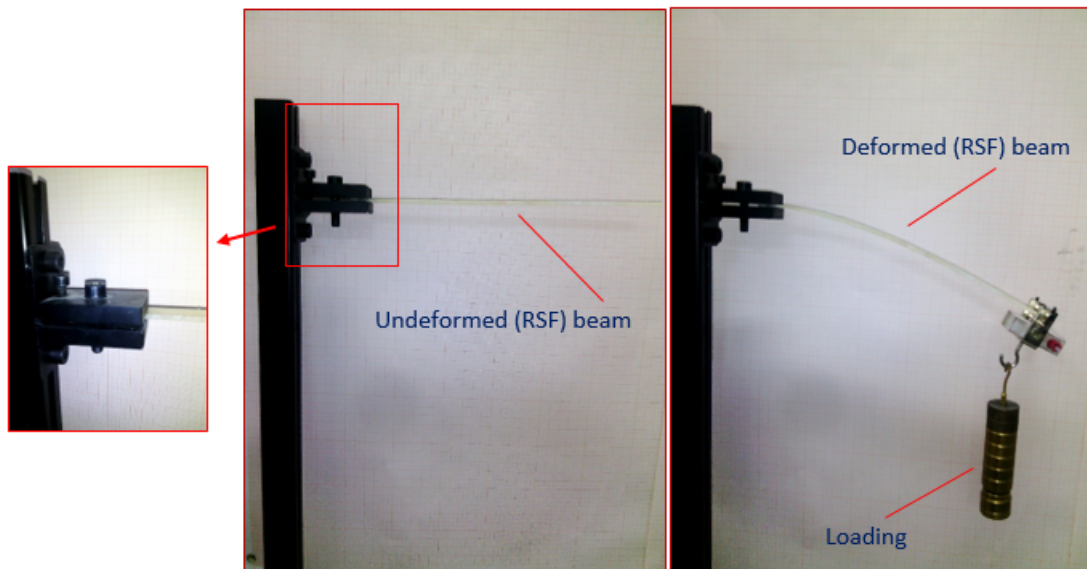


Figure 3.12: Bending experiments for **(RSF)** beams.

The accuracy of displacements measurement is one of the main problems that we can observe during the experiments. This is because the difficulties that can be appear when the beams behave in large deflection, especially the displacements measurement of the first part of loading. Also, It has been observed that during the loading when the beams move, the friction between the pencil at the tip of the beams and the graph paper may effect the displacements measurement. On the other hand, it has also been observed that the position of load also may effect the displacements measurement, because it is difficult to ensure the position of load with beam's neutral axis, especially with load increasing.

As result of all observations mentioned early, we have thought how to minimize experiments mistakes from the first side and how to improve the accuracy of displacements measurement from the other side. So, first we have been looking another alternative solution for **(GFP)** laminated specimens in order to optimize the displacements measurement. Therefore, the suggest idea is to measure the displacements by remote. So, we omitted the graph paper from the metallic stand and change it by a laser electronic telemeter.

It can be seen from Figure 3.13, two laser electronic telemeters with a precision of ($+or - 2mm$) were used for the new way of experiments. A vertical and horizontal metallic rods with a circular section were provided and fixed on a metallic stand. Then, Two metallic cubes with holes were used, in order to place the laser electronic telemeters on rods as well as make a vertical and an horizontal mechanism for displacements measurement, where we can move or fixe the telemeters by hand during the experiments, using a metallic bolt. Also, for loading a serie of different metallic masses whith a metallic axis are used. However, in this case, the metallic axis was hanged at the tip of specimens using a thread, where it was fixed by using a needle during the preparation of specimens. It can be observed that the laser light pass through the specimens because the transparency of laminates, and to avoid this problem a white paper was pasted at the tip of each specimen to insure laser light point from the vertical telemeter. First, the beams were accuratly fixed from one end in the stand using a metallic bolt and loaded from the free end. Then before loading the horizontal and the vertical distances between the laser

telemeters and the tip of beams were measured as a references for displacements measurement. The next step was the loading by hand, where the vertical telemeter was moved carefully until we make sure that laser light point on white paper at the tip of specimens then we measure the vertical and the horizontal distances.

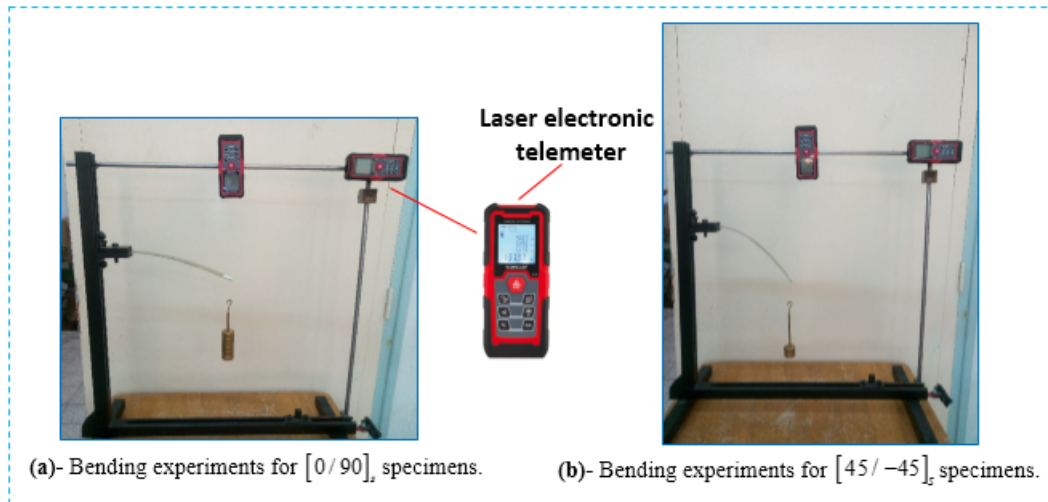


Figure 3.13: Bending experiments for (GFP) laminated beams.

3.4 Experiments Results

In this section, the experimental results from the bending experiments of all materials under consideration in this study are presented. First, the results of (PG)specimens are described and commented. The measured horizontal and vertical displacements u and w are plotted versus the tip load. Note that, these displacements are measured at the tip of beams and that u is actually negative for these experiments.

Figure 3.14, shows the obtained displacements u and w for four (**PG**) specimens subjected to tip concentrated load. From Figure 3.14, we can see clearly that w is quasi-linear. However, u is started small and tends to be curve as load increasing.

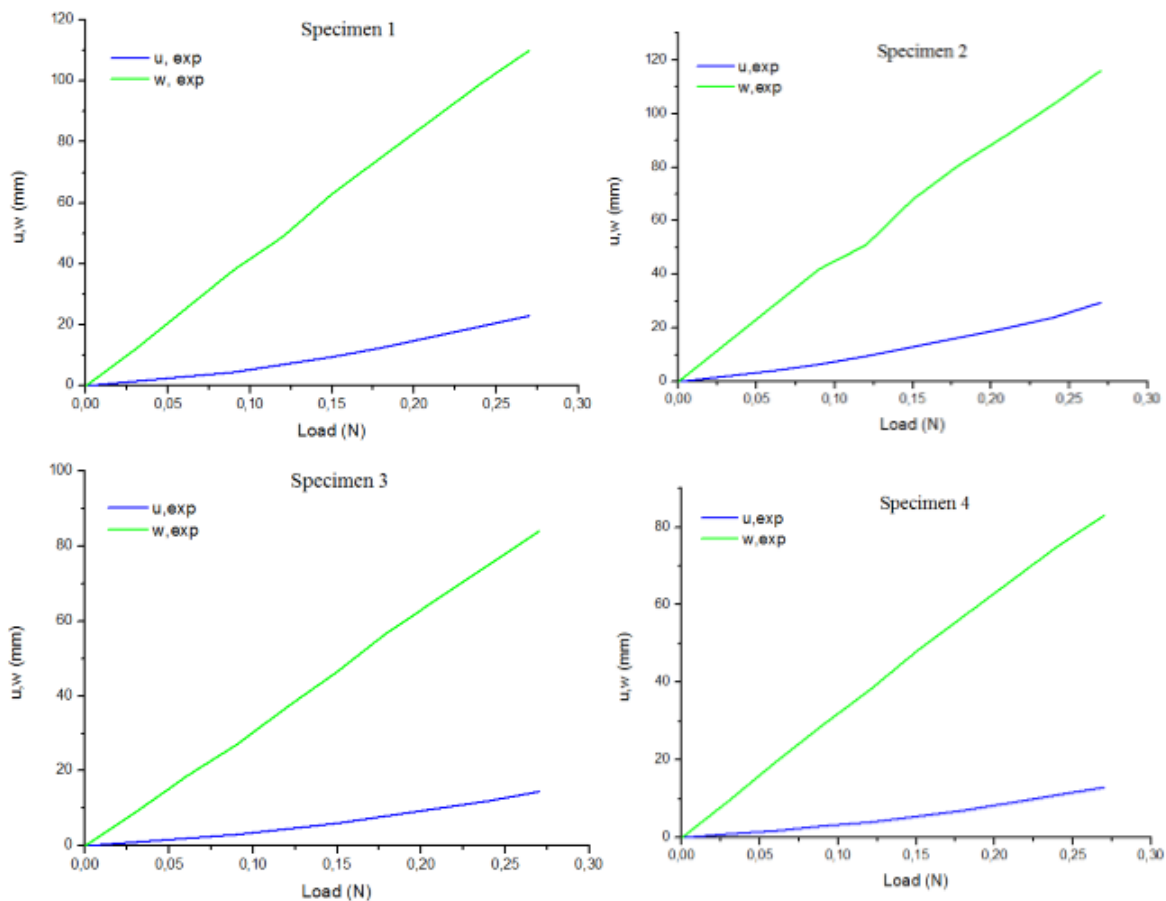


Figure 3.14: Experimental tip displacements for (**PG**) specimens.

Concerning the results of the second group of specimens Figure 3.15, plots displacements curves obtained for six (**RSF**) specimens versus the tip load. As mentioned early, twelve (**RSF**) specimens were prepared for these experiments. However, here we present just the results of six specimens. Thus, from these curves it can be seen that all of them show a similar plot. The behavior for w presents a small initial linear part and start to be an organized curve with load increasing. Also, u shows initially small linear part and tends to be curve in parallel with w .

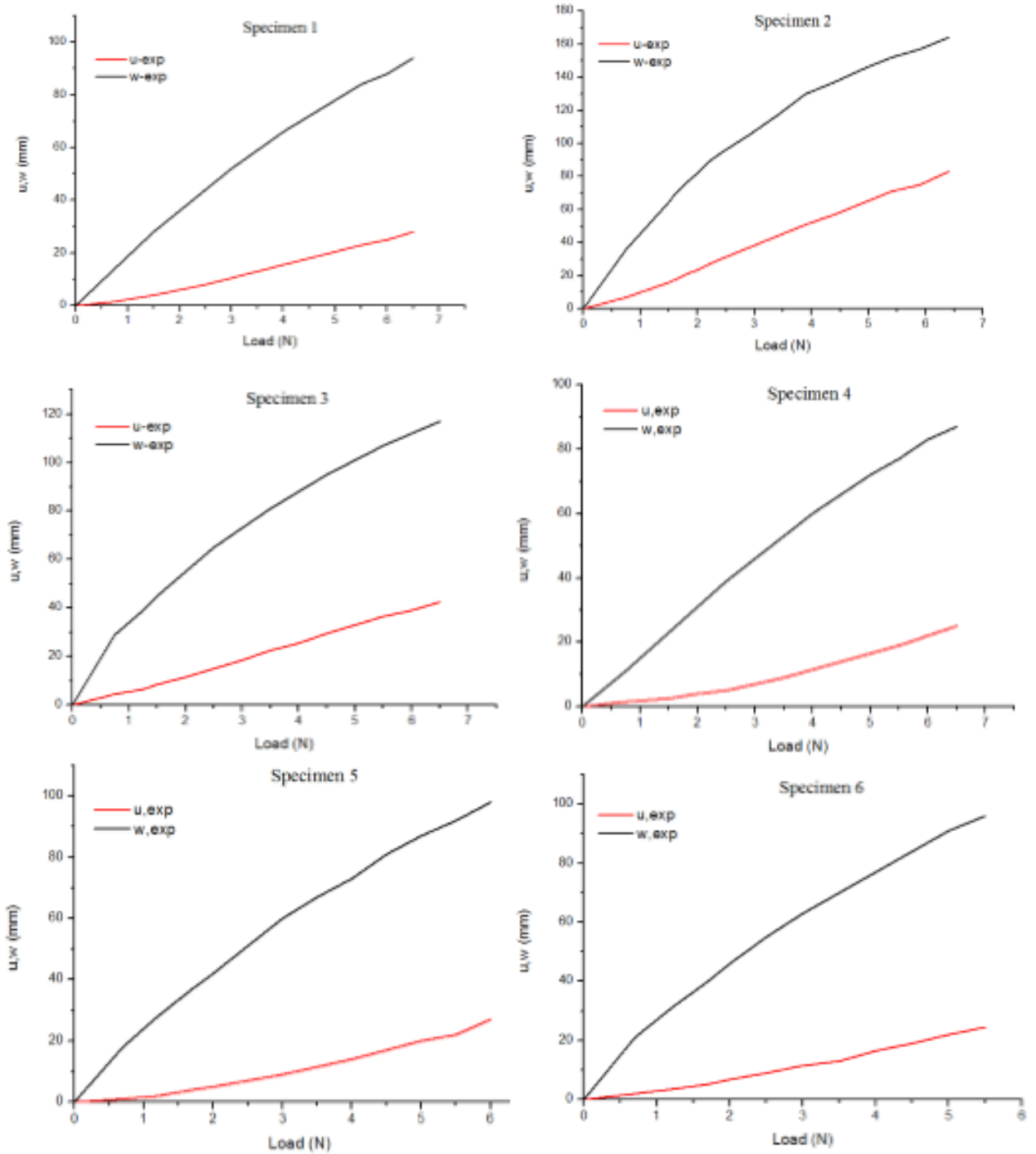


Figure 3.15: Experimental tip displacements for (RSF) specimens.

For the resulting plot of the last group of specimens, Figure 3.16, shows the obtained displacements u, w curves for four (**GFP**) laminate specimens with different fiber orientations. Regarding the first and the second $[0/90/90/0]$ laminated specimens, the curves shows that the initial behavior for w is fairly linear and tends to be disorganized curve with load increasing, this is because the new way of displacements measurement and the difficulties that can appear during setting laser electronic telemeters especially for the first ones. u is initially very small and the tip of beams starts moving on towards the root when significant bending slopes are obtained. However, for the third $[45/-45/-45/45]$ laminated specimen the curves demonstrate an improvement in displacements measurement especially for u . Concerning the last specimen $[0/90/90/0]$ the curves show more improvements for both displacements u, w .

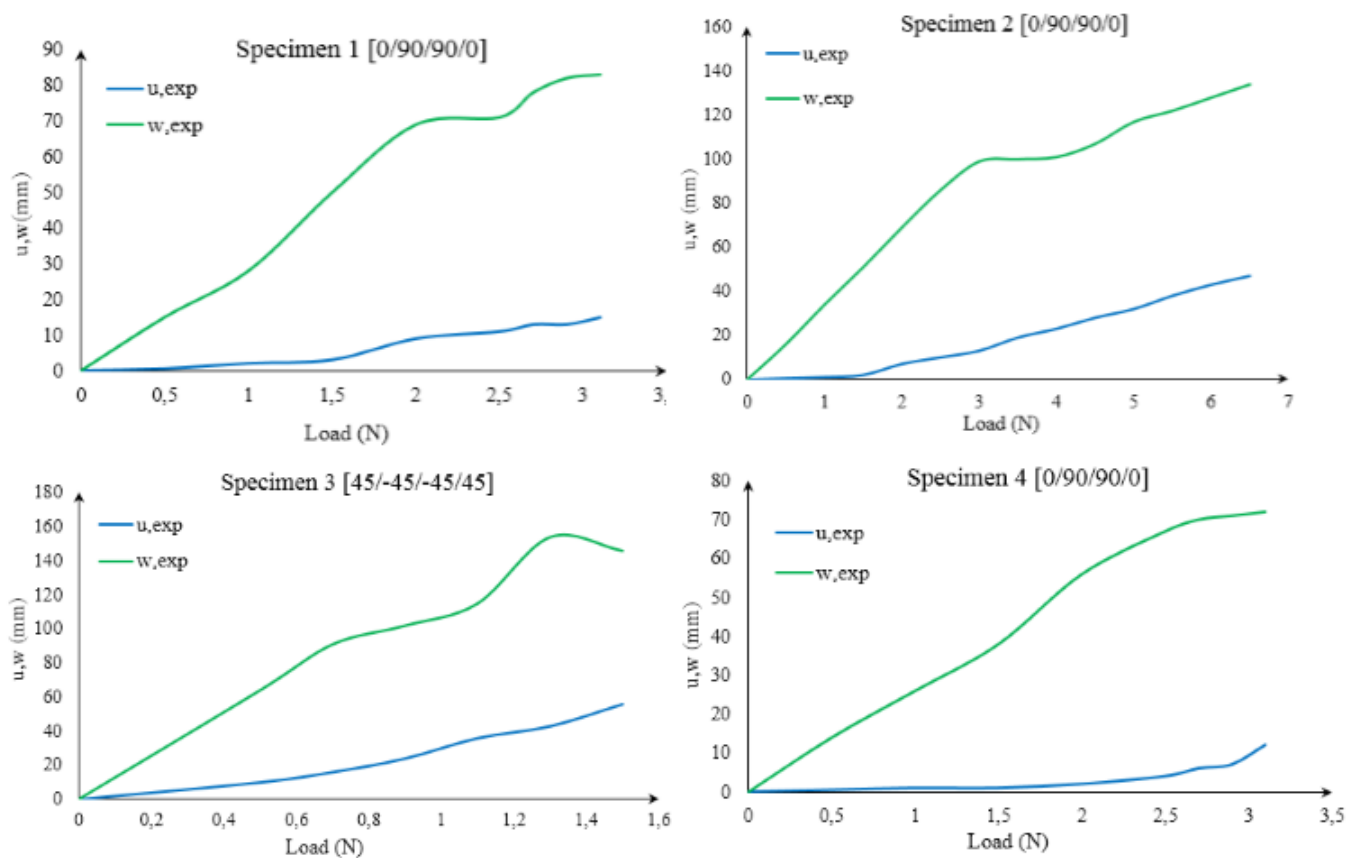


Figure 3.16: Experimental tip displacements for (**GFP**) specimens.

3.5 Conclusion

Several bending experiments were carried out on isotropic and composite cantilever beams in the present experimental program. An isotropic (**PG**), composite (**RSF**) and (**GFP**) laminated specimens were used in this investigation. In addition, the properties of used materials were measured through a series of static tensile tests. Furthermore, a calcination was carried out to define more properties. In the following, the important points that can be concluded from these experiments.

- It has been shown that the curves for (**PG**)specimens group the vertical displacement is quasi-linear. However, the horizontal displacement is started small and tends to be curve as load increasing.
- Concerning the second group of (**RSF**) specimens, the behavior presented a small initial linear part for the vertical displacement and it started to be an organized curve with load increasing. The horizontal displacement has shown initially small linear part and tends to be curve in parallel with the vertical displacement.
- Regarding the first and the second $[0/90/90/0]$ (**GFP**) laminated specimens, the curves shows that the initial behavior for w is fairly linear and tends to be disorganized curve with load increasing, this is because the new way of displacements measurement and the difficulties that can appear during setting laser electronic telemeters especially for the first ones. The horizontal displacement is initially very small and the tip of beams starts moving on towards the root when significant bending slopes are obtained. However, for the third $[45/-45/-45/45]$ laminated specimen the curves demonstrate an improvement in displacements measurement especially for u . Concerning the last specimen $[0/90/90/0]$ the curves show more improvements for both displacements u, w .

Chapter4

Analytical Model for Composite Beams

4.1 Introduction

In this chapter, an analytical formulation has been carried out to analyze the large deflection of composite beams. The proposed formulation is based on the elastica beam model, according to the classical Euler-Bernoulli beam theory, which is prepared to be able to dealing with symmetric and non-symmetric laminated beams. Subsequently, for the purpose of validation, it has been compared with both analytical models and experimental studies existing in the literature. Furthermore, for the sake of comparison, the present formulation has been also compared with the obtained results from the performed experiments in the previous chapter. Also, the varying parameters, such as fiber orientation angle, anisotropic ratio E_1/E_2 and slenderness ratio are examined to discover and understand their effect on the deflections variation of laminated beams.

4.2 Theoretical Approach

An analytical formulation has been carried out in order to analyze the large deflection of composite cantilever beam, subjected to point load applied at its free end. In rectangular coordinates (x, z) , the curvature of bent beam is given by the well known relation from analytical geometry by the following equation:

$$\frac{1}{\rho} = -\frac{\frac{d^2w}{dx^2}}{[1 + (\frac{dw}{dx})^2]^{\frac{3}{2}}} \quad (4.1)$$

Where ρ is the curvature radius.

Figure 4.1, depicts a deformed geometry of a cantilever beam in $x - z$ plane, which is deformed due to some loading, where Ψ is the rotation angle of any beam section.

We have also according to Figure 4.1, the relation

$$\frac{dw}{dx} = tg\Psi \quad (4.2)$$

By differentiating the right side of Eq(4.2) we can have

$$\frac{d}{dx}(tg\Psi) = \frac{\frac{d\Psi}{dx}}{\cos^2\Psi} = (1 + tg^2\Psi)\frac{d\Psi}{dx} \quad (4.3)$$

By substituting Eq(4.2) and Eq(4.3) into Eq(4.1), the curvature can be re-written as a function of Ψ as follows

$$\frac{1}{\rho} = -\cos\Psi\frac{d\Psi}{dx} \quad (4.4)$$

According to Figure 4.1, we can also have

$$\frac{1}{\rho} = \frac{d\Psi}{ds} \quad (4.5)$$

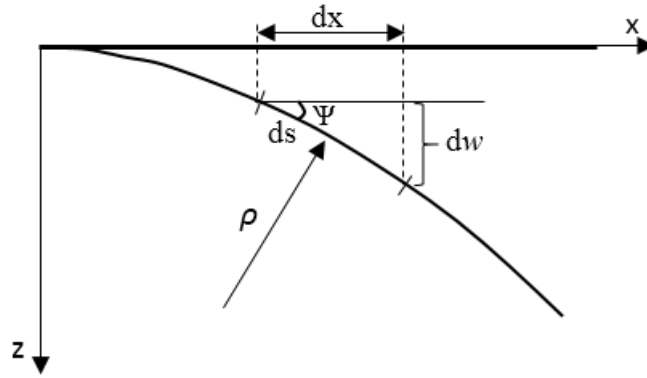


Figure 4.1: Deformed geometry of a cantilever beam.

While finitely the Euler-Bernoulli beam theory may be used in such practical problems, it will be essential and very popular when the the large deflection problem is studied. Neglecting shear deformation, the Euler-Bernoulli kinematics can be expressed in the following way.

$$u(x, z) = u_0(x) - \mathbf{z} \sin \Psi \quad (4.6)$$

$$w(x, z) = w_0(x)$$

Where u_0 and w_0 are the axial and transverse displacements of a point on the neutral axis. The strain-displacement relationship is given by

$$E_{xx} = \frac{du}{dx} = \frac{du_0}{dx} - \mathbf{z} \cos \Psi \frac{d\Psi}{dx} \quad (4.7)$$

From Eqs (4.4) and (4.5), Eq (4.7) can be rewritten as follows

$$E_{xx} = \frac{du_0}{dx} + \mathbf{z} \frac{d\Psi}{ds} \quad (4.8)$$

This expression can be rewritten as follows

$$E_{xx} = \varepsilon_{xx}^0 + \mathbf{z} K_s \quad (4.9)$$

4.2.1 Constitutive equations

The constitutive equations for an orthotropic k^{th} layer of a laminated in the local coordinate system (1,2,3) can be written in terms of stresses-strains relationships Figure 4.2, as follows

$$\begin{Bmatrix} \sigma_{11}^k \\ \sigma_{22}^k \\ \sigma_{12}^k \end{Bmatrix} = \begin{bmatrix} Q_{11}^k & Q_{12}^k & 0 \\ Q_{12}^k & Q_{22}^k & 0 \\ 0 & 0 & Q_{66}^k \end{bmatrix} \begin{Bmatrix} E_{11}^k \\ E_{22}^k \\ E_{12}^k \end{Bmatrix} \quad (4.10)$$

Where subscripts 1 and 2 indicate the fibers direction and in-plane transverse to the fibers direction, respectively; subscript 3 is the direction normal to the plate Figure 4.2. The reduced stiffness components are given by

$$\begin{aligned} Q_{11}^k &= \frac{E_1^k}{1 - \nu_{12}^k \nu_{21}^k} \\ Q_{22}^k &= \frac{E_2^k}{1 - \nu_{12}^k \nu_{21}^k} \\ Q_{12}^k &= \frac{\nu_{21}^k E_1^k}{1 - \nu_{12}^k \nu_{21}^k} \\ Q_{66}^k &= G_{12}^k \end{aligned}$$

This equation can be rewritten as follows

$$\left\{ \sigma^k \right\} = \left[Q^k \right] \left\{ E^k \right\} \quad (4.11)$$

In the material coordinates (X, Y, Z) , the constitutive equations of each layer can be given by

$$\begin{Bmatrix} \sigma_{xx}^k \\ \sigma_{yy}^k \\ \sigma_{xy}^k \end{Bmatrix} = \begin{bmatrix} \bar{Q}_{11}^k & \bar{Q}_{12}^k & \bar{Q}_{16}^k \\ \bar{Q}_{12}^k & \bar{Q}_{22}^k & \bar{Q}_{26}^k \\ \bar{Q}_{16}^k & \bar{Q}_{26}^k & \bar{Q}_{66}^k \end{bmatrix} \begin{Bmatrix} E_{xx}^k \\ E_{yy}^k \\ E_{xy}^k \end{Bmatrix} \quad (4.12)$$

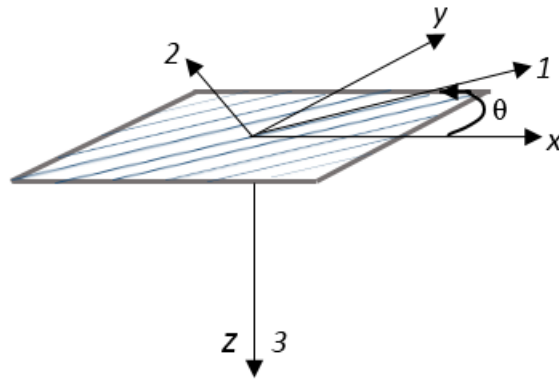


Figure 4.2: A lamina with reference axes (X, Y, Z) and fiber axes $(1, 2, 3)$.

This equation can be rewritten as follows

$$\{\bar{\sigma}^k\} = [\bar{Q}^k] \{\bar{E}^k\} \quad (4.13)$$

Where

$$\{\bar{\sigma}^k\} = \begin{Bmatrix} \sigma_{xx}^k \\ \sigma_{yy}^k \\ \sigma_{xy}^k \end{Bmatrix}, \quad \{\bar{E}^k\} = \begin{Bmatrix} E_{xx}^k \\ E_{yy}^k \\ E_{xy}^k \end{Bmatrix} \quad (4.14)$$

And

$$[\bar{Q}^k] = [T]^{-1}[Q^k][T] \quad (4.15)$$

$[T]$ is the transformation matrix

$$[T] = \begin{bmatrix} c^2 & s^2 & 2cs \\ s^2 & c^2 & -cs \\ -2cs & 2cs & c^2 - s^2 \end{bmatrix} \quad (4.16)$$

The components \bar{Q}_{ij}^k are the stiffness coefficients of a layer in the global coordinates system (X, Y, Z) of the laminate forming an angle θ with the local coordinates system of the lamina, with $c = \cos\theta$ and $s = \sin\theta$. θ is the fiber orientation angle with respect to material coordinates system.

The stiffness coefficients are given by the following

$$\begin{aligned} \bar{Q}_{11}^k &= Q_{11}^k c^4 + Q_{22}^k s^4 + 2(Q_{12}^k + 2Q_{66}^k) s^2 c^2 \\ \bar{Q}_{22}^k &= Q_{11}^k s^4 + Q_{22}^k c^4 + 2(Q_{12}^k + 2Q_{66}^k) s^2 c^2 \\ \bar{Q}_{12}^k &= (Q_{11}^k + Q_{22}^k - 4Q_{66}^k) s^2 c^2 + Q_{12}^k (s^4 + c^4) \\ \bar{Q}_{66}^k &= (Q_{11}^k + Q_{22}^k - 2Q_{12}^k - 2Q_{66}^k) s^2 c^2 + Q_{66}^k (s^4 + c^4) \\ \bar{Q}_{16}^k &= (Q_{11}^k - Q_{12}^k - 2Q_{66}^k) s c^3 - (Q_{11}^k - Q_{12}^k - 2Q_{66}^k) s^3 c \\ \bar{Q}_{26}^k &= (Q_{11}^k - Q_{12}^k - 2Q_{66}^k) s^3 c - (Q_{11}^k - Q_{12}^k - 2Q_{66}^k) s c^3 \end{aligned} \quad (4.17)$$

In case of beams, and accordingly to Bernoulli theory, it may have the following equation

$$\sigma_{yy} = \sigma_{xy} = 0 \quad (4.18)$$

This may lead to have the following equation

$$\sigma_{xx}^k = \bar{Q}_{eq}^k \mathbf{E}_{xx}^k \quad (4.19)$$

Where the equivalent stiffness coefficient of a layer is expressed as

$$\bar{Q}_{eq}^k = \bar{Q}_{11}^k + \bar{Q}_{12}^k \left[-\frac{\bar{Q}_{12}^k \bar{Q}_{66}^k - \bar{Q}_{16}^k \bar{Q}_{26}^k}{\bar{Q}_{22}^k \bar{Q}_{66}^k - (\bar{Q}_{26}^k)^2} \right] + \bar{Q}_{16}^k \left[-\frac{\bar{Q}_{16}^k}{\bar{Q}_{66}^k} \right] - \bar{Q}_{26}^k \left[-\frac{\bar{Q}_{66}^k \bar{Q}_{12}^k + \bar{Q}_{26}^k \bar{Q}_{16}^k}{\bar{Q}_{66}^k (\bar{Q}_{22}^k \bar{Q}_{66}^k - (\bar{Q}_{26}^k)^2)} \right] \quad (4.20)$$

4.2.2 Resultant efforts

By integrating the stress through the thickness, the force and moment resultants are obtained as follows

$$N = \int_{-\frac{h}{2}}^{\frac{h}{2}} \sigma_{xx} \cdot dz = \sum_{k=1}^{k=n} \left(\int_{z^k}^{z^{k+1}} \bar{Q}_{eq}^k \cdot \mathbf{E}_{xx} dz \right) \quad (4.21)$$

$$N = \sum_{k=1}^{k=n} \int_{z^k}^{z^{k+1}} \bar{Q}_{eq}^k \left(\varepsilon_{xx}^0 - \mathbf{z} \frac{d\Psi}{ds} \right) dz = \sum_{k=1}^{k=n} \left(\int_{z^k}^{z^{k+1}} \bar{Q}_{eq}^k \cdot \varepsilon_{xx}^0 dz \right) - \sum_{k=1}^{k=n} \left(\int_{z^k}^{z^{k+1}} \bar{Q}_{eq}^k \cdot \mathbf{z} \frac{d\Psi}{ds} dz \right) \quad (4.22)$$

The force resultant can be written

$$N = A \cdot \varepsilon_{xx}^0 + B \cdot K_s \quad (4.23)$$

$$M = \int_{-\frac{h}{2}}^{\frac{h}{2}} \sigma_{xx} \cdot \mathbf{z} dz = \sum_{k=1}^{k=n} \left(\int_{z^k}^{z^{k+1}} \bar{Q}_{eq}^k \cdot \mathbf{E}_{xx} \mathbf{z} dz \right) \quad (4.24)$$

$$M = \sum_{k=1}^{k=n} \int_{z^k}^{z^{k+1}} \bar{Q}_{eq}^k z \left(\varepsilon_{xx}^0 - \mathbf{z} \frac{d\Psi}{ds} \right) dz = \sum_{k=1}^{k=n} \left(\int_{z^k}^{z^{k+1}} \bar{Q}_{eq}^k \cdot \varepsilon_{xx}^0 \mathbf{z} dz \right) - \sum_{k=1}^{k=n} \left(\int_{z^k}^{z^{k+1}} \bar{Q}_{eq}^k \cdot \mathbf{z}^2 \frac{d\Psi}{ds} dz \right) \quad (4.25)$$

The moment resultant can be written

$$M = B.\varepsilon_{xx}^0 + D.K_s \quad (4.26)$$

Where n is the layers number, with A, B and D are the extensional, coupling and bending rigidity scalars, respectively, and are defined as

$$A = \sum_{k=1}^{k=n} \bar{Q}_{eq}^k (h_k - h_{k-1}) \quad (4.27)$$

$$B = \frac{1}{2} \sum_{k=1}^{k=n} \bar{Q}_{eq}^k (h_k^2 - h_{k-1}^2) \quad (4.28)$$

$$D = \frac{1}{3} \sum_{k=1}^{k=n} \bar{Q}_{eq}^k (h_k^3 - h_{k-1}^3) \quad (4.29)$$

4.2.3 Neutral axis position change

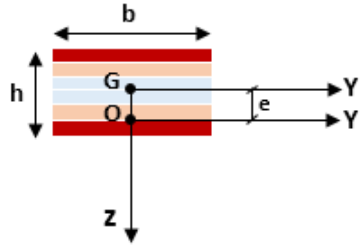


Figure 4.3: Neutral axis positions.

When the asymmetric laminated section is considered, the neutral axis is not located at the middle of the beam section as shown in Figure 4.3, which this shift between them is expressed by the coupling rigidity. For purpose omitting the coupling rigidity and in order to determine the position of the neutral axis, a new coordinate system $z' = z - e$ is considered as follows

$$x = x'$$

$$z = z' + e$$

Where e is the distance between the median axis of the beam section and the neutral axis, Figure 4.3

Then, to calculate the distance, the coupling rigidity with respect to axis z' must be 0

$$B' = \sum_{k=1}^n \int_{z'_{k-1}}^{z'_k} Q_{eq}^k z' dz' = 0 \quad (4.30)$$

$$B' = \sum_{k=1}^n \int_{z'_{k-1}}^{z'_k} Q_{eq}^k (\mathbf{z} - e) dz = \sum_{k=1}^n \int_{z'_{k-1}}^{z'_k} Q_{eq}^k \mathbf{z} dz - \sum_{k=1}^n \int_{z'_{k-1}}^{z'_k} Q_{eq}^k \cdot e dz = 0 \quad (4.31)$$

$$B' = B - eA \quad (4.32)$$

This leads to

$$e = \frac{B}{A} \quad (4.33)$$

Once e is determined, the new bending stiffness with respect to z' can be given by

$$D' = \sum_{k=1}^n \int_{z'_{k-1}}^{z'_k} Q_{eq}^k z'^2 dz' = \frac{1}{3} \sum_{k=1}^n Q_{eq}^k [(h_k - e)^3 - (h_{k-1} - e)^3] \quad (4.34)$$

4.2.4 Cantilever beam with tip concentrated load

Laminated cantilever beam, subjected to a concentrated load P at the free end, is shown on Figure 4.4. To determine the horizontal and vertical displacements Δ_x and Δ_z respectively of the free end of the beam, the bending moment-curvature relation is used. [45].

Relation is given by

$$D' \frac{d\Psi}{ds} = -M(x) \quad (4.35)$$

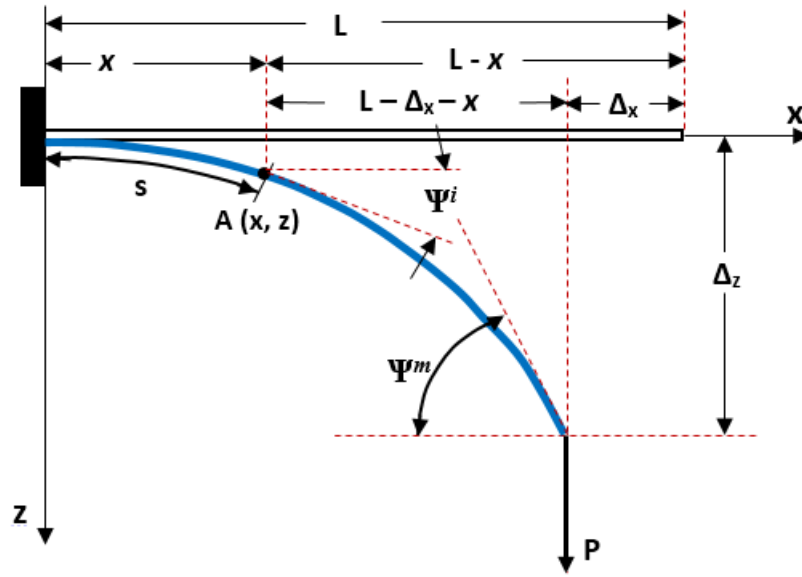


Figure 4.4: Schematic view of a cantilever.

$M(x)$ is the bending moment at location x , which can be expressed as

$$M(x) = -P(L - \Delta_x - x) \quad (4.36)$$

The derivation of Eq.(4.35) with respect to s , yields to

$$D' \frac{d^2 \Psi}{ds^2} = -\frac{dM(x)}{ds} \quad (4.37)$$

Substituting the bending moment expression in Eq.(4.37) we can have

$$D' \frac{d^2 \Psi}{ds^2} = P \cos \Psi \quad (4.38)$$

Multiplying the above Eq. by $\frac{d\Psi}{ds}$ we can have

$$D' \frac{d^2 \Psi}{ds^2} \frac{d\Psi}{ds} + P \cos \Psi \frac{d\Psi}{ds} = 0 \quad (4.39)$$

Integrating Eq.(4.39), can be re-written in the following form

$$\frac{d}{ds} \left[\frac{1}{2} D' \left(\frac{d\Psi}{ds} \right)^2 + P \sin \Psi \right] = 0 \quad (4.40)$$

Integrating Eq.(4.40) and evaluating the constant of integration by using the following boundary conditions $(d\Psi/ds) = 0$ and $(\Psi = \Psi^m)$ at $(s = L)$, which Ψ^m the unknown quantity at free-end, Figure 4.4.

Eq (4.40) becomes

$$\left(\frac{d\Psi}{ds}\right)^2 = \frac{2}{D'}(P\sin\Psi^m - P\sin\Psi) \quad (4.41)$$

By integrating Eq.(4.41), assuming that the beam's length will not change during bending, we can have

$$\sqrt{\frac{2P}{D'}} \int_0^L ds = \int_0^{\Psi^m} \sqrt{\sin\Psi^m - \sin\Psi} d\Psi \quad (4.42)$$

So we can have the expression which makes it possible to obtain the value of the rotation of the free end of the beam Ψ^m

$$L = \sqrt{\frac{D'}{2P}} \int_0^{\Psi^m} \frac{d\Psi}{\sqrt{\sin\Psi^m - \sin\Psi}} \quad (4.43)$$

Once the rotation angle Ψ^m is obtained, the horizontal and vertical displacements Δ_x and Δ_z can be calculated by using the following equations

$$\Delta_x = L - 2\sqrt{\frac{D'}{2P}}[\sin\Psi^m] \quad (4.44)$$

$$\Delta_z = \sqrt{\frac{D'}{2P}} \int_0^{\Psi} \frac{\sin\Psi d\Psi}{\sqrt{\sin\Psi^m - \sin\Psi}} \quad (4.45)$$

4.3 Simpson's Rule

Simpson's rule is one of the most commonly used numerical method to approximate the value of a definite integral using quadratic polynomials. It is used primarily for cases where exact integration is very difficult or impossible to obtain [4, 220]. Of these, it has been used in order to solving Eqs (4.44) and (4.45).

Consider,for example, the integral

$$\int_a^b f(x)dx \quad (4.46)$$

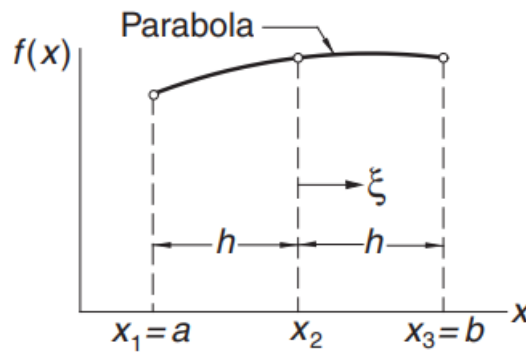


Figure 4.5: Simpson's 1/3 rule [220].

Simpson's 1/3 rule can be obtained by passing a parabolic interpolant through three adjacent nodes, as shown in Figure 4.5. The area under the parabola, which represents an approximation of Eq (4.46), is

$$I = \frac{h}{3} \left[f(a) + 4f\left(\frac{a+b}{2}\right) + f(b) \right] \quad (4.47)$$

To obtain the composite Simpson's 1/3 rule, the integration range (a, b) is divided into $n - 1$ panels of width $h = (b - a)/(n - 1)$ each, as indicated in figure 4.6.

Applying Eq(4.47) to two adjacent panels, we have

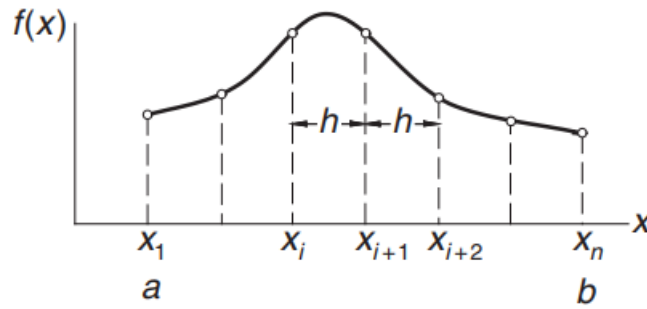


Figure 4.6: Composite Simpson's 1/3 rule [220].

$$\int_{x_i}^{x_{i+2}} f(x)dx \approx \frac{h}{3}[f(x_i) + 4f(x_{i+1}) + f(x_{i+2})] \quad (4.48)$$

Substituting Eq(4.48)into the following Eq

$$\int_a^b f(x)dx = \int_{x_1}^{x_n} f(x)dx = \sum_{i=1,3,\dots}^{n-1} \left[\int_{x_i}^{x_{i+2}} f(x)dx \right] \quad (4.49)$$

yields

$$\int_a^b f(x)dx \approx I = \frac{h}{3}[f(x_1) + 4f(x_2) + 2f(x_3) + 4f(x_4) + \dots \quad (4.50)$$

$$\dots + 2f(x_{n-2}) + 4f(x_{n-1}) + f(x_n)]$$

4.4 Validation of the Analytical Formulation

In order to validate the analytical formulation, three different tests of cantilever beams are considered in this section. The present examples are compared with the available analytical approaches from the literature for isotropic and composite cantilever beams. Furthermore, for the sake of confrontation, the present formulation has been also compared with the obtained results from the performed experiments in the previous chapter.

4.4.1 Isotropic cantilever beam subjected to tip concentrated load

An isotropic cantilever beam subjected to tip load is considered for the first case as illustrated in Figure 4.7. The horizontal and vertical deflections are computed for different load parameter value, where the obtained results are presented in Table 4.1. Figure 4.8, show the present analytical results compared with the analytical results obtained by Mattiasson [221] and Kumar et al. [47]. The curves show that the obtained results are clearly in excellent agreement with those results.

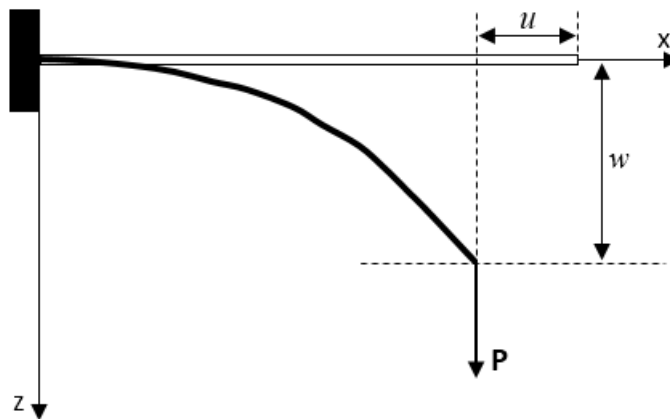


Figure 4.7: Cantilever beam subjected to tip load.

Table 4.1: Non-dimensional deflections as a function of load parameter for isotropic cantilever beam subjected to tip load.

$\frac{PL^2}{EI}$	Mattiasson		Kumar et al.		Present analytical	
	u	w	u	w	u	w
1	0,0564	0,3017	0,0566	0,3019	0,0812	0,3018
2	0,1606	0,4934	0,1616	0,4939	0,1616	0,4936
3	0,2544	0,6032	0,2554	0,6038	0,2453	0,6368
4	0,3289	0,6699	0,3292	0,6704	0,3117	0,6934
5	0,3876	0,7137	0,3882	0,7146	0,3767	0,7322
6	0,4345	0,7445	0,4423	0,7454	0,4273	0,7606
7	0,4729	0,7673	0,4821	0,7682	0,4679	0,7852
8	0,5048	0,7849	0,511	0,7861	0,5013	0,7971
9	0,5318	0,799	0,5428	0,803	0,5293	0,8118
10	0,555	0,8106	0,5621	0,8206	0,5531	0,8262

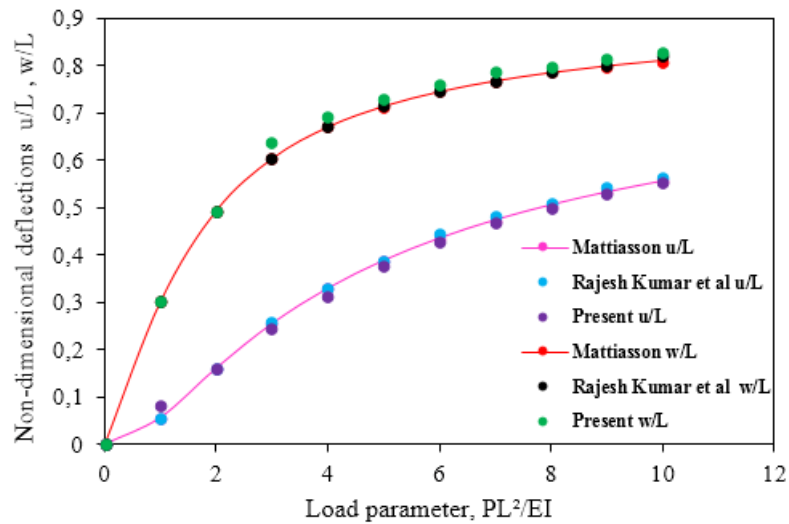


Figure 4.8: Non-dimensional deflections as a function of load parameter for isotropic cantilever beam subjected to tip load.

4.4.2 Composite cantilever beams subjected to tip concentrated load

Another two cases for composite laminated cantilever beams subjected to tip load are now presented. The second case considered for validation is a symmetric 12-layer cross-ply $[0/90]_{3s}$ cantilever beam of length $L = 550mm$, width $W = 30mm$, and thickness $t = 0.124mm$. The third case is an antisymmetric cantilever beam $[20/-70_2/20]_{2a}$ of length $L = 560mm$, width $W = 30mm$, and thickness $t = 0.134mm$. The mechanical properties of the material used, are as follows: $E_1 = 142GPa$, $E_2 = 9.8GPa$, $\nu_{12} = 0.3$ and $G_{12} = 6GPa$. The cantilever beam was loaded at free end, where the vertical and the horizontal displacements are measured at a distance $a = 50mm$ from the free end as shown in Figure 4.9.

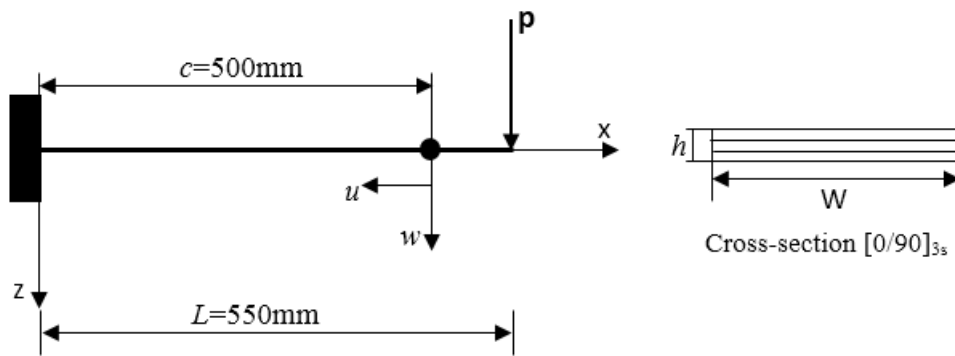


Figure 4.9: Laminated cantilever beam subjected to tip load.

Table 4.2 and Table 4.3, shows the horizontal and the vertical displacements obtained by the present analytical formulation with those obtained analytically and experimentally by Minguet et al. [62]. Figures 4.10 and 4.11, show the present analytical results compared with the experimental and the analytical results obtained by Minguet et al. [62]. The curves show that the results compare well for a symmetric beam. However, there are some differences in the results of vertical displacement in case of antisymmetric beam. The large deflection shapes of the symmetrical 12-layer cross-ply cantilever beam subjected to various vertical concentrated loads at free end respectively are shown in Figure 4.12.

Table 4.2: Analytical horizontal and vertical displacements of symmetric laminated $[0/90]_{3s}$ cantilever beam end.

Load (g)	Experimental [62]		Present analytical		Analytical [62]	
	u (mm)	w (mm)	u (mm)	w (mm)	u (mm)	w (mm)
77.58	2.81	50.56	3.86	47.61	2.8	47.75
103.44	4.77	68.1	2.68	63.91	5.61	61.79
146.55	8.02	94.91	4.55	89.47	11.23	89.88
202.58	19.66	125.01	14.35	116.7	18.25	117.97
405.17	58.8	206.46	50.55	201.2	57.58	202.24

Table 4.3: Comparison Analytical horizontal and vertical displacements of antisymmetric laminated $[20/-70_2/20]_{2a}$ cantilever beam end.

Load (g)	Experimental [62]		Present analytical		Analytical [62]	
	u (mm)	w (mm)	u (mm)	w (mm)	u (mm)	w (mm)
51.61	1.82	27.37	1.69	39.02	1.5	27.37
103.22	5.47	52.91	7.78	74.8	4.74	49.27
206.45	16.42	102.18	17.38	139.7	9.12	93.06
303.22	32.84	144.16	39.83	187.2	21.89	131.38
406.45	49.27	178.83	64.79	225.9	34.67	167.88
516.12	65.69	208.02	87.21	259.4	49.27	198.91

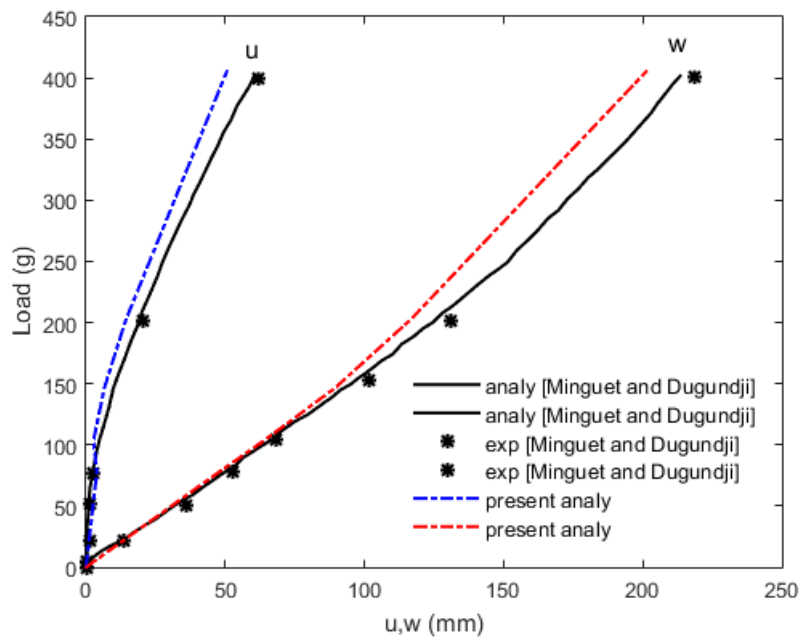


Figure 4.10: Load-displacement curves for a $[0/90]_{3s}$ cantilever beam.

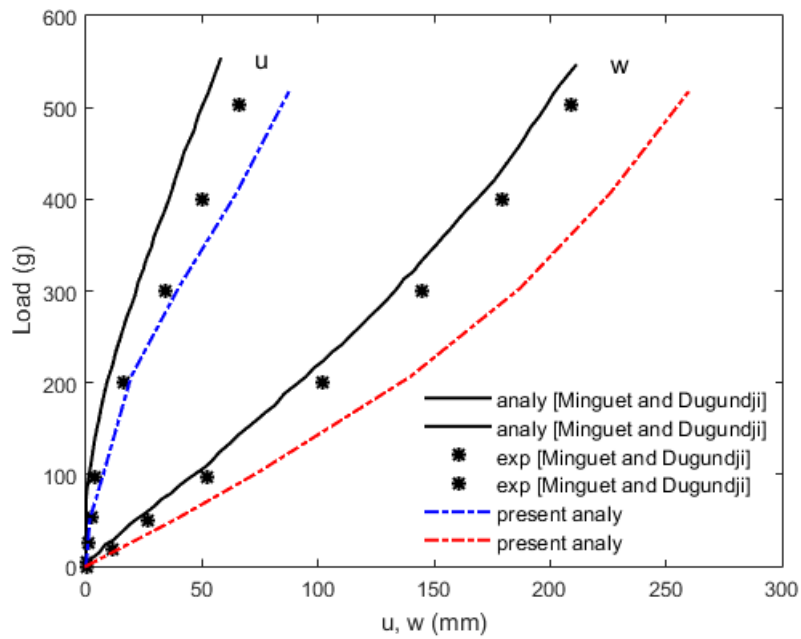


Figure 4.11: Load-displacement curves for a $[20/-70_2/20]_{2a}$ cantilever beam.

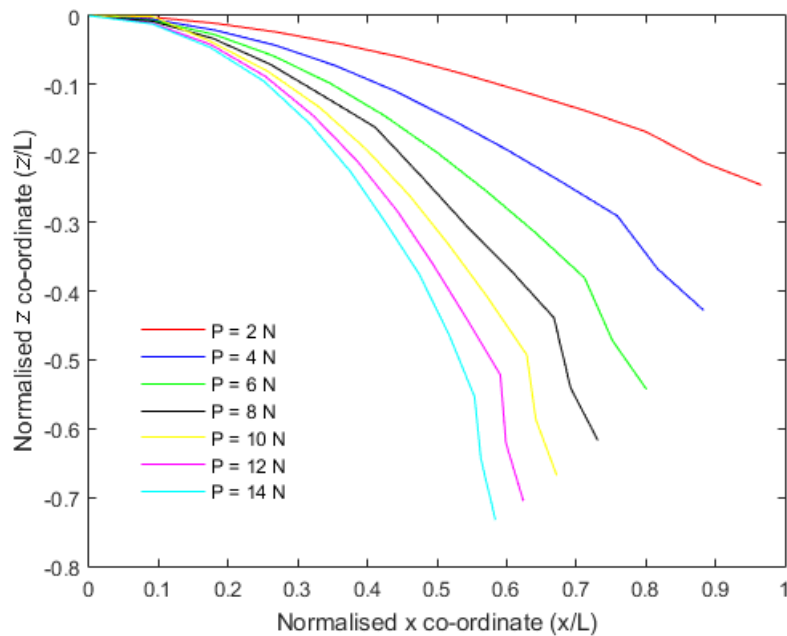


Figure 4.12: Deflection shape of a $[0/90]_{3s}$ cantilever beam for various loads.

4.4.3 Comparison with the current experimental large displacements of (PG) and (RSF) beams.

In the previous section, the analytical formulation has been validated by comparing the obtained results with those obtained analytically and experimentally in the literature. The formulation is preceded in the previous chapter by an experimental analysis of bending of (PG) and (RSF) beams, to determine the horizontal and the vertical displacements measured at the tip of the beams. For comparison purpose, the experimental results in terms of horizontal and vertical displacements and those obtained using the present analytical formulation for both (PG) and (RSF) beams, are presented in this section in. Table 4.4 and Table 4.5.

Figure 4.13, compares the horizontal and vertical displacements, of (PG) beam end, obtained experimentally and those obtained, using the present formulation. The curves, having the same paces, show the well agreement between the two approaches especially the horizontal displacement. Figure 4.14 depicts the comparison between the load-displacements curves of the analytical and the experimental analysis for (RSF) cantilever beam. It can be seen that the analytical curves are going well with the experimental ones.

Table 4.4: Horizontal and vertical displacements of (PG) cantilever beam end.

Load (N)	Present analytical		Present experimental	
	u (mm)	w (mm)	u (mm)	w (mm)
0.12	2.4	43	4	38
0.15	4.3	54.1	5.5	48
0.18	6	64.4	7	57
0.21	8	75	9	66
0.24	10.11	84.2	11	75
0.27	11.27	95	12.5	83

Table 4.5: Horizontal and vertical displacements of **(RSF)** cantilever beam end.

Load (N)	Present analytical		Present experimental	
	u (mm)	w (mm)	u (mm)	w (mm)
0.7	4.31	38.28	7	36
1.5	13.15	70.86	16	64.5
1.6	15.03	74.72	17.5	69
1.8	17.72	82.04	21	76
2	20.16	88.74	23.5	82
2.2	24.07	95.35	27	89
2.4	27.56	102.2	30	94
2.9	33.83	117.6	37	105
3.4	40.43	129.4	44	117
3.9	46.41	138.7	51	130
4.4	53.83	144.9	57	137
4.9	62.45	153.1	64	145
5.4	68.02	158.2	71	152
5.9	73.92	163.1	75	157
6.4	79.91	168.6	83	164

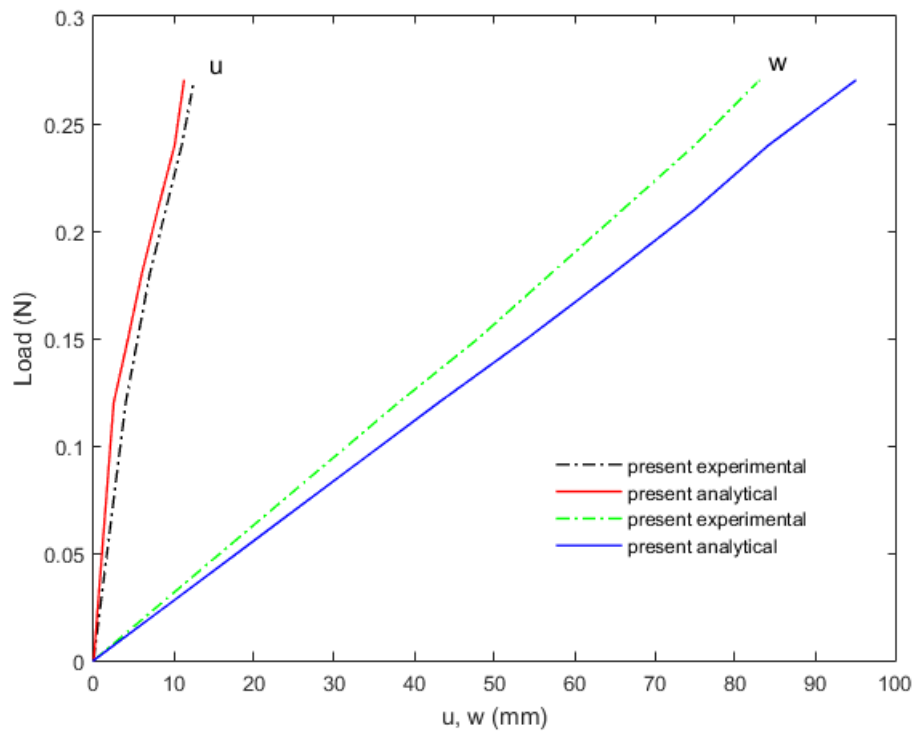


Figure 4.13: Load-displacements curves for a **(PG)** cantilever beam.

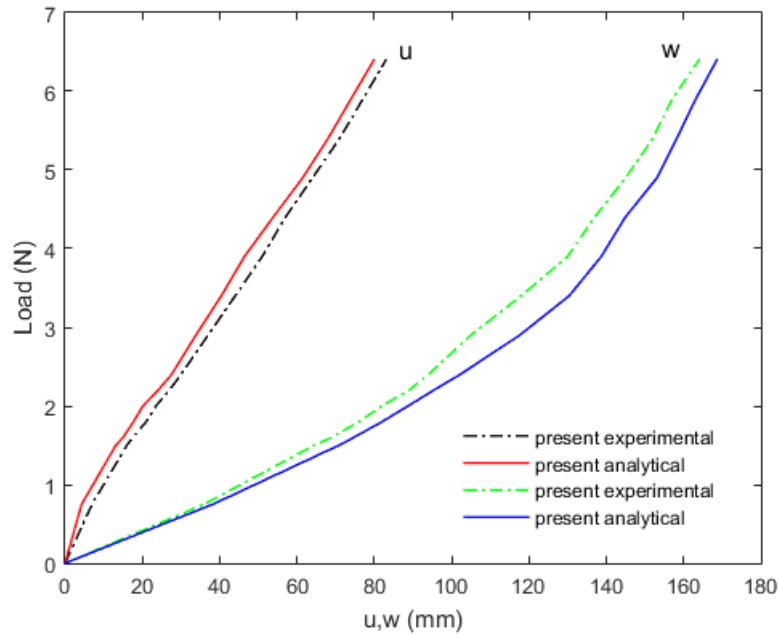


Figure 4.14: Load-displacements curves for a (RSF) cantilever beam.

4.5 Factors affecting large displacements variation

After validating the performance of the analytical formulation in the previous section, by comparing the obtained results with some analytical solutions available in the literature. This section is aimed to discover and understand the effect of fiber orientation angle, anisotropic ratio, slenderness ratio on the horizontal and the vertical displacements in symmetric and nonsymmetric laminated beams under tip load.

4.5.1 Effect of fiber orientation

For our examples here, the mechanical properties of the fabricated long glass fiber/polyester resin (GFP) laminates that were presented in the previous chapter are considered. A symmetric four layers $[\theta/ - \theta/ - \theta/\theta]$ and anti-symmetric eight layers $[\theta/ - \theta/\theta/ - \theta/\theta/ - \theta/\theta/ - \theta]$ cantilever beams under tip load are considered for the first two examples respectively. The horizontal and vertical displacements corresponding to fiber orientation angle ranging from 0° to 90° are shown in Figures 4.15 and 4.16 respectively.

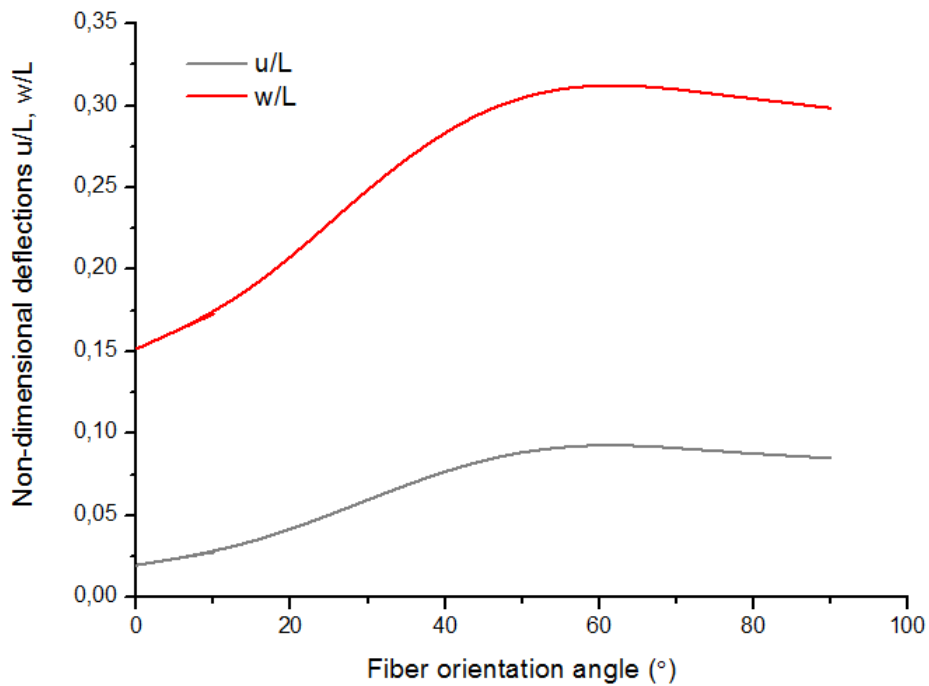


Figure 4.15: Effect of fiber orientation angle on non-dimensional deflections for a symmetric angle-ply (**GFP**) beam under tip load.

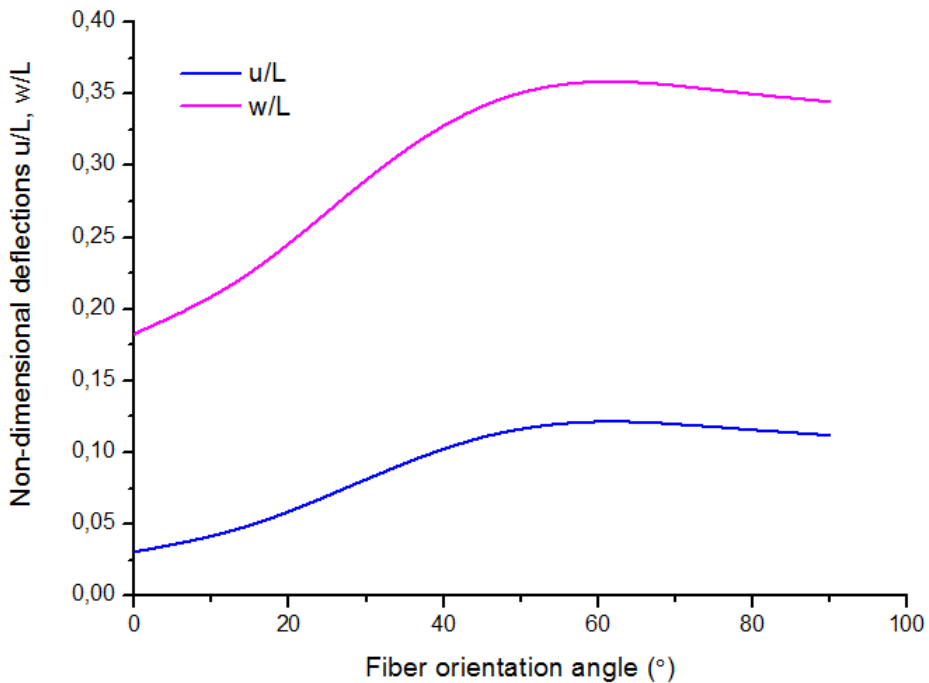


Figure 4.16: Effect of fiber orientation angle on non-dimensional deflections for antisymmetric angle-ply (**GFP**) beam under tip load.

As shown in Figures 4.15 and 4.16, we can see that the effect of fiber orientation angle on displacements is similar for both symmetric and anti-symmetric laminates. It is observed that with an increase in fiber orientation angle, there is an increase in deflections values until the angle $\theta = 45^\circ$ where the deflections reaches its maximum values, then it decrease slowly toward the angle $\theta = 90^\circ$, and we can also note that for $\theta = 0^\circ$ the deflections have the minimum value, which means that the beam's rigidity is at the maximum value.

4.5.2 Effect of degree of anisotropic

It has been found from our examples in the previous section that the deflection values vary as the fiber orientation changes. Additionally, the deflection values also change, depending on the ratio the elasticity modulus of the fiber direction to the transverse one, E_1/E_2 . Thus, the effect of modulus ratio E_1/E_2 on the deflection values on symmetric and antisymmetric angle-ply beams under tip load corresponding to fiber orientation angle ranging from 0° to 90° . The material proprieties in this study are $E_1 = 1\delta, E_2 = 1, G_{12} = 0.5, \nu_{12} = 0.25$, with δ ranging from 1 to 80. Consediring these examples, the effect of modulus ratio on non-dimensional deflection for a symmetric and antisymmetric angle-ply beam with various fiber orientation angles under tip load are presented in Figures 4.17 and 4.18, repectively.

As shown in Figures 4.17 and 4.18, both of symmetric and antisymmetric beams behave in a similar way. It is seen that, the deflection values are affected by the changes of E_1/E_2 when the fiber orientations are between 0° and 45° , the deflection decrease with the increase in modulus ratio until $E_1/E_2 = 30$ for 0° and $E_1/E_2 = 10$ for $15^\circ, 30^\circ, 45^\circ$ the deflection is not affected much by the increase in modulus ratio. However, when the angle values are $60^\circ, 75^\circ, 90^\circ$ the deflection values are not affected by the changes of modulus ratio.

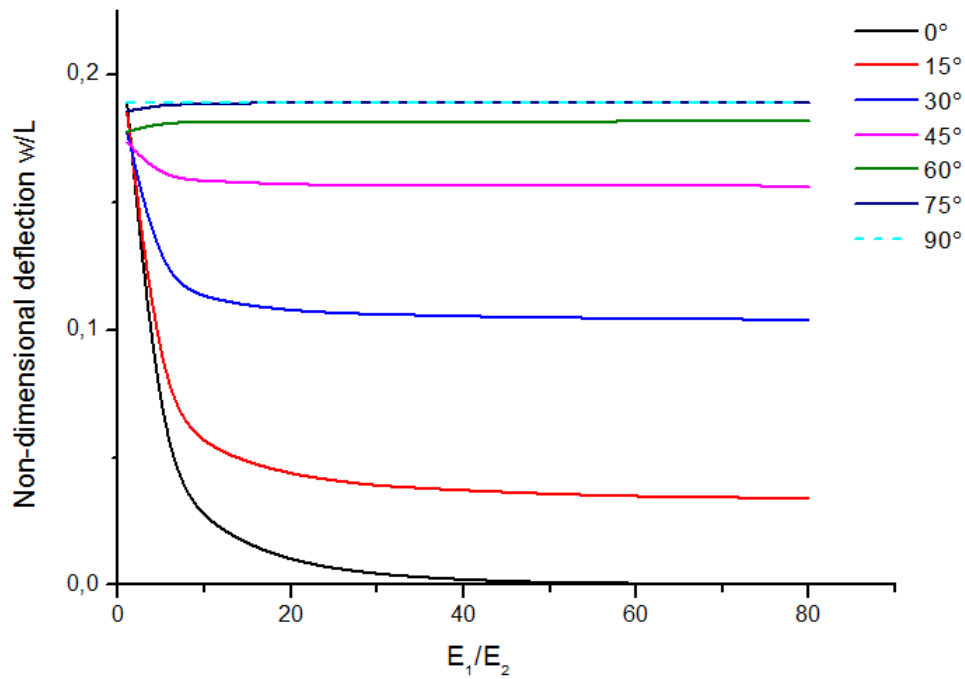


Figure 4.17: Effect of modulus ratio on non-dimensional deflections for a symmetric angle-ply beam with various fiber orientation angles under tip load.

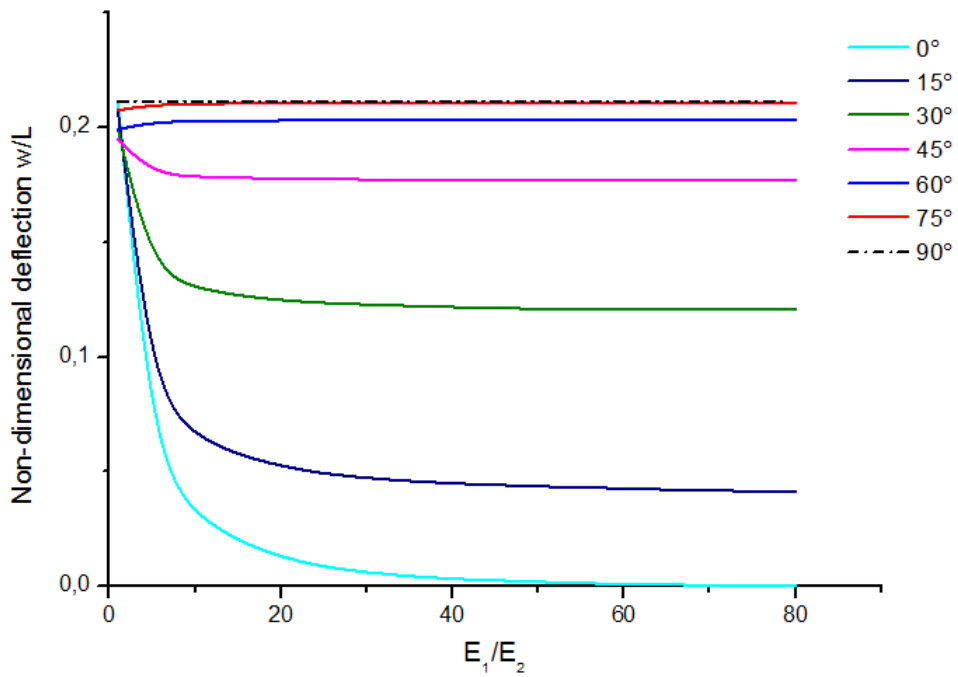


Figure 4.18: Effect of modulus ratio on non-dimensional deflections for antisymmetric angle-ply beam with various fiber orientation angles under tip load.

4.5.3 Effect of slenderness ratio

Another important parameter which can effect the behavior of the beams is the slenderness ratio. Different anisotropy ratio values are considered. A four (**GFP**) layers with a symmetric as well as antisymmetric angle-ply cantilever beams subjected to tip load are considered here for our two examples respectively. The anisotropy ratio E_1/E_2 values are ranging from 1 to 5. The effect of slenderness ratio on non-dimensional deflections values for laminated (**GFP**) cantilever beams under tip load are shown in Figures 4.19 and 4.20, for symmetric and antisymmetric angle-ply laminated beam respectively.

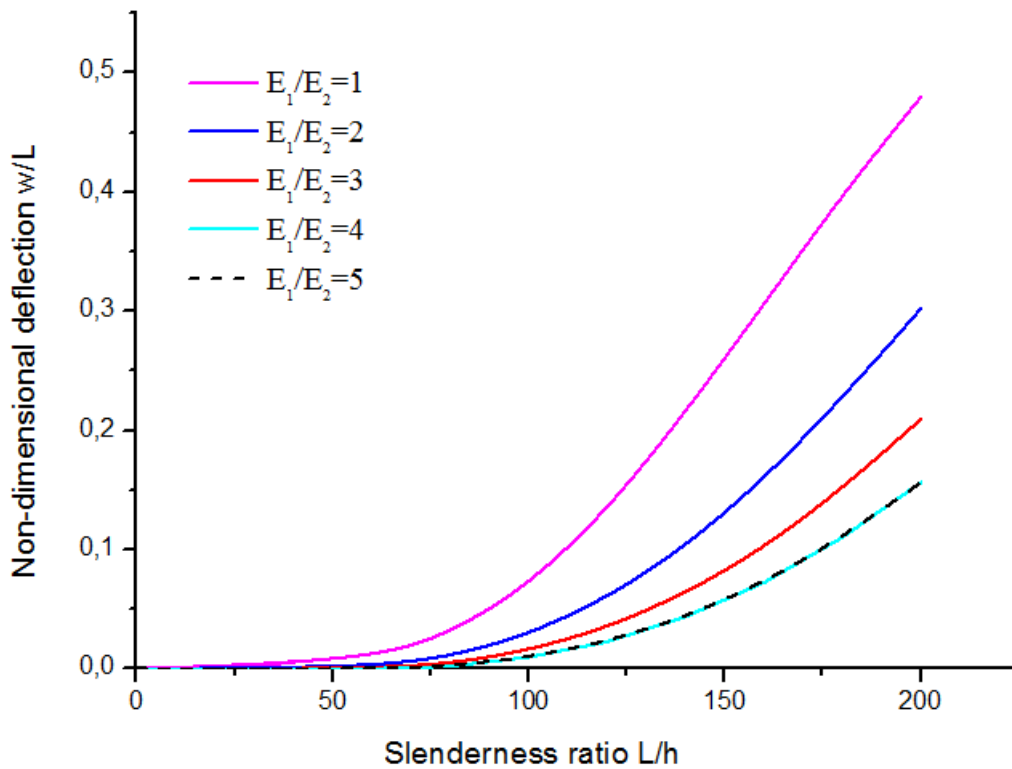


Figure 4.19: Effect of slenderness ratio on non-dimensional deflections for a symmetric angle-ply (**GFP**) beam under tip load with various orthotropy ratio values.

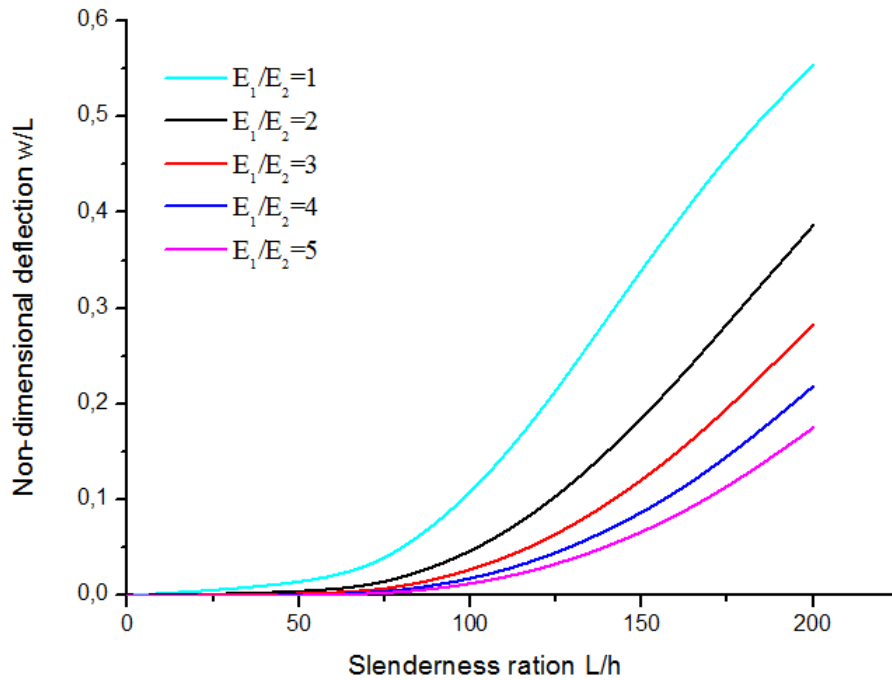


Figure 4.20: Effect of slenderness ratio on non-dimensional deflections for antisymmetric angle-ply (GFP) beam under tip load with various orthotropy ratio values.

Considering these two cases, we can note from both Figures 4.19 and 4.20, that the curves are consistent for all anisotropy ratio values. It is also observed that the deflections values increase with the increase of slenderness ratio, the deflections values also are increasing. Then, as shown in Figures, we can see that there is a decrease in deflection values with the increase in anisotropy ratio values.

4.6 Conclusion

An analytical formulation has been carried out in this chapter, to analyze the large deflection of composite beams. The proposed formulation is based on the elastica beam model, according to the classical Euler-Bernoulli beam theory, which is prepared to be able to dealing with symmetric and non-symmetric laminated beams. Subsequently, for the purpose of validation, the obtained results have been compared with both analytical models and experimental studies existing in the literature. It has been shown that for isotropic beam case the obtained results are clearly in excellent agreement with those obtained in the literature. Also, for symmetric

as well as antisymmetric laminated beams cases the results are compare well with those. Furthermore, for the sake of comparison, the present formulation has been also compared with the obtained results from the performed experiments in the previous chapter. It has been seen that the present analytical results are going well with the experimental ones. In addition, the varying parameters, such as fiber orientation angle, anisotropic ratio E_1/E_2 and slenderness ratio were examined to discover and understand their effect on the deflections variation of laminated beams. As result, some of the important observations from the parametric study are in the following points

- It has been seen, that the effect of fiber orientation angle on displacements is similar for both symmetric and antisymmetric laminates. It has been also observed that with an increase in fiber orientation angle, there is an increase in deflections values until the angle $\theta = 45^\circ$ where the deflections reaches its maximum values, then it decrease slowly toward the angle $\theta = 90^\circ$, and we can also note that for $\theta = 0^\circ$ the deflections have the minimum value, which means that the beam's rigidity is at the maximum value.
- It has been seen that, the deflection values are affected by the changes of E_1/E_2 when the fiber orientations are between 0 *degree* and 45° , the deflection decrease with the increase in modulus ratio until $E_1/E_2 = 30$ for 0° and $E_1/E_2 = 10$ for $15^\circ, 30^\circ, 45^\circ$ the deflection is not affected much by the increase in modulus ratio. However, when the angle values are $60^\circ, 75^\circ, 90^\circ$ the deflection values are not affected by the changes of modulus ratio.
- It has been observed, that the deflections values increase with the increase of slenderness ratio for different values of anisotropy ratio.

Chapter 5

Numerical Analysis of Nonlinear Bending of Beams

5.1 Introduction

In this chapter, one-dimensional finite element formulation based on the Euler-Bernoulli beam theory has been developed for the nonlinear bending analysis of symmetric and non-symmetric laminated beams. The present element has been defined by two nodes and three degree of freedom per node. The principle of total potential energy has been used for the derivation of stiffness and geometrical matrices. The direct iterative method has been used to solve the nonlinear equations. Subsequently, for the purpose of validation the present element has been compared with the available analytical models, experimental studies from the literature as well as the present analytical model presented in the previous chapter. In addition, a parametric study is presented in order to examine the effect of some parameters such as fiber orientation angle and slenderness ratio on the deflection variation of laminated beams with different boundary conditions.

5.2 Strain Tensor (Measures of Deformations)

The forces that act on a solid body produce its deformation. One of the basic problems in continuum mechanics is to describe, quantitatively, the deformation that the body undergoes. This is achieved by introduction of measures of deformations. Measures of deformation are based on geometrical quantities that describe deformation of the body. When the body is in motion, in general, its points experience displacement; that is, the position vector of an arbitrary particle changes, with respect to a fixed coordinate, system. One way to describe, quantitatively, the deformation at a given point, P , is to determine relative changes of length of linear elements originating at P as well as changes in the angle between any pair of linear elements originating at P . In differential geometry it is shown that the length of linear elements as well as the angle between them could be determined if the metric is known at a given point. Thus, to define measures of deformation we have to calculate the metric at P in the undeformed and deformed states and then compare those two metrics [222].

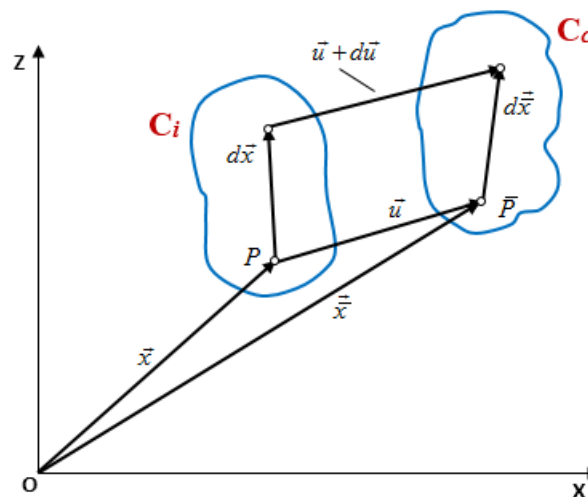


Figure 5.1: Transformation of a point and a vector.

The point P of the undeformed configuration C_i becomes \bar{P} of the deformed configuration C_c Figure 5.1.

$$\overrightarrow{OP} = x\vec{i} + z\vec{k} \quad (5.1)$$

$$\overrightarrow{OP} = \bar{x}\vec{i} + \bar{z}\vec{k} \quad (5.2)$$

The displacement vector of the point P is defined as

$$\vec{u} = \overrightarrow{PP} = \overrightarrow{OP} - \overrightarrow{OP} = u\vec{i} + w\vec{k} \quad (5.3)$$

The coordinates \bar{x}, \bar{z} of point \bar{P} can be written using the Lagrange representation as

$$\begin{Bmatrix} \bar{x}(x, z) \\ \bar{z}(x, z) \end{Bmatrix} = \begin{Bmatrix} x \\ z \end{Bmatrix} + \begin{Bmatrix} u(x, z) \\ w(x, z) \end{Bmatrix} \quad (5.4)$$

The infinitely vector $d\vec{x}$ at P becomes $d\vec{\bar{x}}$ at \bar{P} in the deformed configuration C_c Figures 5.2 and 5.3.

$$d\vec{\bar{x}} = d\vec{x} + d\vec{u} \quad (5.5)$$

$$\begin{Bmatrix} d\bar{x} \\ d\bar{z} \end{Bmatrix} = \begin{Bmatrix} dx \\ dz \end{Bmatrix} + \begin{Bmatrix} \frac{\partial u}{\partial x} dx + \frac{\partial u}{\partial z} dz \\ \frac{\partial w}{\partial x} dx + \frac{\partial w}{\partial z} dz \end{Bmatrix} \quad (5.6)$$

The vector $d\vec{\bar{x}}$ can be given in matrix form by the following

$$\{d\bar{x}\} = \{dx\} + \{du\} = ([I] + [\mathbf{L}])dx = [\mathbf{F}]dx \quad (5.7)$$

The above equation can be written

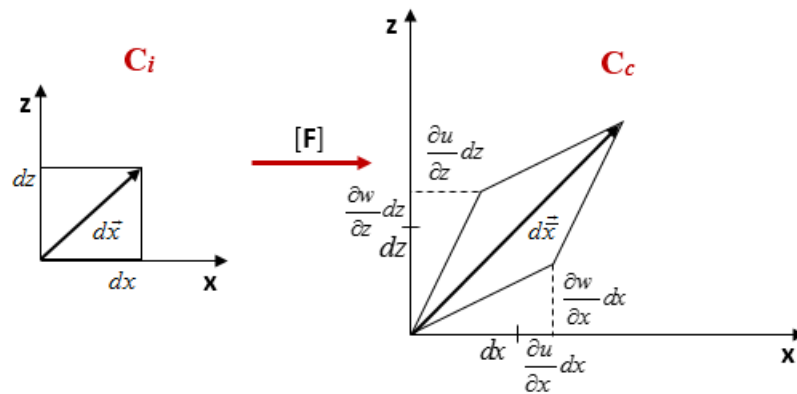


Figure 5.2: Transformation of a vector.

$$\begin{Bmatrix} d\bar{x} \\ d\bar{z} \end{Bmatrix} = \begin{bmatrix} 1 + \frac{\partial u}{\partial x} & \frac{\partial u}{\partial z} \\ \frac{\partial w}{\partial x} & 1 + \frac{\partial w}{\partial z} \end{bmatrix} \begin{Bmatrix} dx \\ dz \end{Bmatrix} \quad (5.8)$$

Where $[F]$ is the transformation gradient tensor and $[L]$ is the deformation gradient tensor

$$[L] = \begin{bmatrix} \frac{\partial u}{\partial x} & \frac{\partial u}{\partial z} \\ \frac{\partial w}{\partial x} & \frac{\partial w}{\partial z} \end{bmatrix} \quad (5.9)$$

• **Dilatation tensor**

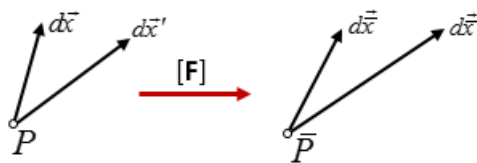


Figure 5.3: Transformation of a vectors.

Consider two infinitely vectors $d\vec{x}$ and $d\vec{x}'$ at point P figure 5.3, becomes $d\vec{x}$ and $d\vec{x}'$ in the deformed configuration C_c .

$$\{d\bar{x}\} = [\mathbf{F}]\{dx\} \quad (5.10)$$

$$\{d\bar{x}'\} = [\mathbf{F}]\{dx'\}$$

The multiplication of vectors $d\vec{\bar{x}}$ and $d\vec{\bar{x}'}$ can be written as

$$\begin{aligned} \{d\bar{x}\}^T \{d\bar{x}'\} &= \{dx\}^T [\mathbf{F}]^T [\mathbf{F}] \{dx'\} \\ &= \{dx\}^T [\mathbf{C}] \{dx'\} \end{aligned} \quad (5.11)$$

Where the dilatation tensor $[\mathbf{C}]$ can be given by the following

$$[\mathbf{C}] = [\mathbf{F}]^T [\mathbf{F}] = ([\mathbf{L}]^T + [I])([\mathbf{L}] + [I]) = [\mathbf{L}]^T [\mathbf{L}] + [\mathbf{L}]^T + [\mathbf{L}] + [I] \quad (5.12)$$

Let ds be the length of the vector $d\vec{x}$ and $d\bar{s}$ the length of the vector $d\vec{\bar{x}}$

$$\begin{aligned} ds^2 &= d\vec{x} \cdot d\vec{x} = \{dx\}^T \cdot \{dx\} \\ d\bar{s}^2 &= d\vec{\bar{x}} \cdot d\vec{\bar{x}} = \{d\bar{x}\}^T \cdot \{d\bar{x}\} \end{aligned} \quad (5.13)$$

The difference $d\bar{s}^2 - ds^2$ can be written by the following

$$\begin{aligned} d\bar{s}^2 - ds^2 &= d\vec{\bar{x}} \cdot d\vec{\bar{x}} - d\vec{x} \cdot d\vec{x} \\ &= \{d\bar{x}\}^T \cdot \{d\bar{x}\} - \{dx\}^T \cdot \{dx\} = \{dx\}^T ([\mathbf{C}] - [I]) \{dx\} \\ &= \{dx\}^T (2[\mathbf{E}]) \{dx\} \end{aligned} \quad (5.14)$$

Where \mathbf{E} is The Green-Lagrange strain tensor defined by

$$[\mathbf{E}] = \underbrace{\frac{[\mathbf{L}]^T + [\mathbf{L}]}{2}}_{\text{Linear-terms}} + \underbrace{\frac{[\mathbf{L}]^T[\mathbf{L}]}{2}}_{\text{Nonlinear-terms}} \quad (5.15)$$

By substituting Eq (5.9) in Eq(5.15) it can be written

$$\begin{aligned} \mathbf{E}_{xx} &= \frac{\partial u}{\partial x} + \frac{1}{2} \left[\left(\frac{\partial u}{\partial x} \right)^2 + \left(\frac{\partial w}{\partial x} \right)^2 \right] \\ \mathbf{E}_{zz} &= \frac{\partial w}{\partial z} + \frac{1}{2} \left[\left(\frac{\partial u}{\partial z} \right)^2 + \left(\frac{\partial w}{\partial z} \right)^2 \right] \\ \mathbf{E}_{xz} &= \frac{1}{2} \left(\frac{\partial u}{\partial z} + \frac{\partial w}{\partial x} \right) + \frac{1}{2} \left[\frac{\partial u}{\partial x} \frac{\partial u}{\partial z} + \frac{\partial w}{\partial x} \frac{\partial w}{\partial z} \right] \end{aligned} \quad (5.16)$$

By omitting the large strain terms and retaining only the square of $\partial w/\partial x$, which represents the rotation of a transverse normal line in the beam, we obtain the so-called von Karaman strains, where it is used as a nonlinear strain-displacement relations for the formulation of the present finite element in the following.

5.3 Finite Element Formulation

5.3.1 Displacement field

The governing equations of the nonlinear bending of beams are developed from basic considerations. Based on the Euler-Bernoulli hypothesis, the bending of beams with large displacements and moderately large rotations considering small strains case, can be derived, using the following displacement field.

$$\begin{aligned} u(x, z) &= u_0(x) - \mathbf{z} \frac{\partial w}{\partial x} \\ w(x, z) &= w_0(x) \end{aligned} \quad (5.17)$$

Where u and w are the total displacements along the coordinates in x and z directions respectively, while u_0 and w_0 denote the axial and transverse displacements of a point of the neutral axis.

5.3.2 Strain-displacement relationships

Using the nonlinear von-karman strain-displacement relationship, the strain component is given by

$$E_{xx} = \frac{\partial u_0}{\partial x} - \mathbf{z} \frac{\partial w^2}{\partial x^2} + \frac{1}{2} \left(\frac{\partial w}{\partial x} \right)^2 \quad (5.18)$$

Or in other term

$$E_{xx} = \varepsilon^0 + \mathbf{z}K_x \quad (5.19)$$

Where

$$\varepsilon^0 = \varepsilon_0^0 + \varepsilon_{nl}^0 \quad (5.20)$$

$$\varepsilon_0^0 = \frac{\partial u_0}{\partial x} \quad (5.21)$$

$$\varepsilon_{nl}^0 = \frac{1}{2} \left(\frac{\partial w}{\partial x} \right)^2 \quad (5.22)$$

$$K_x = -\frac{\partial w^2}{\partial x^2} \quad (5.23)$$

5.3.3 Stress-strain relationships

The constitutive equations for an orthotropic k^{th} layer of a laminated in the local coordinates system (1,2,3) can be written in terms of stresses-strains relationships Figure 5.4 as follows

$$\begin{Bmatrix} \sigma_{11}^k \\ \sigma_{22}^k \\ \sigma_{12}^k \end{Bmatrix} = \begin{bmatrix} Q_{11}^k & Q_{12}^k & 0 \\ Q_{12}^k & Q_{22}^k & 0 \\ 0 & 0 & Q_{66}^k \end{bmatrix} \begin{Bmatrix} E_{11}^k \\ E_{22}^k \\ E_{12}^k \end{Bmatrix} \quad (5.24)$$

Where subscripts 1 and 2 indicate the fibers direction and in-plane transverse to the fibers direction, respectively; subscript 3 is the direction normal to the plate Figure 5.4. The reduced stiffness components are given by

$$\begin{aligned} Q_{11}^k &= \frac{E_1^k}{1 - \nu_{12}^k \nu_{21}^k} \\ Q_{22}^k &= \frac{E_2^k}{1 - \nu_{12}^k \nu_{21}^k} \\ Q_{12}^k &= \frac{\nu_{21}^k E_1^k}{1 - \nu_{12}^k \nu_{21}^k} \\ Q_{66}^k &= G_{12}^k \end{aligned} \quad (5.25)$$

This equation can be rewritten as follows

$$\left\{ \sigma^k \right\} = \left[Q^k \right] \left\{ E^k \right\} \quad (5.26)$$

In the material coordinates (x, y, z) , the constitutive equations can be given by

$$\begin{Bmatrix} \sigma_{xx}^k \\ \sigma_{yy}^k \\ \sigma_{xy}^k \end{Bmatrix} = \begin{bmatrix} \bar{Q}_{11}^k & \bar{Q}_{12}^k & \bar{Q}_{16}^k \\ \bar{Q}_{12}^k & \bar{Q}_{22}^k & \bar{Q}_{26}^k \\ \bar{Q}_{16}^k & \bar{Q}_{26}^k & \bar{Q}_{66}^k \end{bmatrix} \begin{Bmatrix} E_{xx}^k \\ E_{yy}^k \\ E_{xy}^k \end{Bmatrix} \quad (5.27)$$

This equation can be rewritten as follows

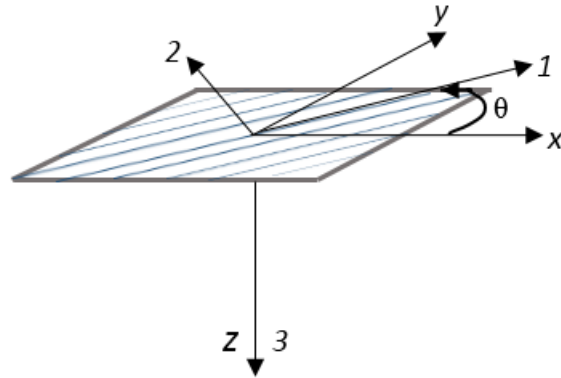


Figure 5.4: A lamina with reference axes (x,y,z) and fiber axes $(1,2,3)$.

$$\{\bar{\sigma}^k\} = [\bar{Q}^k] \{\bar{E}^k\} \quad (5.28)$$

Where

$$\{\bar{\sigma}^k\} = \begin{Bmatrix} \sigma_{xx}^k \\ \sigma_{yy}^k \\ \sigma_{xy}^k \end{Bmatrix}, \{\bar{E}^k\} = \begin{Bmatrix} E_{xx}^k \\ E_{yy}^k \\ E_{xy}^k \end{Bmatrix} \quad (5.29)$$

And

$$[\bar{Q}^k] = [T]^{-1}[Q^k][T] \quad (5.30)$$

$[T]$ is the transformation matrix

$$[T] = \begin{bmatrix} c^2 & s^2 & 2cs \\ s^2 & c^2 & -cs \\ -2cs & 2cs & c^2 - s^2 \end{bmatrix} \quad (5.31)$$

The components \bar{Q}_{ij} are the stiffness coefficients of a layer in the global coordinate system (x, y, z) of the laminate forming an angle θ with the local coordinates system of the lamina, with $c = \cos\theta$ and $s = \sin\theta$. θ is the fiber orientation angle with respect to material coordinates system.

The stiffness coefficients are given by

$$\begin{aligned}
 \bar{Q}_{11}^k &= Q_{11}^k c^4 + Q_{22}^k s^4 + 2(Q_{12}^k + 2Q_{66}^k) s^2 c^2 \\
 \bar{Q}_{22}^k &= Q_{11}^k s^4 + Q_{22}^k c^4 + 2(Q_{12}^k + 2Q_{66}^k) s^2 c^2 \\
 \bar{Q}_{12}^k &= (Q_{11}^k + Q_{22}^k - 4Q_{66}^k) s^2 c^2 + Q_{12}^k (s^4 + c^4) \\
 \bar{Q}_{66}^k &= (Q_{11}^k + Q_{22}^k - 2Q_{12}^k - 2Q_{66}^k) s^2 c^2 + Q_{66}^k (s^4 + c^4) \\
 \bar{Q}_{16}^k &= (Q_{11}^k - Q_{12}^k - 2Q_{66}^k) s c^3 - (Q_{11}^k - Q_{12}^k - 2Q_{66}^k) s^3 c \\
 \bar{Q}_{26}^k &= (Q_{11}^k - Q_{12}^k - 2Q_{66}^k) s^3 c - (Q_{11}^k - Q_{12}^k - 2Q_{66}^k) s c^3
 \end{aligned} \tag{5.32}$$

In case of beams, and accordingly to Bernoulli theory, we can have the following

$$\sigma_{yy} = \sigma_{xy} = 0 \tag{5.33}$$

This may lead to have the following equation

$$\sigma_{xx}^k = \bar{Q}_{eq}^k E_{xx}^k \tag{5.34}$$

Where the equivalent stiffness coefficient of a layer is expressed as

$$\bar{Q}_{eq}^k = \bar{Q}_{11}^k + \bar{Q}_{12}^k \left[-\frac{\bar{Q}_{12}^k \bar{Q}_{66}^k - \bar{Q}_{16}^k \bar{Q}_{26}^k}{\bar{Q}_{22}^k \bar{Q}_{66}^k - (\bar{Q}_{26}^k)^2} \right] + \bar{Q}_{16}^k \left[-\frac{\bar{Q}_{16}^k}{\bar{Q}_{66}^k} \right] - \bar{Q}_{26}^k \left[-\frac{\bar{Q}_{66}^k \bar{Q}_{12}^k + \bar{Q}_{26}^k \bar{Q}_{16}^k}{\bar{Q}_{66}^k (\bar{Q}_{22}^k \bar{Q}_{66}^k - (\bar{Q}_{26}^k)^2)} \right] \tag{5.35}$$

5.3.3.1 Resultant efforts

By integrating the stress through the thickness, the axial force and moment resultants are obtained as follows

$$N = \int_{-\frac{h}{2}}^{\frac{h}{2}} \sigma_{xx} \cdot dz = \sum_{k=1}^{k=n} \left(\int_{z^k}^{z^{k+1}} \bar{Q}_{eq}^k \cdot E_{xx} dz \right) \quad (5.36)$$

$$N = \sum_{k=1}^{k=n} \int_{z^k}^{z^{k+1}} \bar{Q}_{eq}^k \left(\varepsilon_0 + \mathbf{z}K_x \right) dz = \sum_{k=1}^{k=n} \left(\int_{z^k}^{z^{k+1}} \bar{Q}_{eq}^k \cdot \varepsilon_0 dz \right) + \sum_{k=1}^{k=n} \left(\int_{z^k}^{z^{k+1}} \bar{Q}_{eq}^k \cdot \mathbf{z}K_x \right) \quad (5.37)$$

The axial force resultant can be written

$$N = A \cdot \varepsilon_0 + B \cdot K_x \quad (5.38)$$

$$M = \int_{-\frac{h}{2}}^{\frac{h}{2}} \sigma_{xx} \cdot \mathbf{z} dz = \sum_{k=1}^{k=n} \left(\int_{z^k}^{z^{k+1}} \bar{Q}_{eq}^k \cdot E_{xx} \mathbf{z} dz \right) \quad (5.39)$$

$$M = \sum_{k=1}^{k=n} \int_{z^k}^{z^{k+1}} \bar{Q}_{eq}^k z \left(\varepsilon_0 + \mathbf{z}K_x \right) dz = \sum_{k=1}^{k=n} \left(\int_{z^k}^{z^{k+1}} \bar{Q}_{eq}^k \cdot \varepsilon_0 z dz \right) + \sum_{k=1}^{k=n} \left(\int_{z^k}^{z^{k+1}} \bar{Q}_{eq}^k \cdot \mathbf{z}^2 K_x dz \right) \quad (5.40)$$

The moment resultant can be written

$$M = B \cdot \varepsilon_0 + D \cdot K_x \quad (5.41)$$

Where n is the layers number, with A, B and D are the extensional, coupling and bending rigidity scalars, respectively, and are defined as

$$A = \sum_{k=1}^{k=n} \bar{Q}_{eq}^k (h_k - h_{k-1}) \quad (5.42)$$

$$B = \frac{1}{2} \sum_{k=1}^{k=n} \bar{Q}_{eq}^k (h_k^2 - h_{k-1}^2) \quad (5.43)$$

$$D = \frac{1}{3} \sum_{k=1}^{k=n} \bar{Q}_{eq}^k (h_k^3 - h_{k-1}^3) \quad (5.44)$$

$$K_x = -\frac{\partial w^2}{\partial x^2} \quad (5.45)$$

5.3.3.2 Neutral axis position change

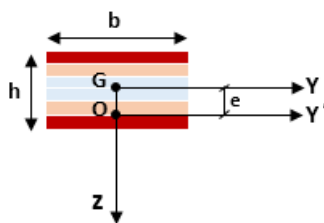


Figure 5.5: Neutral axis position.

When the atisymmetric laminated section is considered, the neutral axis is not located at the middle of the beam section as shown in Figure 5.5, which this shift between them is expressed by the coupling rigidity. For purpose omitting the coupling rigidity and in order to determine the position of the neutral axis, a new coordinates system ($z' = z - e$) is considered

$$x = x'$$

$$z = z' + e$$

With e is the distance between the median axis of the beam section and the neutral axis, Figure 5.5. Then, to calculate the distance, the coupling rigidity with respect to axis z' must be 0

$$B' = \sum_{k=1}^n \int_{z'^{k-1}}^{z'^k} \bar{Q}_{eq}^k z' dz' = 0 \quad (5.46)$$

$$B' = \sum_{k=1}^n \int_{z'_{k-1}}^{z'_k} Q_{eq}^k (\mathbf{z} - e) dz = \sum_{k=1}^n \int_{z'_{k-1}}^{z'_k} Q_{eq}^k \mathbf{z} dz - \sum_{k=1}^n \int_{z'_{k-1}}^{z'_k} Q_{eq}^k \cdot e dz = 0 \quad (5.47)$$

$$B' = B - eA \quad (5.48)$$

This leads to

$$e = \frac{B}{A} \quad (5.49)$$

Once e is determined, the new bending stiffness with respect to z' can be given by

$$D' = \sum_{k=1}^n \int_{z'_{k-1}}^{z'_k} Q_{eq}^k z'^2 dz' = \frac{1}{3} \sum_{k=1}^n Q_{eq}^k [(h_k - e)^3 - (h_{k-1} - e)^3] \quad (5.50)$$

5.3.4 Displacement interpolation and shape functions

The displacements field vector of the present finite element can be defined in the following form

$$\delta(x) = \sum_{i=1}^n N(x) \delta_i \quad (5.51)$$

where $\delta(x)$ is the displacement vector of a given point along the element.

$\delta_i = \{u_i w_i \phi_i\}^T$ is the nodal displacement vector, i is the number of the considered node ($i = 1, 2$) and $N_k(x)$ are the Lagrange and Hermit shape functions given in the following

$$\begin{aligned}
 N_1 &= 1 - \frac{x}{L} \\
 N_2 &= \frac{x}{L} \\
 N_3 &= 1 - \frac{3}{L^2}x^2 + \frac{2}{L^3}x^3 \\
 N_4 &= x - \frac{2}{L}x^2 + \frac{x^3}{L^2} \\
 N_5 &= \frac{3}{L^2}x^2 - \frac{2}{L^3}x^3 \\
 N_6 &= -\frac{1}{L}x^2 + \frac{1}{L^2}x^3
 \end{aligned} \tag{5.52}$$

The strain-displacement relationship of Eqs.(5.18)and (5.19) can be rewritten as follows

$$\begin{aligned}
 \{\varepsilon_0\} &= [B_m]\{\delta\} \\
 \{K_x\} &= [B_f]\{\delta\} \\
 \frac{\partial w}{\partial x} &= [G]\{\delta\} \\
 \{\varepsilon_{nl}\} &= \frac{1}{2}\{\delta\}^T[G]^T[G]\{\delta\}
 \end{aligned} \tag{5.53}$$

Where

$$[B_m] = \begin{bmatrix} \frac{\partial N_1}{\partial x} & 0 & 0 & \frac{\partial N_2}{\partial x} & 0 & 0 \end{bmatrix} \tag{5.54}$$

$$[B_f] = \begin{bmatrix} 0 & \frac{\partial N_2^2}{\partial x^2} & \frac{\partial N_3^2}{\partial x^2} & 0 & \frac{\partial N_5^2}{\partial x^2} & \frac{\partial N_6^2}{\partial x^2} \end{bmatrix} \tag{5.55}$$

$[B_m]$ and $[B_f]$ are (1×6) matrices, and the subscripts m and f denote the membrane and the bending strains, respectively.

5.3.5 Evaluation of stiffness matrix

The principle of total potential energy is used to derivate the elementary stiffness matrix of the element. It is defined by

$$\Pi = U - W \quad (5.56)$$

U and W are the deformation potential energy and the external forces work, respectively. In order to establish the relationships between displacements and forces, the first variation of the total potential energy must be equal 0.

$$\partial\Pi = \partial U - \partial W = 0 \quad (5.57)$$

The potential energy of deformation can be given by

$$U = \frac{1}{2} \int_v \sigma_{xx} \varepsilon_{xx} dv \quad (5.58)$$

Where

$$U = \frac{1}{2} \int_0^L N \varepsilon_0 dx + \frac{1}{2} \int_0^L M K_x dx \quad (5.59)$$

By substituting Eq(5.38)and (5.41)into the above equation, it can be written as

$$U = \frac{1}{2} \int_0^L (\{\varepsilon_0\}^T [A\varepsilon_0 + BK_x]) dx + \frac{1}{2} \int_0^L (\{K_x\}^T [B\varepsilon_0 + DK_x]) dx \quad (5.60)$$

And

$$U = \frac{1}{2} \int_0^L (\{\varepsilon_0\}^T A \{\varepsilon_0\}) dx + \frac{1}{2} \int_0^L (\{\varepsilon_0\}^T B \{K_x\}) dx + \frac{1}{2} \int_0^L (\{K_x\}^T B \{\varepsilon_0\}) dx + \int_0^L (\{K_x\}^T D \{K_x\}) dx \quad (5.61)$$

By substituting Eq (5.20) into Eq (5.61) it can be written as

$$U = \frac{1}{2} \int_0^L (\{\varepsilon_0^0\} + \{\varepsilon_{nl}^0\})^T A (\{\varepsilon_0^0\} + \{\varepsilon_{nl}^0\}) dx + \frac{1}{2} \int_0^L (\{\varepsilon_0^0\} + \{\varepsilon_{nl}^0\})^T B (\{K_x\}) dx \\ + \frac{1}{2} \int_0^L (\{K_x\})^T B (\{\varepsilon_0^0\} + \{\varepsilon_{nl}^0\}) dx + \frac{1}{2} \int_0^L (\{K_x\})^T D (\{K_x\}) dx \quad (5.62)$$

In the present formulation, a new position of the beam neutral axis had been determined for omitting the coupling rigidity purpose. Then, with respect to the new coordinates, a new bending stiffness D' had been determined at the new neutral axis. Of these, even when the laminated section is considered as a non-symmetric, the coupling rigidity is equal zero $B = 0$. So, in this case the axial resultant force and the resultant moment are given by

$$N = A\varepsilon^0 \\ M = D'K_x \quad (5.63)$$

By substituting Eq (5.63) in Eq (5.61), the Eq (5.62) become

$$U = \frac{1}{2} \int_0^L (\{\varepsilon_0^0\}^T A \{\varepsilon_0^0\}) dx + \frac{1}{2} \int_0^L (\{\varepsilon_0^0\}^T A \{\varepsilon_{nl}^0\}) dx + \frac{1}{2} \int_0^L (\{\varepsilon_{nl}^0\}^T A \{\varepsilon_0^0\}) dx \\ + \frac{1}{2} \int_0^L (\{\varepsilon_{nl}^0\}^T A \{\varepsilon_{nl}^0\}) dx + \frac{1}{2} \int_0^L (\{K_x\}^T D' \{K_x\}) dx \quad (5.64)$$

substituting the strain-displacement relationship Eqs (5.53) in the above equation, we find

$$U = \frac{1}{2} \int_L ((\{\delta\}^T [B_m]^T A [B_m] \{\delta\}) + (\{\delta\}^T [B_m]^T A \frac{1}{2} \{\delta\}^T [G]^T [G] \{\delta\}) \\ + (\frac{1}{2} \{\delta\}^T [G]^T [G] \{\delta\} A [B_m] \{\delta\}) + (\frac{1}{2} \{\delta\}^T [G]^T [G] \{\delta\} A \frac{1}{2} \{\delta\}^T [G]^T [G] \{\delta\}) \\ + ([B_f]^T D' [B_f]) + ([G]^T N [G])) dx \quad (5.65)$$

The stiffness matrix can be given by

$$\begin{aligned}
 [K_e] = \int_0^L & \left(\underbrace{([B_m]^T A [B_m])}_{\text{Linear-membrane}} + \frac{3}{4} \underbrace{([B_m]^T A \{\delta\}^T [G]^T [G])}_{\text{Nonlinear-membrane}} + \frac{3}{4} \underbrace{([G]^T [G] \{\delta\} A [B_m])}_{\text{Nonlinear-membrane}} \right. \\
 & \left. + \frac{1}{2} \underbrace{([G]^T [G] \{\delta\} A \{\delta\}^T [G]^T [G])}_{\text{Nonlinear-membrane}} + \underbrace{([B_f]^T D' [B_f])}_{\text{Linear-flexional}} + ([G]^T N [G]) \right) dx \quad (5.66)
 \end{aligned}$$

5.4 Resolution Method

The iterative solution method and the calculation steps used to solve the present nonlinear finite element equations are presented here. Consider the nonlinear finite element equilibrium equation can be written as

$$K(\delta)\delta = F \quad (5.67)$$

Where δ is the unknown to be determined, $K(\delta)$ is a function of δ , F is the known force.

The nonlinear Eq (5.67) can be linearized using the iterative procedure. We begin with an initial guess for δ , say $\delta^{(0)}$, ($\delta^{(0)} = 0$) and determine the first approximation to δ by solving the equation

$$\delta^{(1)} = (K(\delta^{(0)}))^{-1} F \quad (5.68)$$

$\delta^{(1)} \neq \delta$, and a second approximation for δ sought by using the last approximation to evaluate K

$$\delta^{(2)} = (K(\delta^{(1)}))^{-1} F \quad (5.69)$$

This procedure is continued until the difference between two consecutive approximations of δ differ by a preselected value.

5.4.1 Load increments

Examining the expression (5.36) for the axial force N , it is clear that the rotation of a transverse normal contributes to tensile component of N irrespective of the sign of load. As result, beam becomes increasingly stiff with an increase in load. Hence, for large loads the nonlinearity may be too large for the numerical scheme to yeild convergent solution. Therefore, it is necessary to divide the total load F into several smaller load increaments $\delta F_1, \delta F_2, \dots, \delta F_n$ such that

$$F = \sum_{i=1}^n \delta F_i \quad (5.70)$$

For the first load inceament step $F_1 = \delta F_1$, the obtained solution is linear and it is used as the intial "guess" vector for the next load inceament $F_2 = \delta F_2$. This is continued until the total load is reached. Note that the element coordinates are updated after each step.

5.5 Validation of The Present Finite Element

In this section, different tests are considered in order to validate the performance of the present finite element. The obtained results are compared with those obtained analytically, experimentally and numerically approaches available in the literature. Isotropic and composite cantilever beams are considered. Furthermore, for the sake of comparison it has been compared with the obtained results from the analytical formulation presented in the previous chapter.

5.5.1 Isotropic cantilever beam subjected to tip concentrated load

An isotropic cantilever beam subjected to tip load is considered for the first case as illustrated in Figure 5.6. As shown in Figure 5.6, the effort N explained that there is an extension in the length of the beam during loading, because the present finite element was formulated by the requirement that the beam is extensible. The vertical deflections are computed for deferent load parameter value, where the obtained results are presented in Table 5.1. Figure 5.7, show the present finite element results compared with the present analytical and the results obtained by Mattiasson [221], Kumar et al. [47] and Nanakorn and Vu [92]. The curves show that the obtain

results are in good agreement with those results.

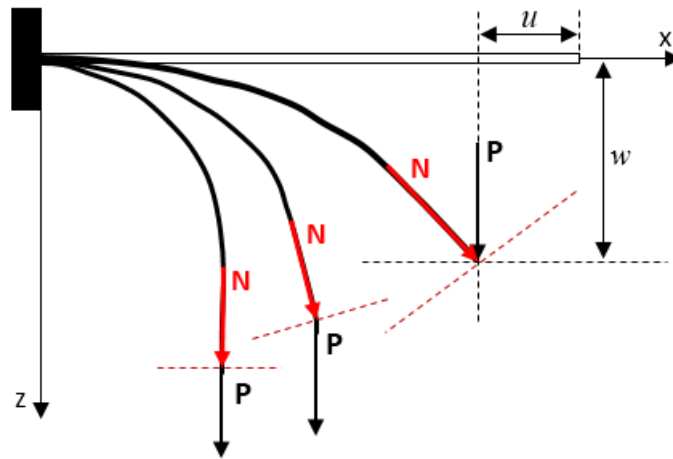


Figure 5.6: Cantilever beam under tip load.

Table 5.1: Non-dimensional deflections as a function of load parameter for isotropic cantilever beam subjected to tip load.

$\frac{PL^2}{EI}$	Mattiasson w	Kumar et al. w	Present analy w	Nanakorn and Vu w	Present finite elem. w
1	0,3017	0,3019	0,3018	0.29946	0,31639
2	0,4934	0,4939	0,4936	0.48748	0,55262
3	0,6032	0,6038	0,6368	0.59534	0,69509
4	0,6699	0,6704	0,6934	0.66126	0,77223
5	0,7137	0,7146	0,7322	0.70479	0,8134
6	0,7445	0,7454	0,7606	0.73550	0,83675
7	0,7673	0,7682	0,7852	0.75831	0,85162
8	0,7849	0,7861	0,7971	0.77597	0,86247
9	0,799	0,803	0,8118	0.79011	0,87136
10	0,8106	0,8206	0,8262	0.80173	0,87923

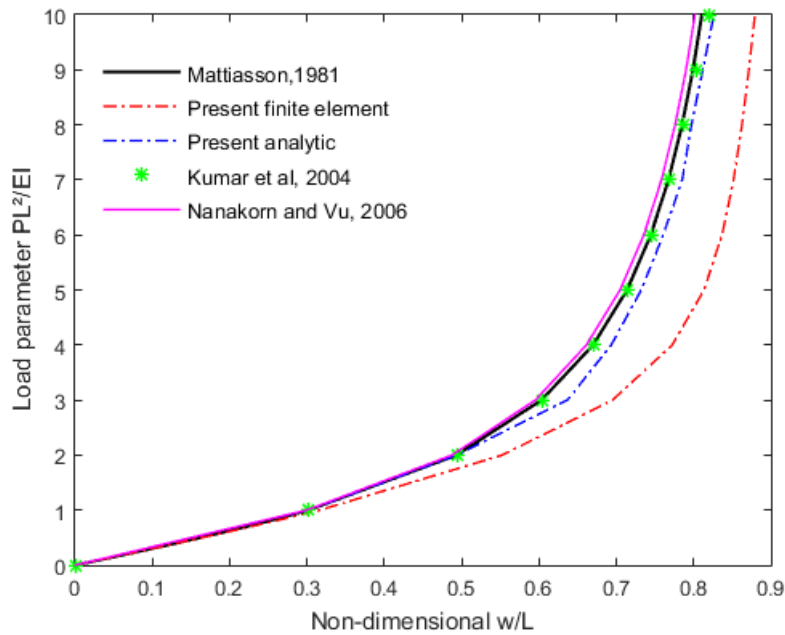


Figure 5.7: Load-deflections curves for cantilever beam with tip load.

5.5.2 Composite cantilever beams subjected to tip concentrated load

Another case for composite laminated cantilever beams subjected to tip load are now presented. The second case considered for validation is a symmetric 12-layer cross-ply $[0/90]_{3s}$ cantilever beam of length $L = 550mm$, width $W = 30mm$, and thickness $t = 0.124mm$. The mechanical properties of the used material, are as follows: $E_1 = 142GPa$, $E_2 = 9.8GPa$, $\nu_{12} = 0.3$ and $G_{12} = 6GPa$. The cantilever beam was loaded at free end, where the vertical and the horizontal displacements are measured at a distance $a = 50mm$ from the free end as shown in Figure 5.8.

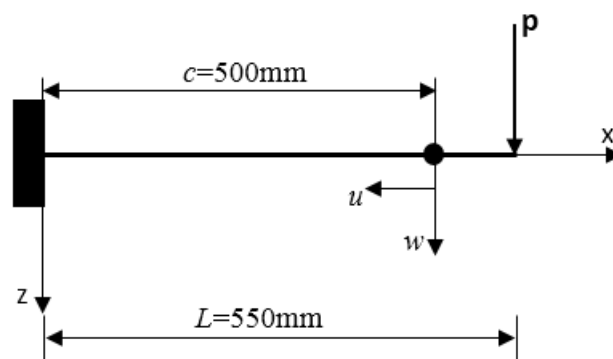


Figure 5.8: Laminated cantilever beam under tip load.

Table 5.2 show the horizontal and the vertical displacements obtained by the present finite element and analytical formulation with the results obtained analytically and experimentally by Minguet et al. [62]. Figure 5.9 show the load-deflections curves of the present numerical and analytical compared with the experimental and the analytical results obtained by Minguet et al. [62]. The curves show that the results are clearly compared well for a symmetric laminated beam.

Table 5.2: Horizontal and vertical displacements of symmetric laminated $[0/90]_{3s}$ cantilever beam .

Load (g)	Experimental [62]		Present analytical		Analytical [62]		Present finite element	
	u (mm)	w (mm)	u (mm)	w (mm)	u (mm)	w (mm)	u (mm)	w (mm)
77.58	2.81	50.56	3.86	47.61	2.8	47.75	4.2856	59.632
103.44	4.77	68.1	2.68	63.91	5.61	61.79	7.5606	79.047
146.55	8.02	94.91	4.55	89.47	11.23	89.88	14.913	110.52
202.58	19.66	125.01	14.35	116.7	18.25	117.97	27.627	149.25
405.17	58.8	206.46	50.55	201.2	57.58	202.24	92.697	262.15

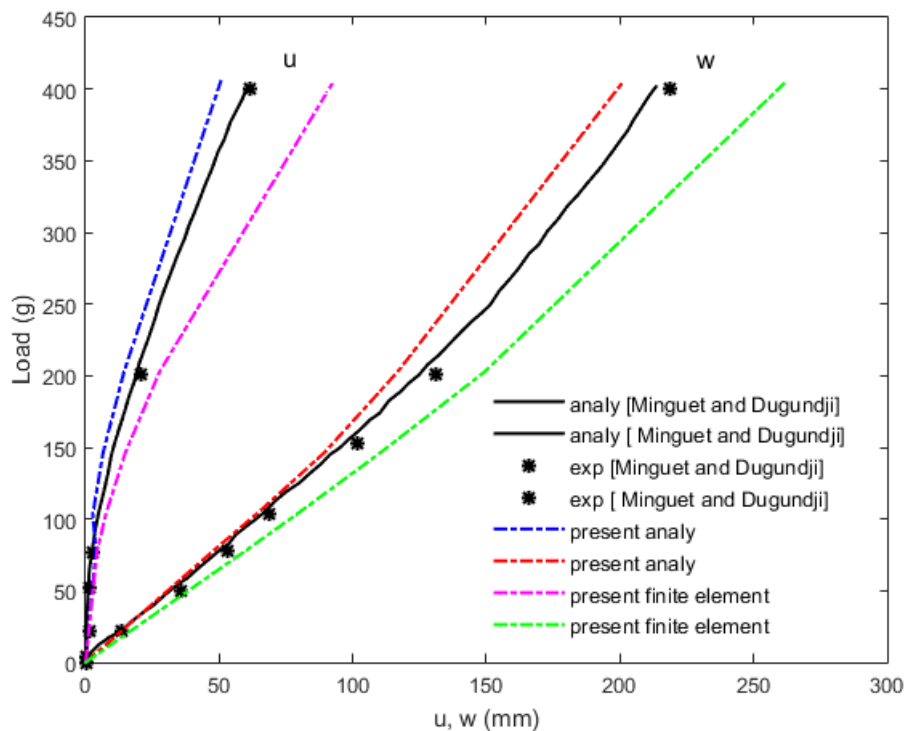


Figure 5.9: Load-deflections curves for $[0/90]_{3s}$ cantilever beam.

5.6 Parametric Study

After validating the performance of the present element in the previous section, by comparing the obtained results with the analytical and the numerical solutions available in the literature. This section is aimed to discover and understand the effect of fiber orientation angle, anisotropic ratio, slenderness ratio on the horizontal and the vertical displacements for symmetric and non-symmetric laminated beams with different boundary conditions.

5.6.1 Effect of fiber orientation angle

For our examples here, the mechanical properties of the fabricated long glass fiber/polyester resin (**GFP**) laminates that were presented in the third chapter are considered. A symmetric $[\theta / -\theta / -\theta / \theta]$ and antisymmetric $[-\theta / \theta / -\theta / \theta]$ are considered for the first two examples for simply supported beam under concentrated load and cantilever beams under tip load, respectively Figures 5.10 and 5.11 . The corresponding horizontal and vertical displacements corresponding to fiber orientation angle ranging from 0° to 90° are shown in Figures 5.12 and 5.13 respectively.

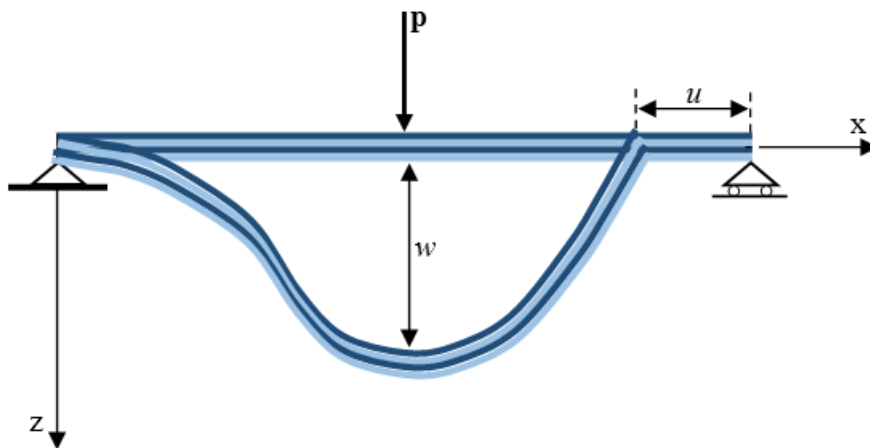


Figure 5.10: Simply supported laminated beam under concentrated load.

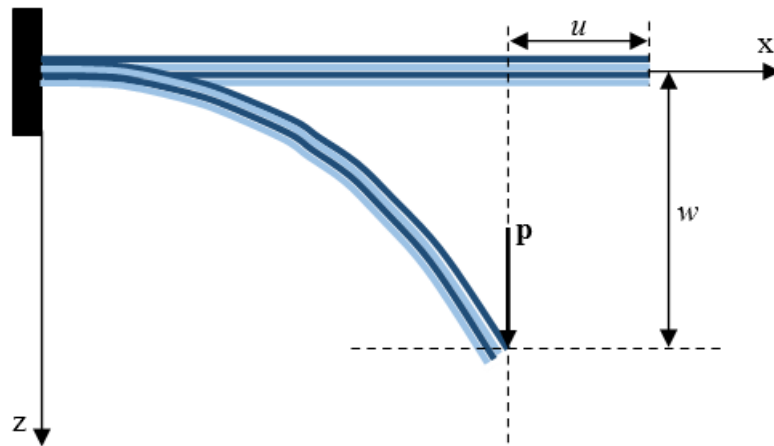


Figure 5.11: Cantilever laminated beam under tip load.

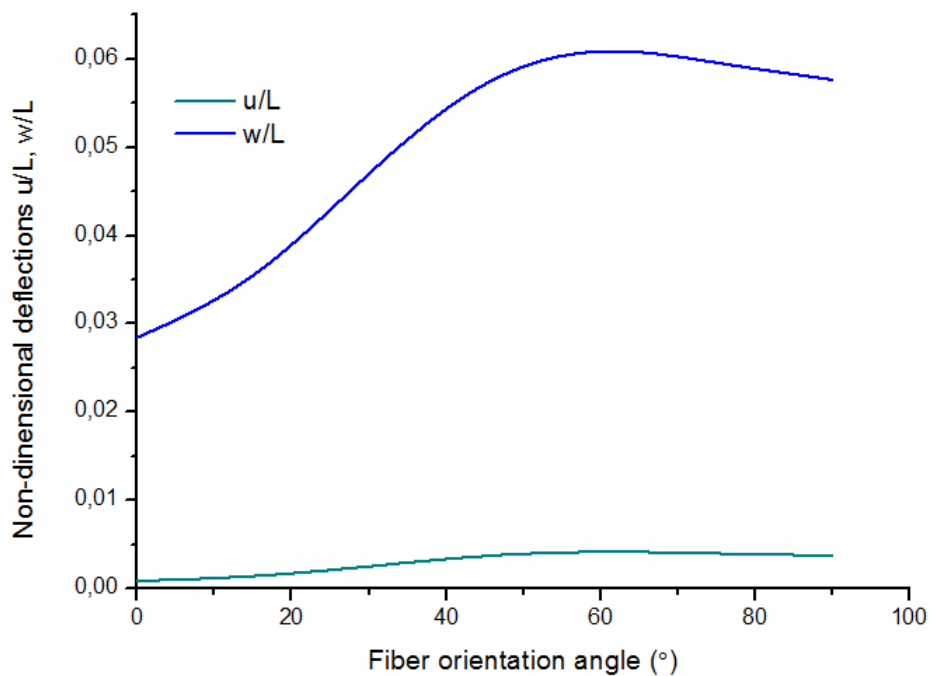


Figure 5.12: Effect of fiber orientation angle on non-dimensional deflections for a symmetric angle-ply (GFP) simply supported beam under concentrated load.

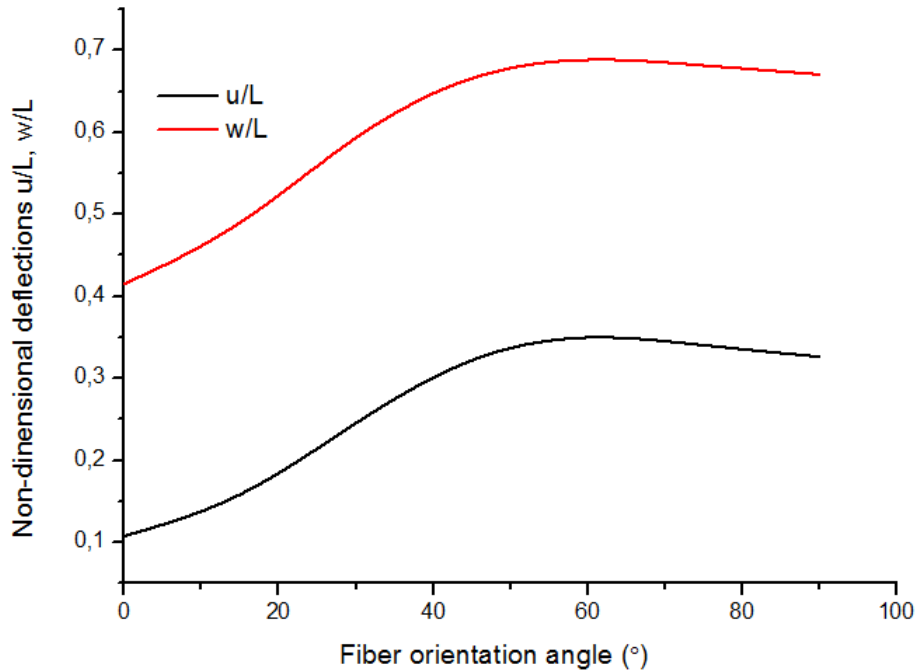


Figure 5.13: Effect of fiber orientation angle on non-dimensional deflections for anisymmetric angle-ply (**GFP**) beam under tip load.

As shown in Figures 5.12 and 5.13, we can see that the behavior under fiber orientation angle affecting is similar for both symmetric and antisymmetric laminates as well as for both considered boundary conditions. It is observed that with an increase in fiber orientation angle, there is an increase in deflections values until the angle $\theta = 45^\circ$ which the deflections reaches the maximum values, then it decrease slowly toward the angle $\theta = 90^\circ$, and we can also note that for $\theta = 0^\circ$ the deflections are in the minimum value.

5.6.2 Effect of slenderness ratio

Now we complete our parametric study here with another important parameter which is the effect of slenderness ratio on deflections values with different anisotropy ratio values. A four (**GFP**) layers with a symmetric as well as antisymmetric angle-ply cantilever beams subjected to tip load and simply supported beam under concentrated load are considered here for our two examples respectively. The anisotropy ratio E_1/E_2 values are ranging from 1 to 5. The effect of slenderness ratio on non-dimensional deflections values for (**GFP**) laminated beams are shown in Figures 5.14 and 5.15, for symmetric and antisymmetric angle-ply respectively.

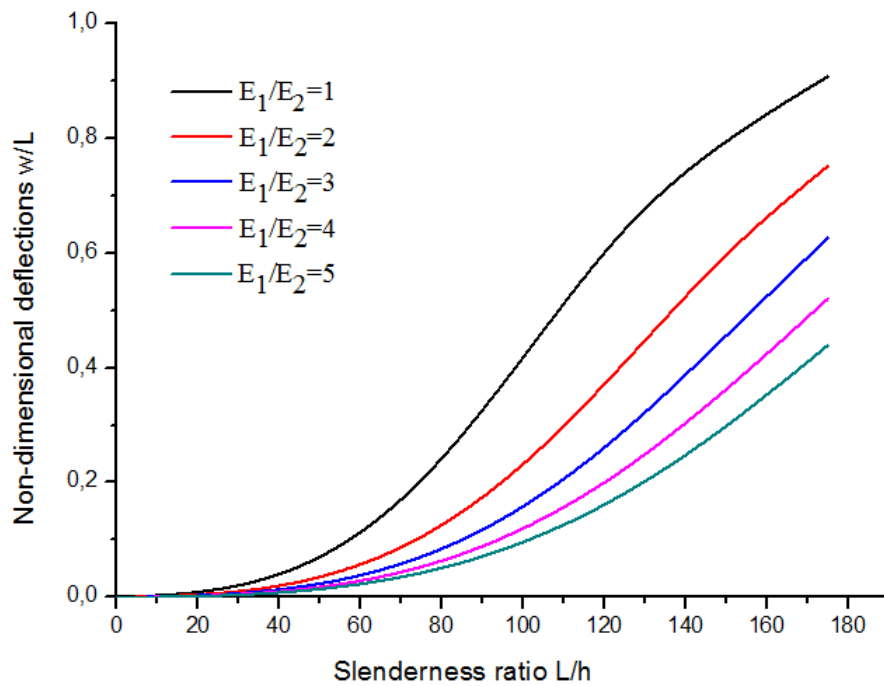


Figure 5.14: Effect of slenderness ratio on non-dimensional deflections for a symmetric angle-ply (**GFP**) beam under tip load with various anisotropy ratio values.

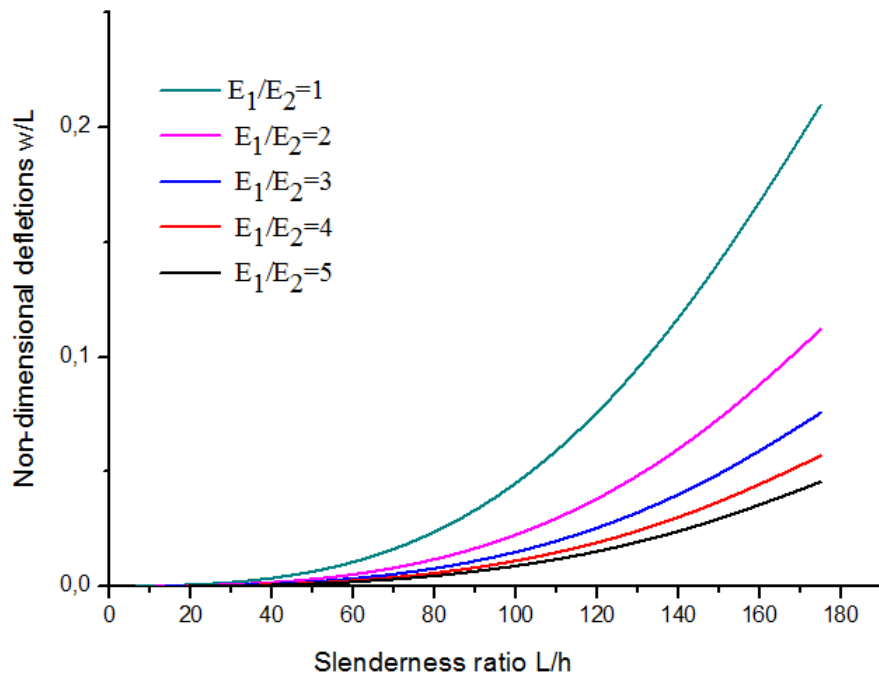


Figure 5.15: Effect of slenderness ratio on non-dimensional deflections for antisymmetric angle-ply (**GFP**) simply supported beam under concentrated load with various anisotropy ratio values.

Considering these two cases, we can note from both figures that the curves are consistent for all anisotropy ratio values. Also, it is observed that with the increase in slenderness ratio, the deflections values also are increasing. Then, as shown in Figures, we can see that there is a decrease in deflection values with the increase in orthotropy ratio values.

5.7 Conclusion

One-dimensional finite element formulation based on the Euler-Bernoulli beam theory has been developed in this chapter, for the nonlinear bending analysis of composite laminated beams. The present finite element, has been defined by two nodes and three degree of freedom per node. The performance and the reliability of the developed element have been evaluated through some applications on nonlinear bending analysis of isotropic and symmetric laminated beams. The obtained results have been compared with the available results obtained analytically and experimentally in the literature as well as the results of the present analytical model. The applications demonstrate that the results goes well with those obtained in the literature. However, it can be seen, that there is some difference with the analytical results, probably because the present element has been formulated, taking in consideration the axial loading effect, while the analytical model have been formulated supposing the inextensibility of the beam. A parametric study was presented to examinte the effect of some parameters such as fiber orientation angle and slenderness ratio on the deflection variation of laminated beams with different boundary conditions. As consequence, Some of the important observations in the following points

- It has been seen, that similar effect of fiber orientation angle on both symmetric and antisymmetric laminates behaviors for both considered boundary conditions cases. With an increase in fiber orientation angle, there is an increase in deflections values until $\theta = 45^\circ$ when the deflections reaches the maximum values, then it decrease slowly until $\theta = 90^\circ$. We can also note that for $\theta = 0^\circ$ the deflection at its minimum value.
- It has been observed, that with the increase in slenderness ratio, the deflections values also are increasing. Also, it can be seen that there is a decrease in deflection values with the increase in orthotropy ratio values.

Part III

Nonlinear Plates Analysis

Chapter6

Numerical Analysis of Thermo-mechanical Loading Effect on Free Vibration of Laminated Composite Plates

6.1 Introduction

Free vibration of angle-ply laminated composite plates under thermal and mechanical loading effect have been analyzed in the current chapter, using a four-nodded rectangular finite element based on first order shear deformation with assumed natural shear strain. Total potential energy and Hamilton' principles have been used to derivate stiffness, geometric and mass matrices. To take into account the large displacements aspect due to thermal and mechanical pre-buckling of laminates composite plates, the von Karman strain tensor has been used. Furthermore, assumed natural strain method has been introduced to elevate the shear locking phenomenon. The convergence of the natural frequency for unloaded plates case and the critical temperature as well as the buckling critical load has been checked. The effects of thickness to side ratio, anisotropy degree of single layer and fibers orientation angle, on free vibration and critical temperature and critical buckling load have been also analyzed.

6.2 Mathematical Formulation

6.2.1 Displacement field and kinematics

According to first-order formulation, the displacement components vector u, v and w in x, y and z directions, respectively, of a point of coordinates (x, y, z) within the laminate, are given by

$$\begin{aligned} u \equiv u(x, y, z, t) &= u_0(x, y, t) + z\varphi_x(x, y, t) \\ v \equiv v(x, y, z, t) &= v_0(x, y, t) + z\varphi_y(x, y, t) \\ w \equiv w(x, y, z, t) &= w_0(x, y, t) \end{aligned} \quad (6.1)$$

Where, u_0 and v_0 are the in-plane displacement vector components at any point $(x, y, 0)$ in x and y directions, respectively. The transverse displacement $w_0(x, y)$ is considered to be constant across the thickness of the plate.

The state of strain at any point in the overall plate is given by the following two strain vectors

$$\begin{aligned} \{E\}^T &= \{E_{xx}, E_{yy}, \gamma_{xy}\} \\ \{\gamma_s\}^T &= \{\gamma_{xz}, \gamma_{xz}\} \end{aligned} \quad (6.2)$$

Using the von Karman strain-displacement relationship, the strain vector components are given by

$$\begin{aligned}
 E_{xx} &= \frac{\partial u}{\partial x} + \frac{1}{2} \left(\frac{\partial w}{\partial x} \right)^2 = \frac{\partial u_0}{\partial x} + z \frac{\partial \varphi_x}{\partial x} + \frac{1}{2} \left(\frac{\partial w}{\partial x} \right)^2 = \varepsilon_x^0 + zK_x + \varepsilon_x^{nl} \\
 E_{yy} &= \frac{\partial v}{\partial y} + \frac{1}{2} \left(\frac{\partial w}{\partial y} \right)^2 = \frac{\partial v_0}{\partial y} + z \frac{\partial \varphi_y}{\partial y} + \frac{1}{2} \left(\frac{\partial w}{\partial y} \right)^2 = \varepsilon_y^0 + zK_y + \varepsilon_y^{nl} \\
 \gamma_{xy} &= \frac{\partial u}{\partial y} + \frac{\partial v}{\partial x} + \frac{\partial w}{\partial x} \frac{\partial w}{\partial y} = \frac{\partial u_0}{\partial y} + \frac{\partial v_0}{\partial x} + z \left(\frac{\partial \varphi_x}{\partial y} + \frac{\partial \varphi_y}{\partial x} \right) + \frac{\partial w}{\partial x} \frac{\partial w}{\partial y} = \gamma_{xy}^0 + zK_{xy} + \gamma_{xy}^{nl} \\
 \gamma_{xz} &= \frac{\partial u}{\partial z} + \frac{\partial w}{\partial x} = \varphi_x + \frac{\partial w}{\partial x} \\
 \gamma_{yz} &= \frac{\partial v}{\partial z} + \frac{\partial w}{\partial y} = \varphi_y + \frac{\partial w}{\partial y}
 \end{aligned}$$

or in other term

$$\begin{aligned}
 \{E\} &= \{\varepsilon^0\} + z\{K\} + \{\varepsilon^{nl}\} \\
 \{\gamma_z\} &= \begin{Bmatrix} \gamma_{xz} \\ \gamma_{yz} \end{Bmatrix}
 \end{aligned} \tag{6.3}$$

Where

$$\{\varepsilon^0\} = \begin{Bmatrix} \varepsilon_x^0 \\ \varepsilon_y^0 \\ \gamma_{xy}^0 \end{Bmatrix} = \begin{Bmatrix} \frac{\partial u_0}{\partial x} \\ \frac{\partial v_0}{\partial y} \\ \frac{\partial u_0}{\partial y} + \frac{\partial v_0}{\partial x} \end{Bmatrix} \tag{6.4}$$

$$\{K\} = \begin{Bmatrix} K_x \\ K_y \\ K_{xy} \end{Bmatrix} = \begin{Bmatrix} \frac{\partial \varphi_x}{\partial x} \\ \frac{\partial \varphi_y}{\partial y} \\ \frac{\partial \varphi_x}{\partial y} + \frac{\partial \varphi_y}{\partial x} \end{Bmatrix} \tag{6.5}$$

$$\{\varepsilon^{nl}\} = \begin{Bmatrix} \varepsilon_x^{nl} \\ \varepsilon_y^{nl} \\ \gamma_{xy}^{nl} \end{Bmatrix} = \begin{Bmatrix} \frac{1}{2} \left(\frac{\partial w}{\partial x} \right)^2 \\ \frac{1}{2} \left(\frac{\partial w}{\partial y} \right)^2 \\ \frac{\partial w}{\partial x} \frac{\partial w}{\partial y} \end{Bmatrix} \tag{6.6}$$

6.2.2 Constitutive equations

The constitutive equations for an orthotropic layer in the local coordinates system (1, 2, 3), by neglecting $\sigma_3^k = 0$ of kth layer, are expressed as:

$$\begin{Bmatrix} \sigma_{11}^k \\ \sigma_{22}^k \\ \tau_{12}^k \end{Bmatrix} = \begin{bmatrix} Q_{11}^k & Q_{12}^k & 0 \\ Q_{12}^k & Q_{22}^k & 0 \\ 0 & 0 & Q_{66}^k \end{bmatrix} \left(\begin{Bmatrix} E_{11}^k \\ E_{22}^k \\ \gamma_{12}^k \end{Bmatrix} - \begin{Bmatrix} \alpha_1^k \\ \alpha_2^k \\ 0 \end{Bmatrix} \right) \Delta T \quad (6.7)$$

$$\begin{Bmatrix} \tau_{13}^k \\ \tau_{23}^k \end{Bmatrix} = \begin{bmatrix} Q_{44}^k & 0 \\ 0 & Q_{55}^{5k^\circ} \end{bmatrix} \begin{Bmatrix} \gamma_{13}^k \\ \gamma_{23}^k \end{Bmatrix} \quad (6.8)$$

where subscripts 1 and 2 indicate the fibers direction and in-plane transverse to the fibers direction, respectively; subscript 3 is the direction normal to the plate, α_1^k and α_2^k are thermal expansion coefficients of kth layer, and ΔT is the temperature rise. The reduced stiffness components $Q_{ij}^{k^\circ}$ are given by:

$$\begin{aligned} Q_{11}^k &= \frac{E_1^k}{1 - \nu_{12}^k \nu_{21}^k} \\ Q_{22}^k &= \frac{E_2^k}{1 - \nu_{12}^k \nu_{21}^k} \\ Q_{12}^k &= \frac{\nu_{21}^k E_1^k}{1 - \nu_{12}^k \nu_{21}^k} \\ Q_{66}^k &= G_{12}^k \\ Q_{44}^k &= G_{13}^k \\ Q_{55}^k &= G_{23}^k \end{aligned} \quad (6.9)$$

Where E_1^k and E_2^k denote the Young modulus of the material in the 1 and 2 directions, respectively, G_{12}^k, G_{23}^k and G_{13}^k are the elasticity transverse modulus in the 1–2, 2–3 and 1–3 planes, respectively, ν_{12}^k, ν_{21}^k are Poisson's ratios.

The stress–strain relationship of each layer in the global coordinate system (x, y, z) is given by:

$$\begin{Bmatrix} \sigma_{xx}^k \\ \sigma_{yy}^k \\ \tau_{xy}^k \end{Bmatrix} = \begin{bmatrix} \bar{Q}_{11} & \bar{Q}_{12} & \bar{Q}_{16} \\ \bar{Q}_{12} & \bar{Q}_{22} & \bar{Q}_{26} \\ \bar{Q}_{61} & \bar{Q}_{62} & \bar{Q}_{66} \end{bmatrix} \left(\begin{Bmatrix} E_{xx}^k \\ E_{yy}^k \\ \gamma_{xy}^k \end{Bmatrix} - \begin{Bmatrix} \alpha_x^k \\ \alpha_y^k \\ \alpha_{xy}^k \end{Bmatrix} \right) \Delta T \quad (6.10)$$

And

$$\begin{Bmatrix} \tau_{xz}^k \\ \tau_{yz}^k \end{Bmatrix} = \begin{bmatrix} \bar{Q}_{44}^k & \bar{Q}_{45}^k \\ \bar{Q}_{54}^k & \bar{Q}_{55}^k \end{bmatrix} \begin{Bmatrix} \gamma_{xz}^k \\ \gamma_{yz}^k \end{Bmatrix} \quad (6.11)$$

Where

$$\begin{aligned} \alpha_x^k &= \alpha_{11}^k \cos^2 \theta + \alpha_{22}^k \sin^2 \theta \\ \alpha_y^k &= \alpha_{22}^k \cos^2 \theta + \alpha_{11}^k \sin^2 \theta \\ \alpha_{xy}^k &= (\alpha_{11}^k - \alpha_{22}^k) \cos \theta \sin \theta \end{aligned} \quad (6.12)$$

And

$$\begin{aligned}
 \bar{Q}_{11}^k &= Q_{11}^k \cos^4 \theta + Q_{22}^k \sin^4 \theta + 2(Q_{12}^k + 2Q_{66}^k) \sin^2 \theta \cos^2 \theta \\
 \bar{Q}_{22}^k &= Q_{11}^k \sin^4 \theta + Q_{22}^k \cos^4 \theta + 2(Q_{12}^k + 2Q_{66}^k) \sin^2 \theta \cos^2 \theta \\
 \bar{Q}_{12}^k &= (Q_{11}^k + Q_{22}^k - 4Q_{66}^k) \sin^2 \theta \cos^2 \theta + Q_{12}^k (\sin^4 \theta + \cos^4 \theta) \\
 \bar{Q}_{66}^k &= (Q_{11}^k + Q_{22}^k - 2Q_{12}^k - 2Q_{66}^k) \sin^2 \theta \cos^2 \theta + Q_{66}^k (\sin^4 \theta + \cos^4 \theta) \\
 \bar{Q}_{16}^k &= (Q_{11}^k - Q_{12}^k - 2Q_{66}^k) \sin \theta \cos^3 \theta - (Q_{11}^k - Q_{12}^k - 2Q_{66}^k) \sin^3 \theta \cos \theta \\
 \bar{Q}_{26}^k &= (Q_{11}^k - Q_{12}^k - 2Q_{66}^k) \sin^3 \theta \cos \theta - (Q_{11}^k - Q_{12}^k - 2Q_{66}^k) \sin \theta \cos^3 \theta \\
 \bar{Q}_{44}^k &= Q_{44}^k \cos^2 \theta + Q_{55}^k \sin^2 \theta \\
 \bar{Q}_{55}^k &= Q_{44}^k \sin^2 \theta + Q_{55}^k \cos^2 \theta \\
 \bar{Q}_{45}^k &= (Q_{44}^k - Q_{55}^k) \sin \theta \cos \theta
 \end{aligned} \tag{6.13}$$

θ is the fiber orientation angle with respect to material coordinate system.

6.2.3 Stress resultants

The stress resultants through thickness of the laminated plate are given by:

$$[NM] = \begin{bmatrix} N_x & M_x \\ N_y & M_y \\ N_{xy} & M_{xy} \end{bmatrix} = \sum_{k=1}^{k=n} \int_{z^k}^{z^{k+1}} \begin{bmatrix} \bar{Q}_{11} & \bar{Q}_{12} & \bar{Q}_{16} \\ \bar{Q}_{12} & \bar{Q}_{22} & \bar{Q}_{26} \\ \bar{Q}_{61} & \bar{Q}_{62} & \bar{Q}_{66} \end{bmatrix} \left(\begin{Bmatrix} E_{xx}^k \\ E_{yy}^k \\ \gamma_{xy}^k \end{Bmatrix} - \begin{Bmatrix} \alpha_x^k \\ \alpha_y^k \\ \alpha_{xy}^k \end{Bmatrix} \Delta T \right) \begin{Bmatrix} 1 \\ z \end{Bmatrix} dz \tag{6.14}$$

$$\begin{bmatrix} Q_{xz} \\ Q_{yz} \end{bmatrix} = \sum_{k=1}^{k=n} \int_{z^k}^{z^{k+1}} \begin{Bmatrix} \tau_{xz}^k \\ \tau_{yz}^k \end{Bmatrix} dz = \sum_{k=1}^{k=n} \int_{z^k}^{z^{k+1}} \begin{bmatrix} \bar{Q}_{44}^k & \bar{Q}_{45}^k \\ \bar{Q}_{54}^k & \bar{Q}_{55}^k \end{bmatrix} \begin{Bmatrix} \gamma_{xz}^k \\ \gamma_{yz}^k \end{Bmatrix} dz \tag{6.15}$$

where n is the layers number.

The earlier equations can be rewritten in the matrix form as follows:

$$\begin{Bmatrix} N \\ M \\ Q \end{Bmatrix} = \begin{bmatrix} [A] & [B] & 0 \\ [B] & [D] & 0 \\ 0 & 0 & [H] \end{bmatrix} \left(\begin{Bmatrix} \varepsilon^0 \\ K \\ \gamma_z \end{Bmatrix} - \Delta T \begin{Bmatrix} \{\alpha\} \\ 0 \\ 0 \end{Bmatrix} \right) \quad (6.16)$$

The elasticity matrices components $A_{ij}, B_{ij}, D_{ij}, H_{ij}$ can be written as follows:

$$(A_{ij}, B_{ij}, D_{ij}) = \sum_{k=1}^{k=n} \int_{z^k}^{z^{k+1}} \bar{Q}_{ij}^k (1zz^2) dz \quad (6.17)$$

$$(H_{ij}) = \sum_{k=1}^{k=n} \int_{z^k}^{z^{k+1}} \bar{Q}_{ij}^k . dz \quad (6.18)$$

The above equations can be rewritten in the following form:

$$\begin{aligned} A_{ij} &= \sum_{k=1}^{k=n} \bar{Q}_{ij}^k (h_k - h_{k-1}) \\ B_{ij} &= \frac{1}{2} \sum_{k=1}^{k=n} \bar{Q}_{ij}^k (h_k^2 - h_{k-1}^2) \\ D_{ij} &= \frac{1}{3} \sum_{k=1}^{k=n} \bar{Q}_{ij}^k (h_k^3 - h_{k-1}^3) \\ H_{ij} &= \sum_{k=1}^{k=n} \bar{Q}_{ij}^k (h_k - h_{k-1}) \end{aligned} \quad (6.19)$$

6.3 Finite Element Formulation

A four-noded rectangular finite element having five degrees of freedom per node, based on the first-order shear deformation theory, is formulated.

6.3.1 Displacement interpolation and shape functions

The displacements field vector of the present finite element can be defined in the following form Figure 6.1.

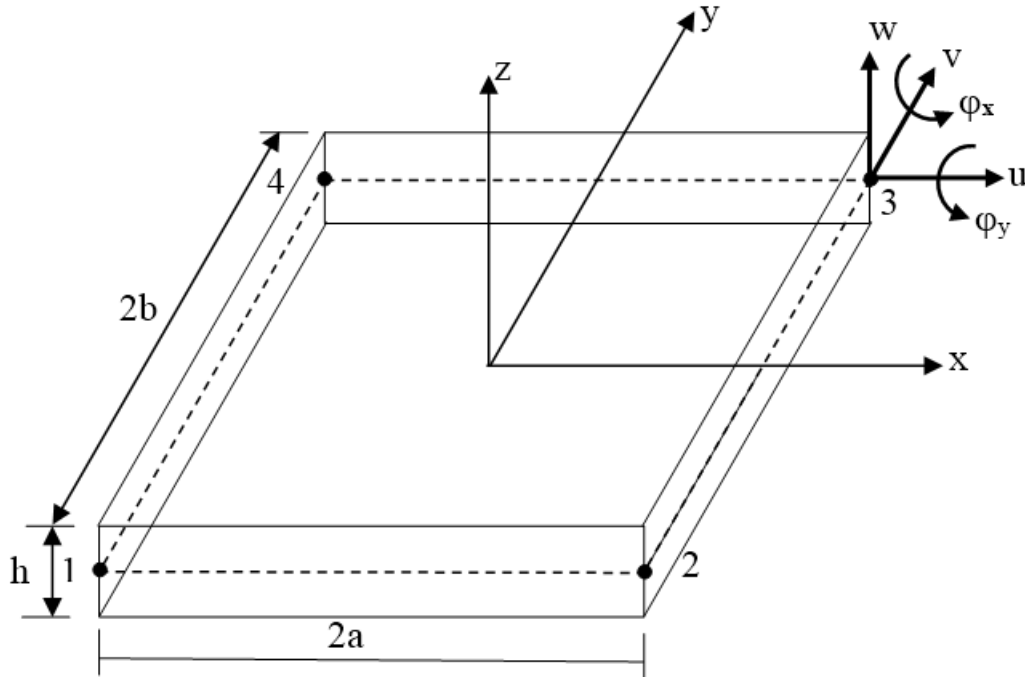


Figure 6.1: Geometry and nodal variables of the element.

$$\delta_i(x, y) = \sum_{\alpha=1}^4 N_{\alpha}(x, y) \delta_i^{\alpha} \quad (i = 1, 5) \quad (6.20)$$

where $\delta_i(x, y)$ is the displacement vector of a given point $M(x, y)$ within the element.

δ_i^{α} and N_{α} are displacement vector and the bilinear Lagrange shape functions associated with node α , respectively.

$$\delta^{\alpha} = u^{\alpha}, v^{\alpha}, w^{\alpha}, \varphi_x^{\alpha} \text{ or } \varphi_y^{\alpha} \quad (a = 1, 2, 3, 4)$$

And

$$\begin{aligned}
 N_1(x, y) &= \frac{1}{4ab}(a-x)(b-y) \\
 N_2(x, y) &= \frac{1}{4ab}(a+x)(b-y) \\
 N_3(x, y) &= \frac{1}{4ab}(a+x)(b+y) \\
 N_4(x, y) &= \frac{1}{4ab}(a-x)(b+y)
 \end{aligned}
 \tag{6.21}$$

6.3.2 Strain-displacement relationship matrices

The strain-displacement relationship of Eq (6.3) can be rewritten as follows:

$$\begin{aligned}
 \{\varepsilon^0\} &= [B_m]\{\delta\} \\
 \{K\} &= [B_b]\{\delta\} \\
 \{\gamma\} &= [B_s]\{\delta\} \\
 \begin{Bmatrix} \frac{\partial w}{\partial x} \\ \frac{\partial w}{\partial y} \end{Bmatrix} &= [G]\{\delta\}
 \end{aligned}
 \tag{6.22}$$

Where

$$\begin{bmatrix} B_m \end{bmatrix} = \begin{bmatrix} \frac{\partial N_i}{\partial x} & 0 & 0 & 0 & 0 \\ 0 & \frac{\partial N_i}{\partial y} & 0 & 0 & 0 \\ \frac{\partial N_i}{\partial y} & \frac{\partial N_i}{\partial x} & 0 & 0 & 0 \end{bmatrix} \quad (i = 1, 2, 3, 4) \quad (6.23)$$

$$\begin{bmatrix} B_b \end{bmatrix} = \begin{bmatrix} 0 & 0 & 0 & \frac{\partial N_i}{\partial x} & 0 \\ 0 & 0 & 0 & 0 & \frac{\partial N_i}{\partial y} \\ 0 & 0 & 0 & \frac{\partial N_i}{\partial y} & \frac{\partial N_i}{\partial x} \end{bmatrix} \quad (i = 1, 2, 3, 4) \quad (6.24)$$

$$\begin{bmatrix} B_s \end{bmatrix} = \begin{bmatrix} 0 & 0 & \frac{\partial N_i}{\partial x} & N_i & 0 \\ 0 & 0 & \frac{\partial N_i}{\partial y} & 0 & N_i \end{bmatrix} \quad (i = 1, 2, 3, 4) \quad (6.25)$$

$$\begin{bmatrix} G \end{bmatrix} = \begin{bmatrix} 0 & 0 & \frac{\partial N_i}{\partial x} & 0 & 0 \\ 0 & 0 & \frac{\partial N_i}{\partial y} & 0 & 0 \end{bmatrix} \quad (i = 1, 2, 3, 4) \quad (6.26)$$

$\begin{bmatrix} B_m \end{bmatrix}$ and $\begin{bmatrix} B_b \end{bmatrix}$ are (3×20) matrices, and the subscripts m and b denote the membrane and the bending strains, respectively. $\begin{bmatrix} B_s \end{bmatrix}$ and $\begin{bmatrix} D \end{bmatrix}$ are (2×20) matrices, and the subscript “s” denotes the shear strain.

And $\left\{ \delta \right\}$ is (20×1) matrix, given by:

$$\left\{ \delta \right\}^T = \left\{ u_\alpha \quad v_\alpha \quad w_\alpha \quad \varphi_{x\alpha} \quad \varphi_{y\alpha} \right\} \quad (\alpha = 1, 2, 3, 4)$$

6.3.3 Derivation of the elementary matrices

The total potential energy principle is used to derivate the elementary stiffness matrix of the element.

It is defined by:

$$\Pi = U - W \quad (6.27)$$

U and W are the deformation potential energy and the external forces work, respectively.

Eq(6.27) can be written in terms of stress resultants and the corresponding strains as follows:

$$\Pi = \frac{1}{2} \int_A \left(\left\{ \varepsilon_0 \right\}^t \left\{ N \right\} + \left\{ K \right\}^t \left\{ M \right\} + \left\{ \gamma_z \right\}^t \left\{ Q \right\} \right) dA + \frac{1}{2} \int_A \left\{ \varepsilon_{nl} \right\}^t \left\{ N \right\} dA \quad (6.28)$$

where A is the element area.

Using Eqs.(6.16),(6.23),(6.24) and (6.25), the total potential energy can be written as

$$\begin{aligned} \Pi = \frac{1}{2} & \left(\int_{-b}^b \int_{-a}^a \left\{ \delta \right\}^t \left[B_m \right]^t \left[A \right] \left[B_m \right] + \left[B_m \right]^t \left[B \right] \left[B_b \right] \right. \\ & + \left[B_b \right]^t \left[B \right] \left[B_m \right] + \left[B_b \right]^t \left[D \right] \left[B_b \right] + \dots + \left[B_s \right]^t \left[H \right] \left[B_s \right] \left. \right) \left\{ \delta \right\} dx dy \\ & + \int_{-b}^b \int_{-a}^a \frac{1}{2} \left\{ q \right\}^t \left[G \right]^t \left[N \right] \left[G \right] \left\{ \delta \right\} dx dy \quad (6.29) \end{aligned}$$

Where

$$\left[N \right] = \begin{bmatrix} N_x & N_{xy} \\ N_{xy} & N_y \end{bmatrix} \quad (6.30)$$

The cancelation of the second variation of the total potential energy, with respect to the nodal values $\left\{ \delta \right\}$, leads to the following eigenvalue problem

$$\left(\left[K_e \right] + \left[K_g^e \right] \right) \left\{ \delta \right\} = 0 \quad (6.31)$$

Using the loading factor λ , $\left[N \right] = \left[N^0 \right]$.

The eigenvalue problem used to evaluate the critical temperature or the critical load can be given by

$$\det \left(\left[K_e \right] + \lambda \left[K_{g0}^e \right] \right) = 0 \quad (6.32)$$

and the critical temperature rise is given by

$$\Delta T_{cr} = \lambda_{cr} \cdot \Delta T \quad (6.33)$$

The critical load is given by

$$N_{cr} = \lambda_{cr} \cdot \Delta T_{cr} N^0 \quad (6.34)$$

where $\left[K_e \right]$ and $\left[K_{g0}^e \right]$ are the elementary stiffness matrix and the elementary geometrical matrix, respectively.

The stiffness matrix $\left[K_e \right]$ is the sum of five matrices as follows:

$$\left[K_e \right] = \left[K_e^m \right] + \left[K_e^{e1} \right] + \left[K_e^{c2} \right] + \left[K_e^b \right] + \left[K_e^s \right] \quad (6.35)$$

in which

$$\begin{aligned}
 \begin{bmatrix} K_e^m \end{bmatrix} &= \int_{-b}^b \int_{-a}^a ([B_m]^T [A] [B_m]) dx dy \\
 \begin{bmatrix} K_e^{c1} \end{bmatrix} &= \int_{-b}^b \int_{-a}^a ([B_m]^T [A] [B_b]) dx dy \\
 \begin{bmatrix} K_e^{c2} \end{bmatrix} &= \int_{-b}^b \int_{-a}^a ([B_b]^T [A] [B_m]) dx dy \\
 \begin{bmatrix} K_e^b \end{bmatrix} &= \int_{-b}^b \int_{-a}^a ([B_b]^T [A] [B_b]) dx dy \\
 \begin{bmatrix} K_e^s \end{bmatrix} &= \int_{-b}^b \int_{-a}^a ([B_s]^T [A] [B_s]) dx dy
 \end{aligned} \tag{6.36}$$

The geometrical matrix can be written as

$$\begin{bmatrix} K_{g0}^e \end{bmatrix} = \int_{-b}^b \int_{-a}^a ([G]^T [N^0] [G]) dx dy \tag{6.37}$$

Where $\begin{bmatrix} N^0 \end{bmatrix} = \begin{bmatrix} N_x^0 & N_{xy}^0 \\ N_{xy}^0 & N_y^0 \end{bmatrix}$.

6.3.4 Assumed natural shear strain method

To alleviate the locking phenomenon, the assumed strain method is employed.

For natural assumed transverse shear strains $\bar{\gamma}_{xz}^A$ and $\bar{\gamma}_{yz}^A$ the following sampling points are employed as shown in Figure 6.2 [42].

According to Figure 6.2, the sampling point coordinates are given as

$$\bar{\gamma}_{xz}^A : (0, b) \text{ and } (0, -b) \quad \bar{\gamma}_{yz}^A : (a, 0) \text{ and } (-a, 0) \tag{6.38}$$

The assumed natural strains can be defined as follows by

$$\gamma_{xz}^{(0)A} = \sum_1^2 P_i(y) \gamma_{xz}^i, \quad \gamma_{yz}^{(0)A} = \sum_1^2 Q_i(x) \gamma_{yz}^i \tag{6.39}$$

in which i denotes the position of the sampling point and $P_i(y)$ and $Q_i(x)$ are the interpolation functions given by

$$\begin{aligned} P_1(y) &= \frac{1}{2b}(b+y), P_2(y) = \frac{1}{2b}(b-y) \\ Q_1(x) &= \frac{1}{2a}(a+x), Q_2(x) = \frac{1}{2a}(a-x) \end{aligned} \quad (6.40)$$

The relations of Eq.(6.39) can be rewritten in the following matrix form

$$\left\{ \bar{\gamma}_z \right\} = \left[\bar{B}_s \right] \left\{ \delta \right\} \quad (6.41)$$

Where $\left[\bar{B}_s \right]$ is the assumed natural strain–displacement relationship matrix, given by

$$\begin{aligned} \left[\bar{B}_s \right] &= \left\{ P_1(y) \quad Q_1(x) \right\} \begin{bmatrix} 0 & 0 & \frac{\partial N_i}{\partial x}(0, b) & N_i(0, b) & 0 \\ 0 & 0 & \frac{\partial N_i}{\partial y}(a, 0) & 0 & N_i(a, 0) \end{bmatrix} \\ &+ \left\{ P_2(y) \quad Q_2(x) \right\} \begin{bmatrix} 0 & 0 & \frac{\partial N_i}{\partial x}(0, -b) & N_i(0, -b) & 0 \\ 0 & 0 & \frac{\partial N_i}{\partial y}(-a, 0) & 0 & N_i(-a, 0) \end{bmatrix} \end{aligned} \quad (6.42)$$

$\left[B_s \right]$ is substituted by $\left[\bar{B}_s \right]$ in the shear stiffness matrix $\left[K_e^s \right]$

6.3.5 Natural vibration of pre-stressed plates

Hamilton principle is defined by

$$\delta \int_{t_1}^{t_2} (\Pi - T) dt = 0 \quad (6.43)$$

where T is the kinetic energy and t_1 and t_2 are initial and final instant, respectively.

Using Lagrange equation, the equation of motion can be expressed by

$$\left[M \right] \left\{ \ddot{\delta} \right\} + \left[K_T \right] \left\{ \delta \right\} = 0 \quad (6.44)$$

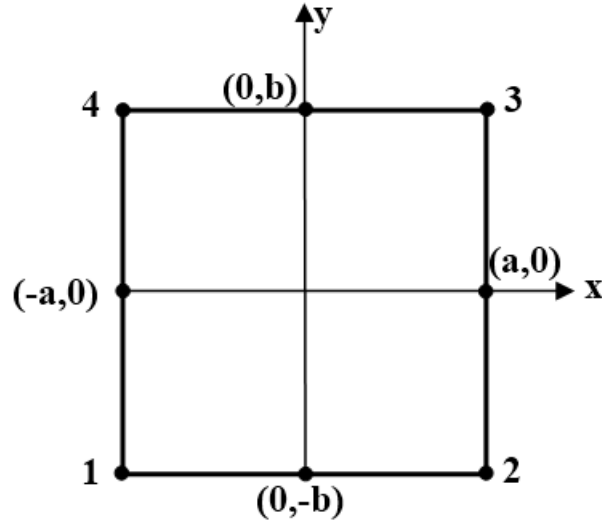


Figure 6.2: Sampling point $\bar{\gamma}_{xz}^A$ and $\bar{\gamma}_{yz}^A$.

where $[M]$ is the mass matrix, $[K_T]$ is the stiffness matrix, including the thermal effect and $\left\{ \ddot{\delta} \right\} = \frac{d^2}{dt^2} \left\{ \delta \right\}$

$$[K_T] = [K^e] + [K_g^e] \quad (6.45)$$

• **Derivation of mass matrix**

The variation of kinetic energy, with respect to time, is given by

$$\delta T = \int_v \rho (\ddot{u} \cdot \delta u + \ddot{v} \cdot \delta v + \ddot{w} \cdot \delta w) dV \quad (6.46)$$

where ρ and V are the material density and element volume, respectively.

This expression can be rewritten as

$$\begin{aligned} \delta T = \int_A I_0 (\ddot{u}_0 \cdot \delta u_0 + \ddot{v}_0 \cdot \delta v_0 + \ddot{w} \cdot \delta w) + I_1 (\ddot{u}_0 \delta \varphi_x + \ddot{\varphi}_x \delta u_0 + \ddot{v}_0 \delta \varphi_y + \ddot{\varphi}_y \delta v_0 \\ + I_2 (\ddot{\varphi}_x \delta \varphi_x + \ddot{\varphi}_y \delta \varphi_y)) dA \quad (6.47) \end{aligned}$$

Where

$$(I_0, I_1, I_2) = \int_{-\frac{h}{2}}^{\frac{h}{2}} \frac{1}{h} \rho(1, z, z^2) dz \quad (6.48)$$

The inertia matrix is given by

$$[m] = \begin{bmatrix} I_0 & 0 & 0 & I_1 & 0 \\ 0 & I_0 & 0 & 0 & I_1 \\ 0 & 0 & I_0 & 0 & 0 \\ I_1 & 0 & 0 & I_2 & 0 \\ 0 & I_1 & 0 & 0 & I_2 \end{bmatrix} \quad (6.49)$$

The mass matrix is given by

$$[M] = \int_{-b}^b \int_{-a}^a ([N]^T [m] [N]) dx dy \quad (6.50)$$

Substituting $\{\ddot{\delta}\}$ by $-\omega^2 \{\delta\}$ in Eq(6.43), we obtain the following eigenvalue problem

$$\left([K_e] + [K_g^e] - \omega^2 [M] \right) \{\delta\} = 0 \quad (6.51)$$

6.4 Effect of Thermal Loading on Free Vibration of Angle-Ply Laminated Composite Plates

In this section, the finite element, based on the first order shear deformation theory with assumed natural strain method, is used to analyze the effect of temperature load on the fundamental natural frequencies of laminated plates. The general geometry of the plate and boundary conditions considered in the present analysis are shown in Figure 6.3.

Boundary conditions, employed in numerical tests, are as follows

Simply supported plate at all edges

$$u_0 = v_0 = w = \varphi_y = 0 \text{ at } x = 0, x = L$$

$$u_0 = v_0 = w = \varphi_x = 0 \text{ at } y = 0, y = l$$

The material properties of the individual layer are taken as follows

$$\frac{E_1}{E_2} = 15, \frac{G_{12}}{E_2} = \frac{G_{13}}{E_2} = 0.5, \frac{G_{23}}{E_2} = 0.3356, \nu_{12} = 0.3, \frac{\alpha_1}{\alpha_0} = 0.015, \frac{\alpha_2}{\alpha_0} = 1, \rho = 1$$

Where α_0 is a normalization factor of thermal expansion coefficients.

Subscripts 1 and 2 stand for parallel and perpendicular directions to the fibers, respectively.

The dimensionless temperature rise is defined as

$$\bar{\lambda} = \alpha_0 \Delta T$$

and the dimensionless critical temperature is defined as

$$\bar{\lambda}_{cr} = \alpha_0 \Delta T_{cr}$$

The natural frequencies are normalized by the following equation

$$\varpi = \omega \times h \sqrt{\frac{\rho}{E_2}}$$

and for Figures 6.4, 6.5 and 6.6, $\varpi = \omega \times L \sqrt{\frac{\rho}{E_2}}$.

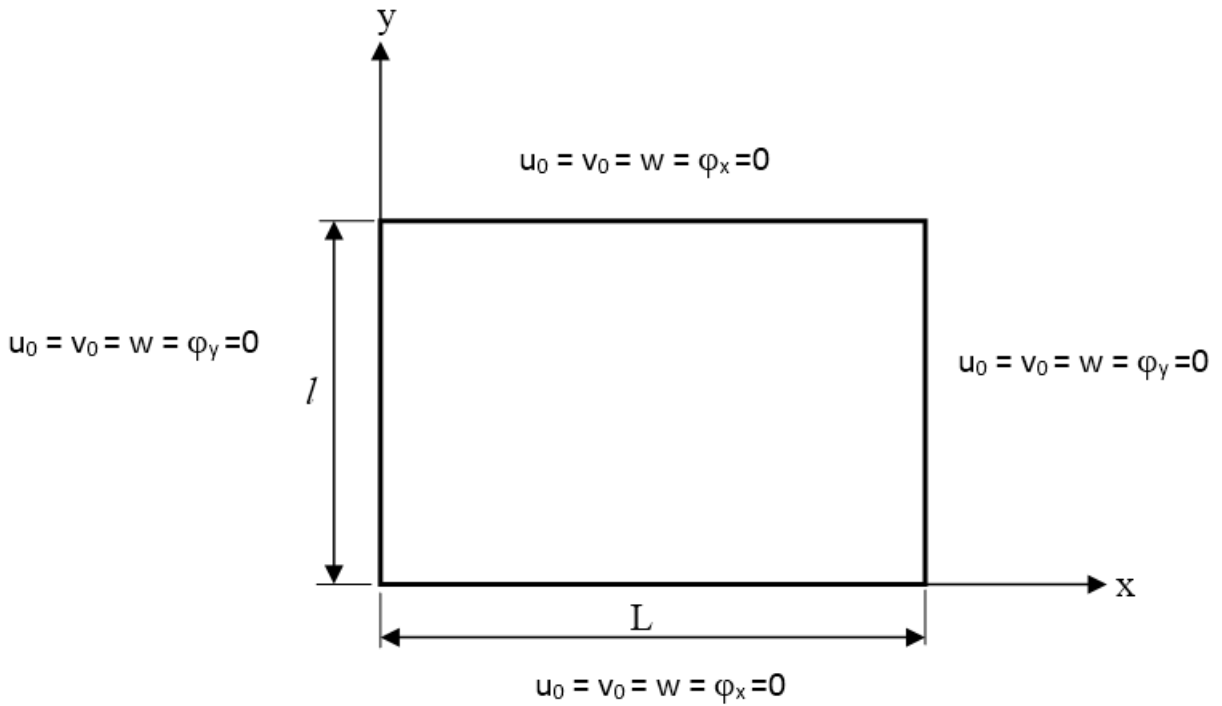


Figure 6.3: Geometry and boundary conditions.

6.4.1 Convergence of the first natural frequency

A simply supported 10-layered anti-symmetric cross-ply $(0/90/\dots/0/90)_{10}$ square plate with $(L/h = 5)$ is analyzed to check the convergence of the first natural frequencies, for $k = 0$ and for different degree of anisotropy values. Four cases with 4×4 , 8×8 , 12×12 and 16×16 meshes are considered. The numerical results of the dimensionless first natural frequency, obtained by the present element and those obtained by 3D analysis of Noor [188], are given in Table 6.1.

Table 6.1: Convergence of non-dimensional natural frequency $\varpi \times 10$ for $\bar{\lambda}$ of 10-layer cross-ply $[0/90/\dots]_{10}$ square laminated composite plate with $(L/h = 5)$

E_1/E_2	3	10	20	30	40
4×4	2.7640	3.6111	4.2520	4.5431	4.8785
8×8	2.6608	3.4641	4.0939	4.4676	4.7159
12×12	2.6457	3.4409	4.0645	4.4362	4.6861
16×16	2.6457	3.4292	4.0546	4.4272	4.6736
3D (Noor) [188]	2.6583	3.4250	4.0497	4.4011	4.6498

6.4.2 Convergence of the critical temperature

Critical temperature of cross-ply 0/90/0, simply supported plate, subjected to uniform temperature rise is analyzed for different side-to-thickness ratio. The plate is analyzed with 4×4 , 8×8 , 12×12 and 16×16 mesh divisions. Table 6.2 shows that the results obtained by the present element are in agreement with Cetkovic [199], 3D [188], and HDST [198,206].

Table 6.2: Convergence of non-dimensional critical temperatures $\bar{\lambda}_{cr}$ of 3-layer cross-ply [0/90/0] square laminated composite plates for different L/h ratios

L/h	5	10	20	100
4×4	0.1934	0.08220	0.02540	0.001100
8×8	0.1865	0.07770	0.02360	0.001000
12×12	0.1853	0.07570	0.02320	0.001000
16×16	0.1791	0.07530	0.02310	0.001000
3D [188]	0.1763	0.07467	0.02308	0.000996
Cetkovic [199]	0.1784	0.07498	0.02303	0.000996
HSDT [206]	0.1763	0.07442	0.02297	0.000996
HSDT [198]	0.1828	0.07439	0.02308	0.000992

6.4.3 Free vibration of angle-ply laminated composite plates, under thermal loading

Free vibration of angle-ply simply supported square laminated composite plates are analyzed under dimensionless thermal loading $\bar{\lambda}$, for different side-to-thickness ratios (L/h). The same previous material proprieties are used.

Tables 6.3,6.4,6.5 show the values of the square of the first natural frequency ϖ^2 , corresponding to dimensionless temperature rise $\bar{\lambda}$. The results show that ϖ^2 decrease with the increase in $\bar{\lambda}$. Thus, this shows that the plate loses its rigidity until reaching 0 for $\bar{\lambda} = \bar{\lambda}_{cr}$.

Table 6.3: Effect of the non-dimensional temperature $\bar{\lambda}$ on non-dimensional natural frequency $(\varpi^2)L/h = 100$.

$\theta = 15^\circ$		$\theta = 30^\circ$		$\theta = 45^\circ$	
$\bar{\lambda}$	ϖ^2	$\bar{\lambda}$	ϖ^2	$\bar{\lambda}$	ϖ^2
0.0000000	0.01801	0.0000000	0.02347	0.000000	0.02619
0.0002272	0.01455	0.000308	0.01877	0.000338	0.02104
0.0004544	0.01109	0.000616	0.01408	0.000677	0.01588
0.0006816	0.00763	0.000924	0.00940	0.001015	0.01073
0.0009088	0.00417	0.001232	0.00470	0.001354	0.00556
0.001136	0.00000	0.001540	0.00000	0.001692	0.00000

Table 6.4: Effect of the non-dimensional temperature $\bar{\lambda}$ on non-dimensional natural frequency $(\varpi^2)L/h = 10$.

$\theta = 15^\circ$		$\theta = 30^\circ$		$\theta = 45^\circ$	
$\bar{\lambda}$	ϖ^2	$\bar{\lambda}$	ϖ^2	$\bar{\lambda}$	ϖ^2
0.0000	1.3600	0.00000	1.7100	0.00000	1.8700
0.0164	1.1200	0.02262	1.3700	0.02470	1.5000
0.0328	0.8700	0.04524	1.0300	0.04941	1.1300
0.0492	0.6300	0.06786	0.6900	0.07412	0.7500
0.0656	0.3800	0.09048	0.3500	0.09883	0.3800
0.0817	0.0000	0.11309	0.0000	0.12354	0.0000

Table 6.5: Effect of the non-dimensional temperature $\bar{\lambda}$ on non-dimensional natural frequency $(\varpi^2)L/h = 5$.

$\theta = 15^\circ$		$\theta = 30^\circ$		$\theta = 45^\circ$	
$\bar{\lambda}$	ϖ^2	$\bar{\lambda}$	ϖ^2	$\bar{\lambda}$	ϖ^2
0.000000	3.2400	0.00000	3.8600	0.000000	4.1000
0.036444	2.7000	0.04972	3.1100	0.053996	3.2900
0.072888	2.1500	0.09944	2.1700	0.107992	2.4700
0.109332	1.6100	0.14916	1.6200	0.161988	1.6600
0.145776	1.0700	0.19888	0.8700	0.215984	0.8500
0.182220	0.0000	0.24860	0.0000	0.269928	0.0000

The square of the first natural frequency ϖ^2 is plotted with respect to the temperature parameter $\bar{\lambda}$ in Figures 6.4, 6.5 and 6.6, respectively. The frequency curves are shown for $\theta = 15^\circ, 30^\circ$ and 45° . The curves are linear for all side-to-thickness ratios and for all fiber orientations angle, and the value of ϖ^2 vanishes when $\bar{\lambda}$ reaches the value of the dimensionless critical temperature $\bar{\lambda}_{cr}$. According to curves of Figures 6.4, 6.5 and 6.6, the linear relation between the square of the first natural frequencies ϖ^2 and the dimensionless temperature rise $\bar{\lambda}$ can be given by the following expression:

$$\frac{\varpi^2}{\varpi_0^2} = 1 - \frac{\bar{\lambda}}{\bar{\lambda}_{cr}}$$

Where ϖ_0^2 is the square of the first natural frequency of the unloaded plates. The above expression is coincided with that given by Noor and Burton [201], Matsunaga [223] and previously by Lurie in 1952 [200].

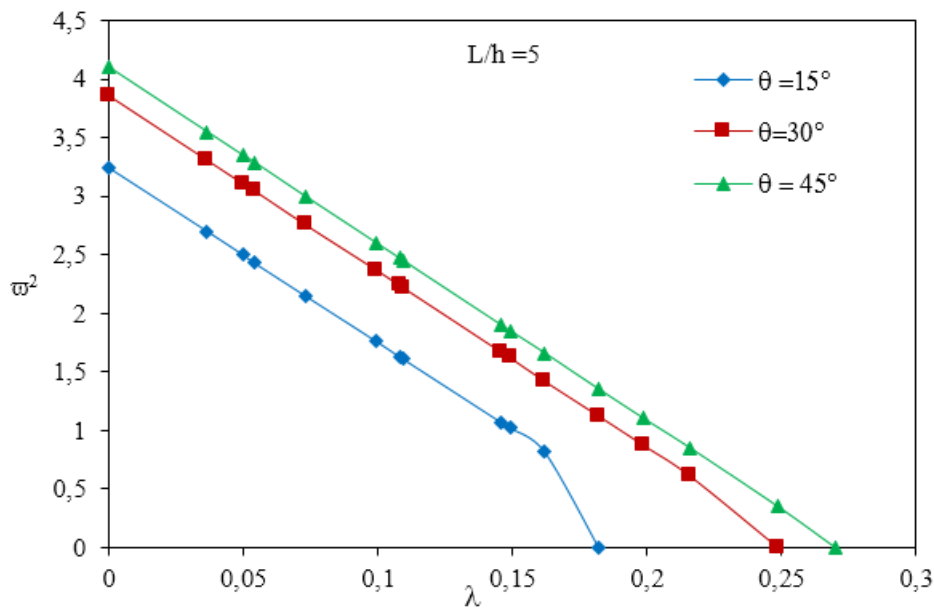


Figure 6.4: Natural frequency ϖ^2 vs temperature $\bar{\lambda}$ of 10-layer angle-ply square laminated composite plates ($L/h = 5$)

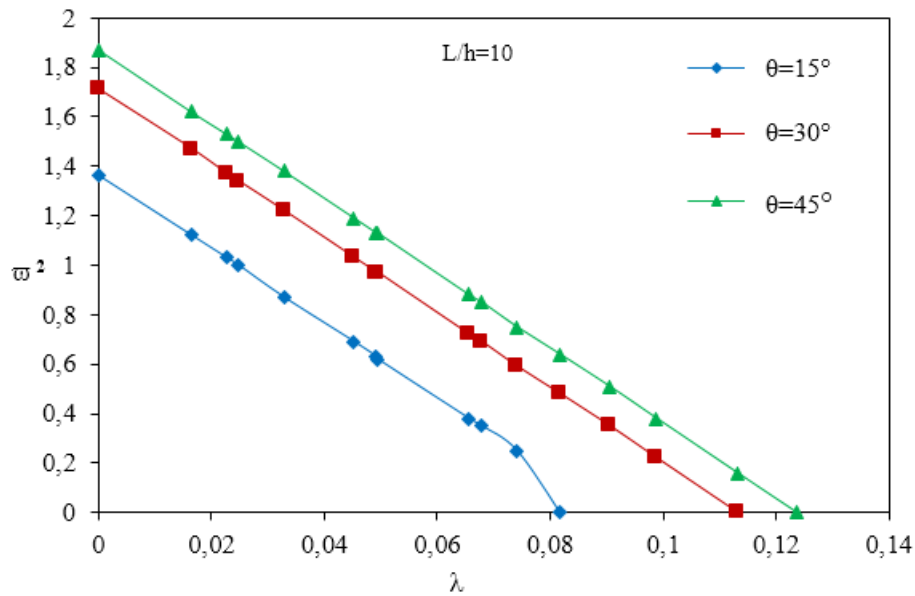


Figure 6.5: Natural frequency ω^2 vs temperature $\bar{\lambda}$ of 10-layer angle-ply square laminated composite plates ($L/h = 10$)

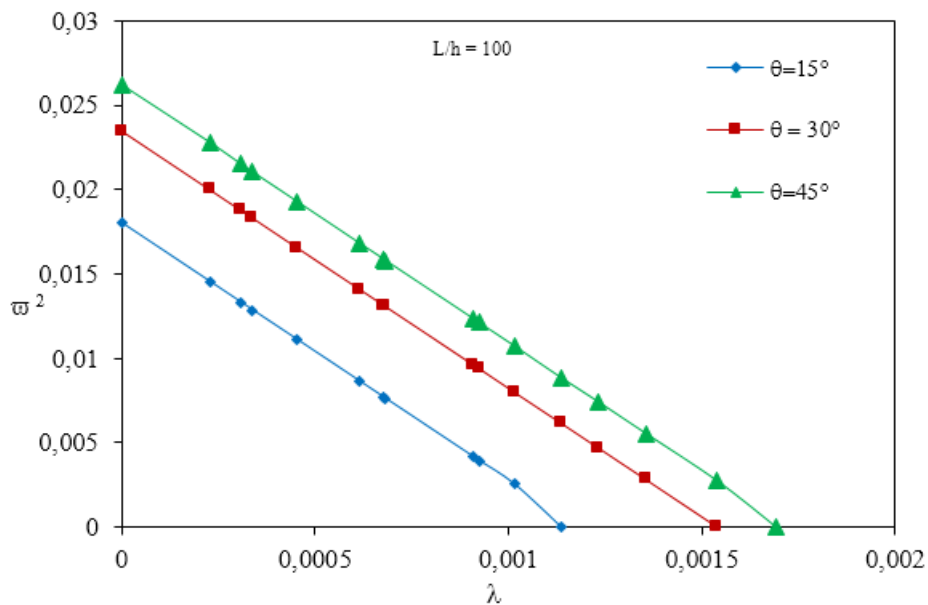


Figure 6.6: Natural frequency ω^2 vs temperature $\bar{\lambda}$ of 10-layer angle-ply square laminated composite plates ($L/h = 100$)

6.4.4 Effect of the side-to-thickness ratio on fundamental natural frequency

A simply supported 10-layered angle-ply $(\theta / - \theta / \dots / \theta / - \theta)_{10}$ square plate is considered to analyze the effect of the plate side-to-thickness ratio, on first natural frequency, for $\bar{\lambda} = 0$ and for different fibers orientation angles ($\theta = 15^\circ, 30^\circ$ and 45°). The dimensionless first natural frequencies obtained by the present finite element and those obtained by Matsunaga [223] are presented in Table 6.6 which shows that the results are in good agreement for all side-to-thickness ratio.

Table 6.6: Non-dimensional frequency $\bar{\omega}$ for ($\bar{\lambda} = 0$) of 10-layer angle-ply square laminated composite plates.

L/h	$\theta = 15^\circ$		$\theta = 30^\circ$		$\theta = 45^\circ$	
	Present	Matsunaga [223]	Present	Matsunaga [223]	Present	Matsunaga [223]
5	0.358900	0.359200	0.391400	0.390500	0.403500	0.401700
10	0.116600	0.116300	0.130700	0.129800	0.136700	0.135500
20	0.032400	0.032020	0.036400	0.036230	0.038407	0.038140
50	0.005339	0.005286	0.006085	0.006009	0.006324	0.006342
100	0.001342	0.001328	0.001532	0.001510	0.001618	0.001595

6.4.5 Effect of side-to-thickness ratio on the critical temperature

The dimensionless critical temperature k_{cr} of 10-layer angle-ply $[\theta / - \theta / \dots]_{10}$ square laminated composite plates for different fiber orientations and for various side-to-thickness ratios is analyzed. Tables 6.7, 6.8 show that the obtained results are in good agreement with those of 3D solution of Noor [201] and those of Matsunaga [223].

Table 6.7: Non-dimensional critical temperatures $\bar{\lambda}_{cr}$ of 10-layer angle-ply $[\theta / - \theta / \dots]_{10}$ square laminated composite plates ($\theta = 0^\circ, 15^\circ$).

L/h	$\theta = 0^\circ$			$\theta = 15^\circ$		
	Present	NOOR [201]	Matsunaga [223]	Present	NOOR [201]	Matsunaga [223]
5	0.14410	0.14360	–	0.182220	0.17530	0.212400
6.67	0.10300	0.10290	–	0.137440	0.132200	–
10	0.05764	0.05780	–	0.081700	0.079040	0.088990
20	0.01740	0.01739	–	0.025900	0.025280	0.027000
100	0.75449×10^3	0.74800×10^{10}	–	0.001136	0.001115	0.001161

Table 6.8: Non-dimensional critical temperatures $\bar{\lambda}_{cr}$ of 10-layer angle-ply $[\theta/-\theta/\dots]_{10}$ square laminated composite plates ($\theta = 30^\circ, 45^\circ$).

L/h	$\theta = 15^\circ$		$\theta = 30^\circ$		$\theta = 45^\circ$	
	Present	Matsunaga [223]	Present	Matsunaga [223]	Present	Matsunaga [223]
5	0.2486	0.2377	0.251100	0.269928	–	0.2656
6.67	0.192200	0.185900	–	0.206453	0.1981	–
10	0.113090	0.110000	0.111000	0.123537	0.1194	0.120900
20	0.035209	0.034460	0.034560	0.039056	0.3810	0.038260
100	0.001540	0.001502	0.001502	0.001692	0.001674	0.001675

6.5 Effect of Mechanical Loading on Free Vibration of Angle-Ply Laminated Composite Plates

The effect of in plane compression load on the fundamental natural frequencies of laminated plates is analyzed here using the present finite element. The geometry of the plate and the boundary conditions considered in the present analysis are shown in Figure 6.7.

The plates are simply supported at all edges. In following, boundary conditions which are given as

$$w = \varphi_y = 0 \text{ at } x = 0, x = L$$

$$v_0 = w = \varphi_x = 0 \text{ at } y = 0, y = l$$

The material properties of the individual layer are taken as follows

$$\frac{E_1}{E_2} = 40, \frac{G_{12}}{E_2} = \frac{G_{13}}{E_2} = \frac{G_{23}}{E_2} = 0.5, \nu_{12} = 0.25, \rho = 1$$

The dimensionless critical load is defined as

$$K_{cr} = \frac{N_{cr} a^2}{E_2 h^3}$$

The natural frequencies are normalized by the following equation

$$\varpi = \frac{\omega a^2}{h} \sqrt{\frac{\rho}{E_2}}$$

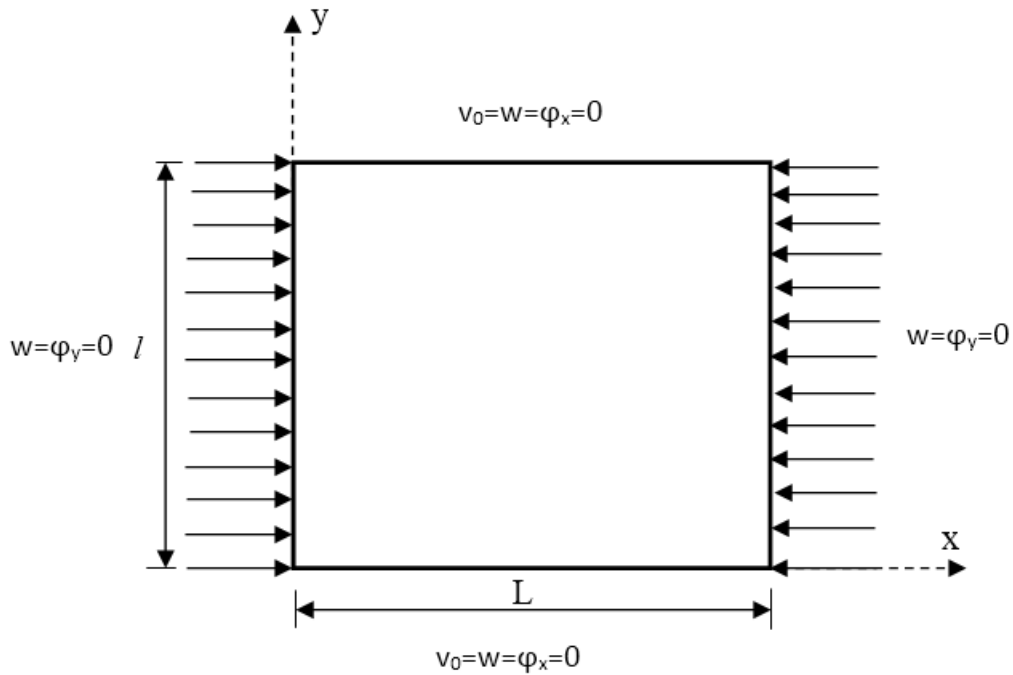


Figure 6.7: Geometry and boundary conditions.

6.5.1 Convergence of the first natural frequency

A simply supported 4-layered anti-symmetric cross-ply ($\theta/ - \theta/\theta/ - \theta$) and 2-layered anti-symmetric angle-ply ($\theta/ - \theta$) square plates with different fiber orientation angle and (L/h) values are analysed here to check the convergence of the first natural frequencies. Five cases with $4 \times 4, 8 \times 8, 12 \times 12, 16 \times 16, 20 \times 20$ meshes are considered. The numerical results of the dimensionless first natural frequency, obtained by the present element and those obtained by Reddy [224], Bert [225] and Viswanathan [226] are given in Tables 6.9, 6.10

Table 6.9: Convergence of non-dimensional natural frequency of 4-layered angle-ply square laminated composite plate with different (L/h) values.

θ	30		45	
(L/h)	10	50	10	50
4×4	18.139	23.393	19.037	24.755
8×8	17.468	22.251	18.350	23.582
12×12	17.347	22.048	18.226	23.302
16×16	17.305	21.978	18.183	23.302
20×20	17.286	21.945	18.163	23.268
Reddy [224]	17.689	-	18.609	24.343
Bert [225]	17.630	-	18.460	23.24
Viswanathan [226]	-	-	23.24	24.348

Table 6.10: Convergence of non-dimensional natural frequency of 2-layered angle-ply square laminated composite plate with different (L/h) values.

θ	30	45
(L/h)	10	10
4×4	13.283	13.689
8×8	12.703	13.111
12×12	12.598	13.007
16×16	12.562	12.971
20×20	12.545	12.954
Reddy [224]	15.001	15.714
Bert [225]	12.680	13.04

6.5.2 Convergence of buckling critical Load

Buckling critical load of 2-layers anti-symmetric cross-ply ($\theta/-\theta$) and 4-layers anti-symmetric angle-ply ($\theta/-\theta/\theta/-\theta$) simply supported square plates, subjected to in plane compression load are analyzed here to check the convergence of buckling critical load. The plates are analyzed with $4 \times 4, 8 \times 8, 12 \times 12, 16 \times 16$ and 20×20 mesh divisions. Tables 6.11, 6.12 shows that the results obtained by the present element are in good agreement with Moita et al. [227], Jones et al. [228] and Senthilnathan et al. [229]

Table 6.11: Convergence of non-dimensional buckling critical load of 2-layered angle-ply square laminated composite plate with different fiber orientation angle and different (L/h) ratios.

θ	0°		30°		45°		60°	
(L/h)	100	10	100	10	100	10	100	10
4×4	39.449	21.618	19.073	17.028	23.524	18.78	21.782	16.558
8×8	36.465	20.682	20.195	16.150	22.292	17.678	20.156	14.393
12×12	35.954	20.516	19.706	16.384	21.840	17.342	19.740	13.552
16×16	35.779	20.459	19.856	15.932	21.754	17.287	19.511	13.453
20×20	35.698	20.432	20.027	15.896	21.715	17.262	19.405	13.407
Moita et al. [227]	36.076	24.203	19.932	16.789	21.642	16.400	19.247	12.668
Jones et al. [228]	35.831	-	20.441	-	21.709	-	19.392	-
Senthilnathan et al. [229]	-	-	-	-	21.666	18.154	-	-

Table 6.12: Convergence of non-dimensional buckling critical load of 4-layered angle-ply square laminated composite plate with different fiber orientation angle and different (L/h) ratios.

θ	0°		30°		45°		60°	
(L/h)	100	10	100	10	100	10	100	10
4×4	39.449	21.618	53.937	31.922	60.340	32.774	53.762	23.950
8×8	36.465	20.683	51.843	30.738	56.808	30.088	46.781	21.710
12×12	35.954	20.516	49.825	30.576	56.194	29.700	45.702	21.431
16×16	35.779	20.459	49.553	30.507	55.982	29.560	45.340	21.341
20×20	35.698	20.432	49.485	30.413	55.884	29.500	45.177	21.300
Moita et al. [227]	35.789	22.550	49.126	29.222	55.285	27.996	44.873	19.910
Jones et al. [228]	35.831	-	49.824	-	56.088	-	45.434	-

6.5.3 Free vibration of angle-ply laminated composite plates, under mechanical loading

Free vibration of angle-ply simply supported square laminated composite plates are analysed here under in plane compression load, for different side-to-thickness ratio (L/h). The same previous material proprieties are used. The square of the first natural frequency ϖ^2 is plotted with respect to in plane compression load parameter N/N_{cr} in Figures 6.8, 6.9, 6.10 and 6.11, respectively. The frequency curves are shown for $\theta = 0^\circ, 30^\circ, 45^\circ$ and 60° . The curves are linear for all side-to-thickness ratios and for all fiber orientations angle, and the value of ϖ^2 vanishes when N reaches the value of the buckling critical load ($N/N_{cr} = 1$), which, show that the plate lose its stiffness.

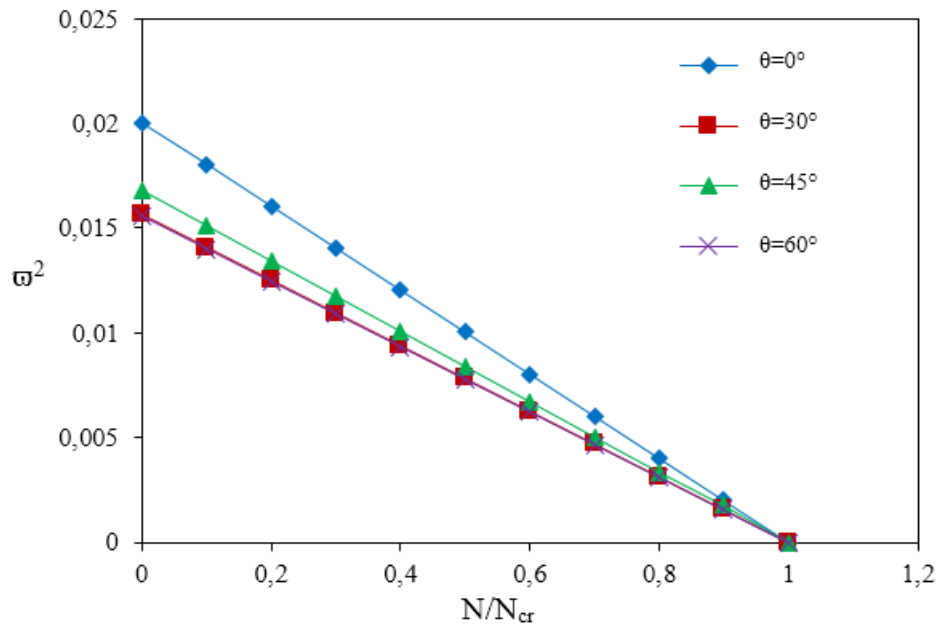


Figure 6.8: Natural frequency ϖ^2 vs in plane compression load N/N_{cr} of anti-symmetric 2 layers square laminated plate ($L/h = 10$).

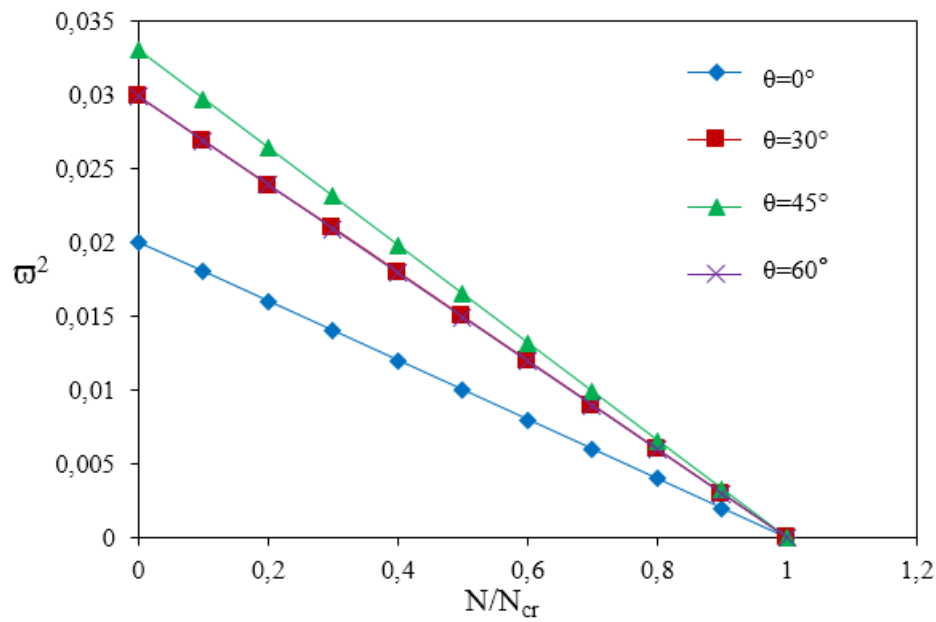


Figure 6.9: Natural frequency ϖ^2 vs in plane compression load N/N_{cr} of anti-symmetric 4 layers square laminated plate ($L/h = 10$).

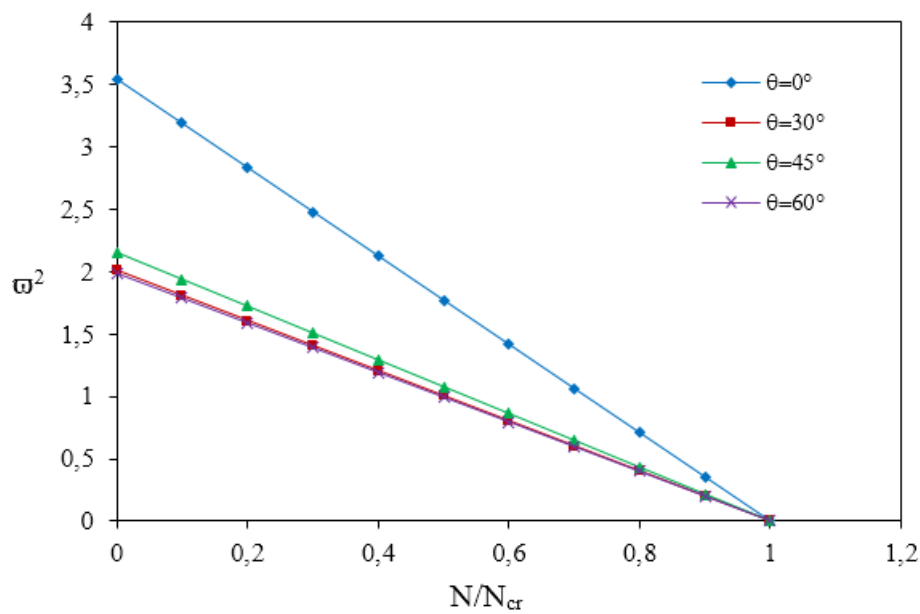


Figure 6.10: Natural frequency ϖ^2 vs in plane compression load N/N_{cr} of anti-symmetric 2 layers square laminated plate ($L/h = 100$).

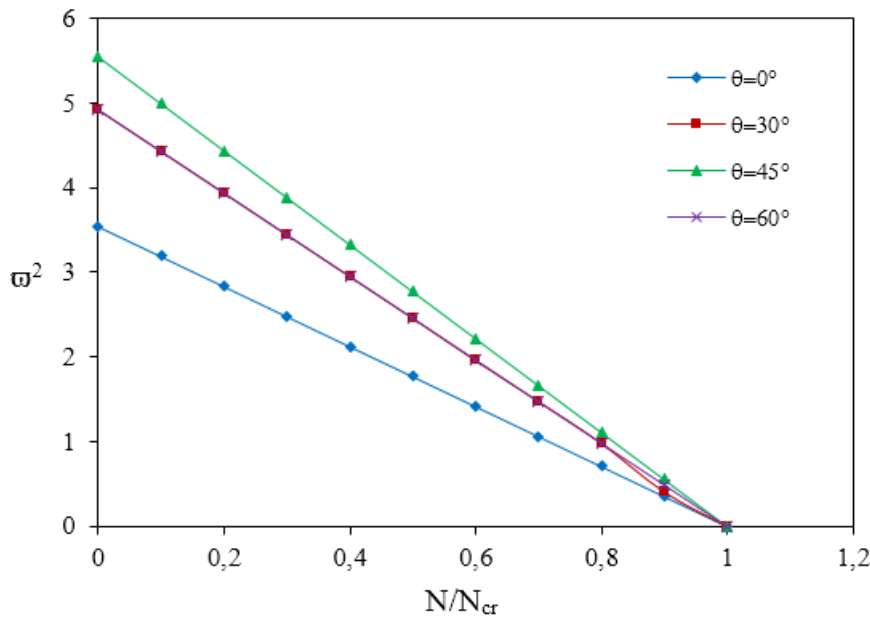


Figure 6.11: Natural frequency ω^2 vs in plane compression load N/N_{cr} of anti-symmetric 4 layers square laminated plate ($L/h = 100$).

6.6 Conclusion

Free vibration of laminated composite plates under thermal and mechanical loading effect have been analyzed, using a four-nodded rectangular finite element based on first order shear deformation with assumed natural shear strain. Total potential energy and Hamilton' principles have been used to derivate stiffness, geometric and mass matrices. Convergence of the natural frequency for unloaded plates case and the critical temperature as well as the buckling critical load is very good, indicating reasonably less number of elements required to get the desired results. The effects of thickness to side ratio, anisotropy degree of single layer and fibers orientation angle, on free vibration, critical buckling temperature and critical buckling load have been also analyzed. The analysis of the effects of thermal and mechanical loading rise on free vibration of angle-ply laminates composite for different thickness to side ratios and for different fibers orientations, shows that the natural frequency decreases in linear way with the increase of loading rise and vanishes for critical value. This relation coincides with the one found in the literature.

General Conclusion

The minimum weight criteria with high performance is essential in the design of aircraft, aerospace vehicles and civil structures until today. This task will be a challenge, especially when the design of wing structures such as aircraft wings, rotor blades, robotic arms or some kind of bridges, is the subject. The behavior of such structures is highly nonlinear due to the deformation of their geometry and the solution of such problems becomes very complex, especially with the use of composite materials. The effects of large displacements may play a primary role in the correct prediction of the behavior of these members, which continue to be modeled as flexible beams. In this way, another difficult task can be imposed here when some structural elements as plates and shells can undergo inplane thermo-mechanical stresses that affect their stiffness and consequently, their dynamic and static behavior. This problem has stimulated the researchers to provide an accurate prediction of free vibration of laminated plates, subjected to inplane thermal or mechanical stresses.

The main objective of the present work was to contribute in nonlinear behavior analysis of beams and plates. This investigation was carried out analytically, experimentally and numerically. This work was divided in two parts. The first part was destined for beams analysis, which an analytical model was firstly developed to analyze the large deflection of laminated cantilever beams. Secondly, an experimental program was prepared in order to carried out several bending experiments on isotropic and composite cantilever beams. In addition, a finite element beam based on the Euler-Bernoulli beam theory, was formulated for beams large deflection analysis. In the second part, the effect of thermo-mechanical loading on free vibration of laminated composite plates was investigated.

In the first chapter of the thesis, basic concepts of nonlinear phenomena were presented. Different types of nonlinearities in solid mechanics were introduced, including geometric, material, kinematic, and force nonlinearities. The importance of nonlinear analysis in structural mechanics was also presented. General solving procedures of nonlinear equations system had been introduced. It was concluded that the geometric nonlinearity is the most important nonlinearity that could appear in the design of some structural elements. Previous works on geometrically nonlinear analysis had been presented in the second chapter which it was concluded that when the large deflection analysis of beams using composite materials, the work is rare in the literature. Several bending experiments were carried out on isotropic and composite cantilever beams in chapter three. In the following, the important points that can be concluded from these experiments.

- It has been shown that the curves for **(PG)** specimens group the vertical displacement is quasi-linear. However, the horizontal displacement is started small and tends to be curve as load increasing.
- Concerning the second group of **(RSF)** specimens, the behavior presented a small initial linear part for the vertical displacement and it started to be an organized curve with load increasing. The horizontal displacement has shown initially small linear part and tends to be curve in parallel with the vertical displacement.
- Regarding the first and the second $[0/90/90/0]$ **(GFP)** laminated specimens, the curves shows that the initial behavior for w is fairly linear and tends to be disorganized curve with load increasing, this is because the new way of displacements measurement and the difficulties that can appear during setting laser electronic telemeters especially for the first ones. The horizontal displacement is initially very small and the tip of beams starts moving on towards the root when significant bending slopes are obtained. However, for the third $[45/-45/-45/45]$ laminated specimen the curves demonstrate an improvement in displacements measurement especially for u . Concerning the last specimen $[0/90/90/0]$ the curves show more improvements for both displacements u, w .

An analytical formulation has been carried out in chapter four, to analyze the large deflection of composite beams. The proposed formulation is based on the elastica beam model, according to the classical Euler-Bernoulli beam theory, which was prepared to be able to dealing with symmetric and non-symmetric laminated beams. Subsequently, for the purpose of validation, the obtained results were compared with both analytical models and experimental studies existing in the literature. It had been shown, that for isotropic beam case the obtained results were clearly in excellent agreement with those obtained in the literature. Also, for symmetric as well as antisymmetric laminated beams cases the results were compared well with those. Furthermore, for the sake of comparison, the present formulation were also compared with the obtained results from the performed experiments. It has been seen, that the present analytical results were going well with the experimental ones. In addition, the varying parameters, such as fiber orientation angle, anisotropic ratio E_1/E_2 and slenderness ratio were examined to discover and understand their effect on the deflections variation of laminated beams. As result, some of the important observations from the parametric study are in the following points

- It has been seen, that the effect of fiber orientation angle on displacements is similar for both symmetric and antisymmetric laminates. It has been also observed that with an increase in fiber orientation angle, there is an increase in deflections values until the angle $\theta = 45^\circ$ where the deflections reaches its maximum values, then it decrease slowly toward the angle $\theta = 90^\circ$, and we can also note that for $\theta = 0^\circ$ the deflections have the minimum value, which means that the beam's rigidity is at the maximum value.
- It has been seen that, the deflection values are affected by the changes of E_1/E_2 when the fiber orientations are between 0 *degree* and 45° , the deflection decrease with the increase in modulus ratio until $E_1/E_2 = 30$ for 0° and $E_1/E_2 = 10$ for $15^\circ, 30^\circ, 45^\circ$ the deflection is not affected much by the increase in modulus ratio. However, when the angle values are $60^\circ, 75^\circ, 90^\circ$ the deflection values are not affected by the changes of modulus ratio.
- It has been observed, that the deflections values increase with the increase of slenderness ratio for different values of anisotropy ratio.

In chapter five, One-dimensional finite element formulation based on the Euler-Bernoulli beam theory has been developed, for the nonlinear bending analysis of composite laminated beams. The present finite element, has been defined by two nodes and three degree of freedom per node. The performance and the reliability of the developed element have been evaluated through some applications on nonlinear bending analysis of isotropic and symmetric laminated beams. The obtained results were compared with the available results obtained analytically and experimentally in the literature as well as the results of the present analytical model. The applications demonstrate that the results goes well with those obtained in the literature. However, it can be seen, that there is some difference with the analytical results, probably because the present element has been formulated, taking in consideration the axial loading effect, while the analytical model have been formulated supposing the inextensibility of the beam. A parametric study was presented to examinte the effect of some parameters such as fiber orientation angle and slenderness ratio on the deflection variation of laminated beams with different boundary conditions. As consequence, Some of the important observations in the following points

- It has been seen, that similar effect of fiber orientation angle on both symmetric and antisymmetric laminates behaviors for both considered boundary conditions cases. With an increase in fiber orientation angle, there is an increase in deflections values until $\theta = 45^\circ$ when the deflections reaches the maximum values, then it decrease slowly until $\theta = 90^\circ$. We can also note that for $\theta = 0^\circ$ the deflection at its minimum value.
- It has been observed, that with the increase in slenderness ratio, the deflections values also are increasing. Also, it can be seen that there is a decrease in deflection values with the increase in orthotropy ratio values.

Free vibration of laminated composite plates under thermal and mechanical loading effect were analyzed the sixth chapter, using a four-nodded rectangular finite element based on first order shear deformation with assumed natural shear strain. Total potential energy and Hamilton' principles were used to derivate stiffness, geometric and mass matrices. Convergence of the natural frequency for unloaded plates case and the critical temperature as well as the buckling critical load was very good, indicating reasonably less number of elements required to get

the desired results. The effects of thickness to side ratio, anisotropy degree of single layer and fibers orientation angle, on free vibration, critical buckling temperature and critical buckling load were also analyzed. The analysis of the effects of thermal and mechanical loading rise on free vibration of angle-ply laminates composite for different thickness to side ratios and for different fibers orientations, were shown that the natural frequency decreases in linear way with the increase of loading rise and vanishes for critical value. This relation coincides with the one found in the literature.

Suggestions for Future Works

- The analytical model as well as the beam finite element can be extended for functionally graded materials analysis.
- The experimental program can be extended for the dynamic behavior.

Bibliography

- [1] E.V. Morozov V.V.Vasiliev. *Mechanics and analysis of composite materials*. Elsevier, 2001.
- [2] P.F.Pai A H.Nayfeh. *Linear and nonlinear structural mechanics*. John Wiley and Sons, 2008.
- [3] J.N.Reddy. *An Introduction to nonlinear finite element analysis: with applications to heat transfer, fluid mechanics, and solid mechanics*. OUP Oxford, 2014.
- [4] D.G.Fertis. *Nonlinear mechanics*. CRC press, 1998.
- [5] N.H.Kim. *Introduction to nonlinear finite element analysis*. Springer Science and Business Media, 2014.
- [6] R.D.Cook. *Finite element modeling for stress analysis*. 1995.
- [7] M.Sathyamoorthy. *Nonlinear analysis of structures*, volume 8. CRC Press, 1997.
- [8] R.D. Ziemian W.McGuire, R.H. Gallagher. *Matrix structural analysis*. 2000.
- [9] M.E.Plesha R.J.Witt R.D.Cook, D.S.Malkus. *Concepts and applications of finite element analysis*. John Willey and Sons, 1989.
- [10] R.L. Taylor O.C.Zienkiewicz. *The finite element method: solid mechanics*, volume 2. Butterworth-heinemann, 2000.
- [11] T.J.Ypma. Historical development of the newton-raphson method. *SIAM review*, 37(4):531–551, 1995.

- [12] E.Riks. The application of newton's method to the problem of elastic stability. *Journal of Applied mechanics*, 39(4):1060–1065, 1972.
- [13] G.A.Wempner. Discrete approximations related to nonlinear theories of solids. *International Journal of Solids and Structures*, 7(11):1581–1599, 1971.
- [14] A.C.Lock A.B.Sabir. Large deflexion, geometrically non-linear finite element analysis of circular arches. *International Journal of Mechanical Sciences*, 15(1):37–47, 1973.
- [15] E.Riks. An incremental approach to the solution of snapping and buckling problems. *International journal of solids and structures*, 15(7):529–551, 1979.
- [16] M.A.Crisfield. A fast incremental/iterative solution procedure that handles “snap-through”. In *Computational Methods in Nonlinear Structural and Solid Mechanics*, pages 55–62. Elsevier, 1981.
- [17] E.Ramm. Strategies for tracing the nonlinear response near limit points. In *Nonlinear finite element analysis in structural mechanics*, pages 63–89. Springer, 1981.
- [18] Y. Bada A.Tati, S. Bouadjadja. Free vibration of thermally stressed angle-ply laminated composite using first-order shear deformation theory model with assumed natural shear strain. *Journal of The Institution of Engineers (India): Series C*, 100(6):937–947, 2019.
- [19] B.C. Lee M.S.Park. Geometrically non-linear and elastoplastic three-dimensional shear flexible beam element of von-mises-type hardening material. *International Journal for Numerical Methods in Engineering*, 39(3):383–408, 1996.
- [20] S.P. Timoshenko. *History of Strength of Materials*. McGRA W-HILL, 1953.
- [21] D.C. Drucker K.E. Bisshopp. Large deflection of cantilever beams. *Quarterly of Applied Mathematics*, 3(3):272–275, 1945.
- [22] J.H. Lau. Large deflections of beams with combined loads. *ASCE.Journal of Engineering Mechanics*, 1974.

- [23] G. Venkateswara.Rao B. Nageswara. Rao. On the large deflection of cantilever beams with end rotational load. *ZAMM-Journal of Applied Mathematics and Mechanics*, 66(10):507–509, 1986.
- [24] B. Nageswara Rao and G. Venkateswara Rao. Large deflections of a nonuniform cantilever beam with end rotational load. *Forschung im Ingenieurwesen A*, 54(1):24–26, 1988.
- [25] L.W. Tsai C.Kimball. Modeling of flexural beams subjected to arbitrary end loads. *Journal of Mechanical Design*, 124(2):223–235, 2002.
- [26] L.Chen. An integral approach for large deflection cantilever beams. *International Journal of Non-Linear Mechanics*, 45(3):301–305, 2010.
- [27] H.D.Conway. The large deflection of simply supported beams. *The London, Edinburgh, and Dublin Philosophical Magazine and Journal of Science*, 38(287):905–911, 1947.
- [28] S.K.L Rao I. K. T Sundara Raja. Large deflections of simply supported beams. *Journal of the Franklin Institute*, 259(6):523–528, 1955.
- [29] P.Seide. Large deflections of a simply supported beam subjected to moment at one end. *Journal of Applied Mechanics*, 51(3):519–525, 1984.
- [30] J. Yang X.Zhang. Inverse problem of elastica of a variable-arc-length beam subjected to a concentrated load. *Acta Mechanica Sinica*, 21(5):444–450, 2005.
- [31] X.Q He S. Chucheepsakul C.M. Wang, K.Y Lam. Large deflections of an end supported beam subjected to a point load. *International Journal of Non-Linear Mechanics*, 32(1):63–72, 1997.
- [32] H.Tari. On the parametric large deflection study of euler–bernoulli cantilever beams subjected to combined tip point loading. *International Journal of Non-Linear Mechanics*, 49:90–99, 2013.
- [33] M. Batista. Large deflections of a beam subject to three-point bending. *International Journal of Non-Linear Mechanics*, 69:84–92, 2015.

- [34] C. M. Wang S.Chucheepsakul, S. Buncharoen. Large deflection of beams under moment gradient. *Journal of engineering mechanics*, 120(9):1848–1860, 1994.
- [35] H. Tseng S. Chucheepsakul, S. Buncharoen. Elastica of simple variable-arc-length beam subjected to end moment. *Journal of engineering mechanics*, 121(7):767–772, 1995.
- [36] T.M. Wang. Nonlinear bending of beams with concentrated loads. *Journal of the Franklin Institute*, 285(5):386–390, 1968.
- [37] T.M. Wang. Non-linear bending of beams with uniformly distributed loads. *International Journal of Non-Linear Mechanics*, 4(4):389–395, 1969.
- [38] R.L. Sierakowski R.D.Schile. Large deflections of a beam loaded and supported at two points. *International Journal of Non-Linear Mechanics*, 2(1):61–68, 1967.
- [39] F. Ellyin A.Ohtsuki. Analytical approach to large deformation problems of frame structures. *JSME International Journal Series A Solid Mechanics and Material Engineering*, 44(1):89–93, 2001.
- [40] S. Kitipornchai M. C.Wang. Shooting—optimization technique for large deflection analysis of structural members. *Engineering Structures*, 14(4):231–240, 1992.
- [41] S.J. Oh B. K.Lee. Elastica and buckling load of simple tapered columns with constant volume. *International Journal of Solids and Structures*, 37(18):2507–2518, 2000.
- [42] K.Lee. Post-buckling of uniform cantilever column under a combined load. *International Journal of Non-Linear Mechanics*, 36(5):813–816, 2001.
- [43] K.Lee. Large deflections of cantilever beams of non-linear elastic material under a combined loading. *International Journal of Non-Linear Mechanics*, 37(3):439–443, 2002.
- [44] E.Solano-Carrillo. Semi-exact solutions for large deflections of cantilever beams of non-linear elastic behaviour. *International Journal of Non-Linear Mechanics*, 44(2):253–256, 2009.

- [45] A. Belendez T.Belendez, C. Neipp. Large and small deflections of a cantilever beam. *European journal of physics*, 23(3):371, 2002.
- [46] A. Belendez T.Belendez, C. Neipp. Numerical and experimental analysis of a cantilever beam: a laboratory project to introduce geometric nonlinearity in mechanics of materials. 2003.
- [47] D. Roy R.Kumar, L.S. Ramachandra. Techniques based on genetic algorithms for large deflection analysis of beams. *Sadhana*, 29(6):589–604, 2004.
- [48] S. Al-Sadder M.Dado. A new technique for large deflection analysis of non-prismatic cantilever beams. *Mechanics Research Communications*, 32(6):692–703, 2005.
- [49] B. S. Shvartsman. Large deflections of a cantilever beam subjected to a follower force. *Journal of Sound and Vibration*, 304(3-5):969–973, 2007.
- [50] S. Liao J. Wang, J.K. Chen. An explicit solution of the large deformation of a cantilever beam under point load at the free tip. *Journal of Computational and Applied Mathematics*, 212(2):320–330, 2008.
- [51] A. K. Mallik A. Banerjee, B.Bhattacharya. Large deflection of cantilever beams with geometric non-linearity: Analytical and numerical approaches. *International Journal of Non-Linear Mechanics*, 43(5):366–376, 2008.
- [52] B.N. Rao M. Mutyalarao, D. Bharathi. On the uniqueness of large deflections of a uniform cantilever beam under a tip-concentrated rotational load. *International Journal of Non-Linear Mechanics*, 45(4):433–441, 2010.
- [53] S.M. Srinivasan A.K.Nallathambi, C.L. Rao. Large deflection of constant curvature cantilever beam under follower load. *International Journal of Mechanical Sciences*, 52(3):440–445, 2010.
- [54] B.S.Shvartsman. Analysis of large deflections of a curved cantilever subjected to a tip-concentrated follower force. *International Journal of Non-Linear Mechanics*, 50:75–80, 2013.

- [55] Z.Y. Li X.J. Hu J.Y. Sun X.T.He, L. Cao. Nonlinear large deflection problems of beams with gradient: A biparametric perturbation method. *Applied Mathematics and Computation*, 219(14):7493–7513, 2013.
- [56] G.B.Sinclair. The non-linear bending of a cantilever beam with shear and longitudinal deformations. *International Journal of Non-linear Mechanics*, 14(2):111–122, 1979.
- [57] M. Obata Y. Goto, T. Yoshimitsu. Elliptic integral solutions of plane elastica with axial and shear deformations. *International Journal of Solids and Structures*, 26(4):375–390, 1990.
- [58] D.T.Spasic T.M.Atanackovic. A model for plane elastica with simple shear deformation pattern. *Acta mechanica*, 104(3-4):241–253, 1994.
- [59] X.I. Song S.Li. Large thermal deflections of timoshenko beams under transversely non-uniform temperature rise. *Mechanics Research Communications*, 33(1):84–92, 2006.
- [60] A. Fereidoon A.Mohyeddin. An analytical solution for the large deflection problem of timoshenko beams under three-point bending. *International Journal of Mechanical Sciences*, 78:135–139, 2014.
- [61] k.y. Lee X.F. Li. Effect of horizontal reaction force on the deflection of short simply supported beams under transverse loadings. *International Journal of Mechanical Sciences*, 99:121–129, 2015.
- [62] J. Dugundji P.Minguet. Experiments and analysis for composite blades under large deflections. i-static behavior. *AIAA journal*, 28(9):1573–1579, 1990.
- [63] D.H. Hodges A.R.Atilgan. Unified nonlinear analysis for nonhomogeneous anisotropic beams with closed cross sections. *AIAA journal*, 29(11):1990–1999, 1991.
- [64] J.N.Reddy A.A.Khdeir. An exact solution for the bending of thin and thick cross-ply laminated beams. *Composite Structures*, 37(2):195–203, 1997.
- [65] M.J. Turner. Large deflections of structures subjected to heating and external loads. *Journal of the Aerospace Sciences*, 27(2):97–106, 1960.

- [66] J.T.Oden. *Finite elements of non-linear continua*. McGraw-Hill Book, 1972.
- [67] M.A.Crisfield. *Non-linear Finite Element Analysis of Solids and Structures*. John Wiley and Sons, 1991.
- [68] M.Kleiber. *Incremental finite element modelling in non-linear solid mechanics*. Ellis Horwood, 1989.
- [69] Z.H.Zhong. *Finite element procedures for contact-impact problems*. Oxford university press, 1993.
- [70] K.J.Bathe. *Finite element procedures in engineering analysis*. Prentice-Hall, Englewood Cliffs, New Jersey, 1982.
- [71] J.R.Thomas T.H.Belytschko. *Computational methods for transient analysis*. North-Holland, 1983.
- [72] G.C. Lee Y.Tada. Finite element solution to an elastica problem of beams. *International Journal for Numerical Methods in Engineering*, 2(2):229–241, 1970.
- [73] T.Y.Yang. Matrix displacement solution to elastica problems of beams and frames. *International Journal of Solids and Structures*, 9(7):829–842, 1973.
- [74] O.C. Zienkiewicz R.D.Wood. Geometrically nonlinear finite element analysis of beams, frames, arches and axisymmetric shells. *Computers and Structures*, 7(6):725–735, 1977.
- [75] D.W.Scharpf J.H.Argyris, P.C. Dunne. On large displacement-small strain analysis of structures with rotational degrees of freedom. *Computer Methods in Applied Mechanics and Engineering*, 14(3):401–451, 1978.
- [76] S.P. Symeonidis J.H.Argyris. Nonlinear finite element analysis of elastic systems under nonconservative loading-natural formulation. part i. quasistatic problems. *Computer Methods in Applied Mechanics and Engineering*, 26(1):75–123, 1981.
- [77] M.A.Crisfield. Incremental/iterative solution procedures for non-linear structural analysis. *Numerical methods for non-linear problems*, pages 261–290, 1980.

- [78] M.A.Crisfield. An arc-length method including line searches and accelerations. *International journal for numerical methods in engineering*, 19(9):1269–1289, 1983.
- [79] M.A.Crisfield. A consistent co-rotational formulation for non-linear, three-dimensional, beam-elements. *Computer methods in applied mechanics and engineering*, 81(2):131–150, 1990.
- [80] J.P. Jameux J.L. Batoz. Large displacements and post-buckling of plane structures. In *European Mechanics Colloquium “Flexible Shells, Theory and Applications”*, Munich, W-Germany, 1983.
- [81] J.P. Jameux J.L.Batoz. Post-flambement et grands déplacements d’arcs plans. *Journal de Mécanique théorique et appliquée*, 5(2):237–257, 1986.
- [82] F.Y. Hou K.M.Hsiao. Nonlinear finite element analysis of elastic frames. *Computers and Structures*, 26(4):693–701, 1987.
- [83] J.E. Churchill A.Chajes. Nonlinear frame analysis by finite element methods. *Journal of structural engineering*, 113(6):1221–1235, 1987.
- [84] J. Oliver E.N.Dvorkin, E.Onte. On a non-linear formulation for curved timoshenko beam elements considering large displacement/rotation increments. *International Journal for Numerical Methods in Engineering*, 26(7):1597–1613, 1988.
- [85] S.H.Lo. Geometrically nonlinear formulation of 3d finite strain beam element with large rotations. *Computers and structures*, 44(1-2):147–157, 1992.
- [86] A.Ibrahimbegovic. On finite element implementation of geometrically nonlinear reissner’s beam theory: three-dimensional curved beam elements. *Computer methods in applied mechanics and engineering*, 122(1-2):11–26, 1995.
- [87] A. Ibrahimbegovic M.A. Mikdad. Interpolation non linéaire pour un élément fini de poutre en grandes rotations tri-dimensionnelles. *Revue Européenne des éléments Finis*, 4(5-6):693–718, 1995.

- [88] W. Wagner F.Gruttmann, R. Sauer. A geometrical nonlinear eccentric 3d-beam element with arbitrary cross-sections. *Computer Methods in Applied Mechanics and Engineering*, 160(3-4):383–400, 1998.
- [89] M.J. Clarke L.H.Teh. Co-rotational and lagrangian formulations for elastic three-dimensional beam finite elements. *Journal of Constructional Steel Research*, 48(2-3):123–144, 1998.
- [90] E.A. Wheeler P.F.Pai, T.J. Anderson. Large-deformation tests and total-lagrangian finite-element analyses of flexible beams. *International Journal of Solids and Structures*, 37(21):2951–2980, 2000.
- [91] M. Saje D. Zupan. Finite-element formulation of geometrically exact three-dimensional beam theories based on interpolation of strain measures. *Computer Methods in Applied Mechanics and Engineering*, 192(49-50):5209–5248, 2003.
- [92] L.N. Vu P. Nanakorn. A 2d field-consistent beam element for large displacement analysis using the total lagrangian formulation. *Finite Elements in Analysis and Design*, 42(14-15):1240–1247, 2006.
- [93] G. Garcea G D. Magisano, L. Leonetti. Advantages of the mixed format in geometrically nonlinear analysis of beams and shells using solid finite elements. *International Journal for Numerical Methods in Engineering*, 109(9):1237–1262, 2017.
- [94] E.Carrera A.Pagani. Unified formulation of geometrically nonlinear refined beam theories. *Mechanics of Advanced Materials and Structures*, 25(1):15–31, 2018.
- [95] D.H.Hodges. *Nonlinear composite beam theory*. American Institute of Aeronautics and Astronautics, 2006.
- [96] T. Merlini M.Borri. A large displacement formulation for anisotropic beam analysis. *Meccanica*, 21(1):30–37, 1986.

- [97] N.G.R Iyengar G.R.Singh, G.V. Rao. Nonlinear bending of thin and thick unsymmetrically laminated composite beams using refined finite element model. *Computers and structures*, 42(4):471–479, 1992.
- [98] K.M.Bangera K.Chandrashekhara. Linear and geometrically non-linear analysis of composite beams under transverse loading. *Composites science and technology*, 47(4):339–347, 1993.
- [99] O.Rand. Nonlinear analysis of orthotropic beams of solid cross-sections. *Composite structures*, 29(1):27–45, 1994.
- [100] A.N. Palazotto S.G.Creaghan. Nonlinear large displacement and moderate rotational characteristics of composite beams incorporating transverse shear strain. *Computers and structures*, 51(4):357–371, 1994.
- [101] A.N. Palazotto D.A.Miller. Nonlinear finite element analysis of composite beams and arches using a large rotation theory. *Finite elements in analysis and design*, 19(3):131–152, 1995.
- [102] E.H. Dowell D.Tang. Experimental and theoretical study on aeroelastic response of high-aspect-ratio wings. *AIAA journal*, 39(8):1430–1441, 2001.
- [103] F A.P.Zielinski, F. Frey. Nonlinear weighted residual approach: application to laminated beams. *Computers and structures*, 81(8-11):1087–1098, 2003.
- [104] S. Gopalakrishnan S. Agarwal, A. Chakraborty. Large deformation analysis for anisotropic and inhomogeneous beams using exact linear static solutions. *Composite structures*, 72(1):91–104, 2006.
- [105] U. Icardi M.D. Sciuva. Large deflection of adaptive multilayered timoshenko beams. *Composite structures*, 31(1):49–60, 1995.
- [106] L. Ragni A. Zona G. Ranzi, A. Dall’Asta. A geometric nonlinear model for composite beams with partial interaction. *Engineering Structures*, 32(5):1384–1396, 2010.

- [107] M. Blair W. Yu. Gebt: A general-purpose nonlinear analysis tool for composite beams. *Composite Structures*, 94(9):2677–2689, 2012.
- [108] S.N. Atluri A.R.Sofi, P.L. Bishay. Explicit tangent stiffness matrix for the geometrically nonlinear analysis of laminated composite frame structures. *Composite Structures*, 187:566–578, 2018.
- [109] Y.Cui X. An, B.C. Khoo. Nonlinear aeroelastic analysis of curved laminated composite panels. *Composite Structures*, 179:377–414, 2017.
- [110] T.Bennett B.Uy M.A.Uddin, A.H. Sheikh. Large deformation analysis of two layered composite beams with partial shear interaction using a higher order beam theory. *International Journal of Mechanical Sciences*, 122:331–340, 2017.
- [111] E. Carrera A.Pagani. Large-deflection and post-buckling analyses of laminated composite beams by carrera unified formulation. *Composite Structures*, 170:40–52, 2017.
- [112] O. Vilnay I.Sheinman Y.Frostig, M. Baruch. High-order theory for sandwich-beam behavior with transversely flexible core. *Journal of Engineering Mechanics*, 118(5):1026–1043, 1992.
- [113] Y. Frostig H.Schwartz-Givli, O. Rabinovitch. High-order nonlinear contact effects in cyclic loading of delaminated sandwich panels. *Composites Part B: Engineering*, 38(1):86–101, 2007.
- [114] I. Sheinman Y.Frostig, O.T. Thomsen. On the non-linear high-order theory of unidirectional sandwich panels with a transversely flexible core. *International Journal of Solids and Structures*, 42(5-6):1443–1463, 2005.
- [115] Y.Frostig. On wrinkling of a sandwich panel with a compliant core and self-equilibrated loads. *Journal of Sandwich Structures and Materials*, 13(6):663–679, 2011.
- [116] K.A. Wang J.L. Abot E.E.Gdoutos, I.M. Daniel. Nonlinear behavior of composite sandwich beams in three-point bending. *Experimental mechanics*, 41(2):182–189, 2001.

- [117] L. Vaikhanski S.R. Nutt S.V.Sokolinsky, H. Shen. Experimental and analytical study of nonlinear bending response of sandwich beams. *Composite Structures*, 60(2):219–229, 2003.
- [118] G.A. Kardomateas M.A. Battley C.N.Phan, N.W. Bailey. Wrinkling of sandwich wide panels/beams based on the extended high-order sandwich panel theory: formulation, comparison with elasticity and experiments. *Archive of Applied Mechanics*, 82(10-11):1585–1599, 2012.
- [119] M. Sadighi S. Dariushi. A new nonlinear high order theory for sandwich beams: An analytical and experimental investigation. *Composite Structures*, 108:779–788, 2014.
- [120] B.H. Rabin A. Kawasaki R.G.Ford Y.Miyamoto, W.A.Kaysser. *Functionally graded materials: design, processing and applications*, volume 5. Springer Science and Business Media, 2013.
- [121] P.E. Duwez M.B.Bever. Gradients in composite materials. *Materials Science and Engineering*, 10:1–8, 1972.
- [122] M.B. Bever M.Shen. Gradients in polymeric materials. *Journal of Materials science*, 7(7):741–746, 1972.
- [123] R.Watanabe Y. Doi M.Niino, A. Kumakawa. Fabrication of a high pressure thrust chamber by the cip forming method. In *20th Joint Propulsion Conference*, page 1227, 1984.
- [124] B.V.Sankar. An elasticity solution for functionally graded beams. *Composites Science and Technology*, 61(5):689–696, 2001.
- [125] S. Gopalakrishnan S.Agarwal, A.Chakraborty. Large deformation analysis for anisotropic and inhomogeneous beams using exact linear static solutions. *Composite structures*, 72(1):91–104, 2006.
- [126] X.F. Li Y.A. Kang. Bending of functionally graded cantilever beam with power-law non-linearity subjected to an end force. *International Journal of Non-Linear Mechanics*, 44(6):696–703, 2009.

- [127] L.W. Byrd V.Birman. Modeling and analysis of functionally graded materials and structures. *Applied mechanics reviews*, 60(5):195–216, 2007.
- [128] X.F. Li Y.A.Kang. Large deflections of a non-linear cantilever functionally graded beam. *Journal of Reinforced Plastics and Composites*, 29(12):1761–1774, 2010.
- [129] A.R.Davoodinik G.H.Rahimi. Large deflection of functionally graded cantilever flexible beam with geometric nonlinearity: analytical and numerical approaches. *Scientia Iranica, Transaction B: Mechanical Engineering*, 17(1):25–40, 2010.
- [130] G.H. Rahimi A.R. Davoodinik. Large deflection of flexible tapered functionally graded beam. *Acta Mechanica Sinica*, 27(5):767, 2011.
- [131] S.D. Akbas T. Kocaturk, M. Simsek. Large displacement static analysis of a cantilever timoshenko beam composed of functionally graded material. *Science and Engineering of Composite Materials*, 18(1-2):21–34, 2011.
- [132] J.N. Reddy. Microstructure-dependent couple stress theories of functionally graded beams. *Journal of the Mechanics and Physics of Solids*, 59(11):2382–2399, 2011.
- [133] I.F.M. Menezes G.H. Paulino C.A. Almeida, J.C.R. Albino. Geometric nonlinear analyses of functionally graded beams using a tailored lagrangian formulation. *Mechanics Research Communications*, 38(8):553–559, 2011.
- [134] M. Saadatfar A. Soleimani. Numerical study of large deflection of functionally graded beam with geometry nonlinearity. In *Advanced Materials Research*, volume 403, pages 4226–4230. Trans Tech Publ, 2012.
- [135] D.W. Lee L.S.Ma. Exact solutions for nonlinear static responses of a shear deformable fgm beam under an in-plane thermal loading. *European Journal of Mechanics-A/Solids*, 31(1):13–20, 2012.
- [136] I.Jafarsadeghi-Poornaki R. Shabani M.Zamanzadeh, G. Rezazadeh. Static and dynamic stability modeling of a capacitive fgm micro-beam in presence of temperature changes. *Applied Mathematical Modelling*, 37(10-11):6964–6978, 2013.

- [137] D.G.Zhang. Nonlinear bending analysis of fgm beams based on physical neutral surface and high order shear deformation theory. *Composite Structures*, 100:121–126, 2013.
- [138] M. Brojan M. Sitar, F. Kosel. Large deflections of nonlinearly elastic functionally graded composite beams. *Archives of Civil and Mechanical Engineering*, 14(4):700–709, 2014.
- [139] B.S.Gan N. D. Kien. Large deflections of tapered functionally graded beams subjected to end forces. *Applied Mathematical Modelling*, 38(11-12):3054–3066, 2014.
- [140] N.D. Kien B.S.Gan. Large deflection analysis of functionally graded beams resting on a two-parameter elastic foundation. *Journal of Asian Architecture and Building Engineering*, 13(3):649–656, 2014.
- [141] N. D. Kien. Large displacement behaviour of tapered cantilever euler-bernoulli beams made of functionally graded material. *Applied Mathematics and Computation*, 237:340–355, 2014.
- [142] M.M. Aghdam H.Niknam, A. Fallah. Nonlinear bending of functionally graded tapered beams subjected to thermal and mechanical loading. *International journal of Non-linear Mechanics*, 65:141–147, 2014.
- [143] D.N. Kim K. Yoon, P.S. Lee. Geometrically nonlinear finite element analysis of functionally graded 3d beams considering warping effects. *Composite Structures*, 132:1231–1247, 2015.
- [144] A.M. Dehrouyeh-Semnani. On the thermally induced non-linear response of functionally graded beams. *International Journal of Engineering Science*, 125:53–74, 2018.
- [145] E. A. Jackson. *Perspectives of nonlinear dynamics*, volume 1. CUP Archive, 1989.
- [146] D.G.Fertis. *Mechanical and structural vibrations*. John Wiley and Sons, 1995.
- [147] A.O. Afonta D.G.Fertis. Free vibration of variable stiffness flexible bars. *Computers and structures*, 43(3):445–450, 1992.

- [148] D.G. Ferris and A.O. Afonta. Small vibrations of flexible bars by using the finite element method with equivalent uniform stiffness and mass methodology. *Journal of sound and vibration*, 163(2):343–358, 1993.
- [149] C.T. Lee D.G. Fertis. Inelastic response of variable stiffness members under cyclic loading. *Journal of engineering mechanics*, 118(7):1406–1422, 1992.
- [150] C.T. Lee D.T. Fertis. Non-linear vibration and instabilities of elastically supported beams with axial restraints. *Journal of sound and vibration*, 165(1):123–135, 1993.
- [151] S. Wojnowsky-Krieger. The effect of an axial force on the vibration of hinged beams. *J. of Applied Mechanics*, 17:35–36, 1950.
- [152] G. Prathap. Nonlinear vibration of beams with variable axial restraint. *AIAA Journal*, 16(6):622–624, 1978.
- [153] T.K. Varadan G. Prathap. The large amplitude vibration of tapered clamped beams. *Journal of Sound and Vibration*, 58(1):87–94, 1978.
- [154] K. Decha-Umphai C. Mei. A finite element method for non-linear forced vibrations of beams. *Journal of Sound and Vibration*, 102(3):369–380, 1985.
- [155] C. Mei. Nonlinear vibration of beams by matrix displacement method. *AIAA Journal*, 10(3):355–357, 1972.
- [156] D.A. Evensen. Nonlinear vibrations of beams with various boundary conditions. *AIAA journal*, 6(2):370–372, 1968.
- [157] G. Prathap G.R. Bhashyam. Galerkin finite element method for non-linear beam vibrations. *Journal of Sound and Vibration*, 72(2):191–203, 1980.
- [158] M.I. Qaisi. Application of the harmonic balance principle to the nonlinear free vibration of beams. *Applied Acoustics*, 40(2):141–151, 1993.
- [159] S.A. Nayfeh A.H. Nayfeh. Nonlinear normal modes of a continuous system with quadratic nonlinearities. *Journal of vibration and acoustics*, 117(2):199–205, 1995.

- [160] Erdog B.Karlik, E. Ozkaya, Serkan Aydin, and Mehmet Pakdemirli. Vibrations of a beam-mass systems using artificial neural networks. *Computers & structures*, 69(3):339–347, 1998.
- [161] R.G. White L. Azrar, R. Benamar. Semi-analytical approach to the non-linear dynamic response problem of s-s and c-c beams at large vibration amplitudes part i: general theory and application to the single mode approach to free and forced vibration analysis. *Journal of Sound and Vibration*, 224(2):183–207, 1999.
- [162] R.G. White L.Azrar, R. Benamar. A semi-analytical approach to the non-linear dynamic response problem of beams at large vibration amplitudes, part ii: Multimode approach to the steady state forced periodic response. *Journal of Sound and Vibration*, 255(1):1–41, 2002.
- [163] S.P. Lim W.C. Xie, H.P. Lee. Normal modes of a non-linear clamped-clamped beam. *Journal of Sound and vibration*, 250(2):339–349, 2002.
- [164] M. Fesanghary T.Pirbodaghi, M.T. Ahmadian. On the homotopy analysis method for non-linear vibration of beams. *Mechanics Research Communications*, 36(2):143–148, 2009.
- [165] N.G.R. Iyengar G. Singh, G.V. Rao. Analysis of the nonlinear vibrations of unsymmetrically laminated composite beams. *AIAA journal*, 29(10):1727–1735, 1991.
- [166] S. Raciti R.K. Kapania. Nonlinear vibrations of unsymmetrically laminated beams. *AIAA journal*, 27(2):201–210, 1989.
- [167] J.Saravanan M. Touratier M.Ganapathi, B.P. Patel. Application of spline element for large-amplitude free vibrations of laminated orthotropic straight/curved beams. *Composites Part B: Engineering*, 29(1):1–8, 1998.
- [168] S.M. Srinivasan B.N.Patel, D.Pandit. A simplified moment-curvature based approach for large deflection analysis of micro-beams using the consistent couple stress theory. *European Journal of Mechanics-A/Solids*, 66:45–54, 2017.

- [169] A.R. Vosoughi P. Malekzadeh. Dqm large amplitude vibration of composite beams on nonlinear elastic foundations with restrained edges. *Communications in Nonlinear Science and Numerical Simulation*, 14(3):906–915, 2009.
- [170] G. Janardhan J.V. Rao J.B. Gunda, R.K. Gupta. Large amplitude vibration analysis of composite beams: simple closed-form solutions. *Composite structures*, 93(2):870–879, 2011.
- [171] H. Salarieh M. Baghani, R.A. Jafari-Talookolaei. Large amplitudes free vibrations and post-buckling analysis of unsymmetrically laminated composite beams on nonlinear elastic foundation. *Applied Mathematical Modelling*, 35(1):130–138, 2011.
- [172] A. Bouazzouni M. Slimani, M. Taazount. Perturbed solution of free non-linear vibrations of composite beams. *Composite Structures*, 94(5):1805–1813, 2012.
- [173] H.R. Ovesy M. Latifi, M. Kharazi. Nonlinear dynamic response of symmetric laminated composite beams under combined in-plane and lateral loadings using full layerwise theory. *Thin-walled Structures*, 104:62–70, 2016.
- [174] J. Yang Y. Xiang S. Kitipornchai, L.L. Ke. Nonlinear vibration of edge cracked functionally graded timoshenko beams. *Journal of Sound and Vibration*, 324(3-5):962–982, 2009.
- [175] S. Kitipornchai Sritawat L.L. Ke, J. Yang. Nonlinear free vibration of functionally graded carbon nanotube-reinforced composite beams. *Composite Structures*, 92(3):676–683, 2010.
- [176] S. Kitipornchai L.L. Ke, J. Yang. An analytical study on the nonlinear vibration of functionally graded beams. *Meccanica*, 45(6):743–752, 2010.
- [177] M. Simsek. Non-linear vibration analysis of a functionally graded timoshenko beam under action of a moving harmonic load. *Composite Structures*, 92(10):2532–2546, 2010.

-
- [178] M.Rafiee A. Shooshtari. Nonlinear forced vibration analysis of clamped functionally graded beams. *Acta Mechanica*, 221(1-2):23, 2011.
- [179] M.M. Aghdam A. Fallah. Nonlinear free vibration and post-buckling analysis of functionally graded beams on nonlinear elastic foundation. *European Journal of Mechanics-A/Solids*, 30(4):571–583, 2011.
- [180] M.M. Aghdam A. Fallah. Thermo-mechanical buckling and nonlinear free vibration analysis of functionally graded beams on nonlinear elastic foundation. *Composites Part B: Engineering*, 43(3):1523–1530, 2012.
- [181] Y. Mao Yiqi Y. Fu, J. Wang. Nonlinear analysis of buckling, free vibration and dynamic stability for the piezoelectric functionally graded beams in thermal environment. *Applied Mathematical Modelling*, 36(9):4324–4340, 2012.
- [182] y. Xiang K.W. Chow S.K.Lai, J. Harrington. Accurate analytical perturbation approach for large amplitude vibration of functionally graded beams. *International Journal of Non-Linear Mechanics*, 47(5):473–480, 2012.
- [183] M. Torabi H. Yaghoobi. Post-buckling and nonlinear free vibration analysis of geometrically imperfect functionally graded beams resting on nonlinear elastic foundation. *Applied Mathematical Modelling*, 37(18-19):8324–8340, 2013.
- [184] D. Das A. Paul. Free vibration analysis of pre-stressed fgm timoshenko beams under large transverse deflection by a variational method. *Engineering Science and Technology, an International Journal*, 19(2):1003–1017, 2016.
- [185] S. Lecca M. Soave E.Carrera, P. Nali. Effects of in-plane loading on vibration of composite plates. *Shock and Vibration*, 19(4):619–634, 2012.
- [186] A.K. Rao S.Srinivas, CV.J Rao. An exact analysis for vibration of simply-supported homogeneous and laminated thick rectangular plates. *Journal of sound and vibration*, 12(2):187–199, 1970.

- [187] S.Srinivas. A refined analysis of composite laminates. *Journal of Sound and Vibration*, 30(4):495–507, 1973.
- [188] A.K.Noor. Free vibrations of multilayered composite plates. *AIAA journal*, 11(7):1038–1039, 1973.
- [189] T. Kuppusamy J.N.Reddy. Natural vibrations of laminated anisotropic plates. *Journal of sound and vibration*, 94(1):63–69, 1984.
- [190] D.M. Sciuva. Bending, vibration and buckling of simply supported thick multilayered orthotropic plates: an evaluation of a new displacement model. *Journal of Sound and Vibration*, 105(3):425–442, 1986.
- [191] R.A. Sheno RA A.K.Nayak, S.S.J. Moy. Free vibration analysis of composite sandwich plates based on reddy’s higher-order theory. *Composites Part B: Engineering*, 33(7):505–519, 2002.
- [192] R. Xiaohui W.Zhen, Ch. Wanji. An accurate higher-order theory and c0 finite element for free vibration analysis of laminated composite and sandwich plates. *Composite Structures*, 92(6):1299–1307, 2010.
- [193] K. Swaminathan T.Kant. Analytical solutions for free vibration of laminated composite and sandwich plates based on a higher-order refined theory. *Composite structures*, 53(1):73–85, 2001.
- [194] W.M. Roberts M.L.Gossard, P. Seide. Thermal buckling of plates. 1952.
- [195] W.S. Burton A.K.Noor. Three-dimensional solutions for thermal buckling of multilayered anisotropic plates. *Journal of engineering mechanics*, 118(4):683–701, 1992.
- [196] J.E. Ashton J.M.Whitney. Effect of environment on the elastic response of layered composite plates. *AIAA Journal*, 9(9):1708–1713, 1971.
- [197] W. Chen Zh.Wu. Thermomechanical buckling of laminated composite and sandwich plates using global–local higher order theory. *International Journal of Mechanical Sciences*, 49(6):712–721, 2007.

- [198] K.K. Shukla S.Singh, J. Singh. Buckling of laminated composite plates subjected to mechanical and thermal loads using meshless collocations. *Journal of Mechanical Science and Technology*, 27(2):327–336, 2013.
- [199] M.Cetkovic. Thermal buckling of laminated composite plates using layerwise displacement model. *Composite Structures*, 142:238–253, 2016.
- [200] F.L.Lurie. Lateral vibrations as related to structural stability. *ASME Journal of applied mechanics*, 19(2):195–204, 1952.
- [201] W.S. Burton A.K.Noor. Three-dimensional solutions for the free vibrations and buckling of thermally stressed multilayered angle-ply composite plates. 1992.
- [202] Ch. Mei Ch. GRAY R.Zhou, D. XUE. Vibration of thermally buckled composite plates with initial deflections using triangular elements. In *34th Structures, Structural Dynamics and Materials Conference*, page 1321, 1993.
- [203] I. D.M.Lee and Lee. Vibration behaviors of thermally postbuckled anisotropic plates using first-order shear deformable plate theory. *Computers and structures*, 63(3):371–378, 1997.
- [204] H.Matsunaga. Vibration and stability of cross-ply laminated composite plates according to a global higher-order plate theory. *Composite Structures*, 48(4):231–244, 2000.
- [205] H.Matsunaga. Vibration and stability of angle-ply laminated composite plates subjected to in-plane stresses. *International journal of mechanical sciences*, 43(8):1925–1944, 2001.
- [206] H.Matsunaga. Thermal buckling of cross-ply laminated composite and sandwich plates according to a global higher-order deformation theory. *Composite Structures*, 68(4):439–454, 2005.
- [207] N. Kaur A.Khanna. Effect of thermal gradient on vibration of non-uniform visco-elastic rectangular plate. *Journal of The Institution of Engineers (India): Series C*, 97(2):141–148, 2016.

- [208] G.Herrmann. The influence of initial stress on the dynamic behavior of elastic and viscoelastic plates. *IABSE publications*, 16, 1955.
- [209] A.E. Armenakas G.Herrmann. Vibrations and stability of plates under initial stress. *Journal of the Engineering Mechanics Division*, 86(3):65–94, 1960.
- [210] S.M. Dickinson S.F.Bassily. Buckling and lateral vibration of rectangular plates subject to inplane loads-a ritz approach. *Journal of Sound and Vibration*, 24(2):219–239, 1972.
- [211] S.R. Robertson E.J.Brunelle. Vibrations of an initially stressed thick plate. *Journal of Sound and Vibration*, 45(3):405–416, 1976.
- [212] P.A.A. Laura G.E.Gianetti, L. Diez. Transverse vibrations of rectangular plates with elastically restrained edges and subject to in-plane shear forces. *Journal of Sound and Vibration*, 54(3):409–417, 1977.
- [213] L.W. Chen J.L.Doong, T.J. Chen. Vibration and stability of an initially stressed laminated plate based on a higher-order deformation theory. *Composite structures*, 7(4):285–309, 1987.
- [214] J.L.Doong. Vibration and stability of an initially stressed thick plate according to a high-order deformation theory. *Journal of Sound and Vibration*, 113(3):425–440, 1987.
- [215] T.J.Craig D.J.Dawe. The vibration and stability of symmetrically-laminated composite rectangular plates subjected to in-plane stresses. *Composite structures*, 5(4):281–307, 1986.
- [216] Palaninathan R.Dhanaraj. Free vibration of initially stressed composite laminates. *Journal of sound and vibration*, 142(3):365–378, 1990.
- [217] S.P. Lim H.P.Lee. Free vibration of isotropic and orthotropic square plates with square cutouts subjected to in-plane forces. *Computers and structures*, 43(3):431–437, 1992.
- [218] H.Matsunaga. Vibration of cross-ply laminated composite plates subjected to initial in-plane stresses. *Thin-walled structures*, 40(7-8):557–571, 2002.

- [219] Ch.P. Fung Ch.S.Chen. Non-linear vibration of initially stressed hybrid composite plates. *Journal of sound and vibration*, 274(3-5):1013–1029, 2004.
- [220] Kiusalaas.J. *Numerical methods in engineering with matlab*. Cambridge University Press, 2009.
- [221] K. Mattiasson. Numerical results from large deflection beam and frame problems analysed by means of elliptic integrals. *International journal for numerical methods in engineering*, 17(1):145–153, 1981.
- [222] A. Guran T.M.Atanackovic. *Theory of elasticity for scientists and engineers*. Springer Science and Business Media, 2012.
- [223] H.Matsunaga. Free vibration and stability of angle-ply laminated composite and sandwich plates under thermal loading. *Composite structures*, 77(2):249–262, 2007.
- [224] J.N.Reddy. Free vibration of antisymmetric, angle-ply laminated plates including transverse shear deformation by the finite element method. *Journal of Sound and Vibration*, 66(4):565–576, 1979.
- [225] T.L.C. Chen C.W.Bert. Effect of shear deformation on vibration of antisymmetric angle-ply laminated rectangular plates. *International Journal of Solids and Structures*, 14(6):465–473, 1978.
- [226] K.S. Kim K.K.Viswanathan. Free vibration of antisymmetric angle-ply-laminated plates including transverse shear deformation: Spline method. *International Journal of Mechanical Sciences*, 50(10-11):1476–1485, 2008.
- [227] C.A.M. Soares J.S. Moita, C.M.M. Soares. Buckling and dynamic behaviour of laminated composite structures using a discrete higher-order displacement model. *Computers and structures*, 73(1-5):407–423, 1999.
- [228] J.M. Whitney R.M. Jones, H.S. Morgan. Buckling and vibration of antisymmetrically laminated angle-ply rectangular plates. *International Journal of Applied Mechanics*, pages 1143–1144, 1973.

- [229] K.H. Lee S.T.Chow N.R.Senthilnathan, S.P. Lim. Buckling of shear-deformable plates.
AIAA journal, 25(9):1268–1271, 1987.